DETECTION OF CLIMATE CHANGES OVER THE GLOBAL AND CARIBBEAN BASIN

by

Oswaldo Martín Julca Benites

A thesis submitted in partial fulfillment of the requirements for the degree of

MASTER OF SCIENCE
in
MECHANICAL ENGINEERING

UNIVERSITY OF PUERTO RICO
MAYAGÜEZ CAMPUS
2007

Approved by:

______________________________ __________________
Nazario Ramírez Beltrán, Ph.D. Date
President, Graduate Committee

______________________________ __________________
Vikram Pandya, Ph.D. Date
Member, Graduate Committee

______________________________ __________________
Gustavo Gutiérrez , Ph.D. Date
Member, Graduate Committee

______________________________ __________________
Sandra Cruz Pol, Ph.D Date
Representative of Graduate Studies

______________________________ __________________
Paul Sundam , Ph.D. Date
Chairperson of the Department

ABSTRACT

The statistical test developed in this research was able to find punctual changes at any time series. In this way the studied variables including sunspot, global carbon dioxide, air surface temperature, cloud cover and sea level showed a change along the course of the time. In addition, almost all the variables are continuously increasing over time.

The reason of the present global warming can not be explained by the increasing amount of sunspot; however, it could be explained by the increase of carbon dioxide in the atmosphere. The global temperature increase is reflected over local region, where each island has a different behavior with respect to the others. In addition, the cloud cover variations have a very important effect in the atmospheric physical processes in our planet.

A statistical relation between the sea level and the middle cloud cover (from 680 until 440 mb), during El Niño event 1997/1998 was found. In the Caribbean region, this relation is clearly observed during the month of March. On the other hand, the mesoscale model RAMS showed that the relation between the middle cloud cover and El Niño 1997/1998 took place due to a very intense sea heating and by an intense vertical wind shear. The intense vertical wind shear cut off the vertical convection, inhibiting the vertical transport of heat and moisture toward the high troposphere. As consequence, the heat and the moisture are stored in the middle levels.

RESUMEN

La prueba estadística desarrollada en la presente investigación fue capaz de hallar cambios puntuales en una serie de tiempo. En ese sentido las variables estudiadas incluyen manchas solares, dióxido de carbono global, temperatura del aire, cobertura de nube y nivel del mar muestran un cambio a lo largo del tiempo. Además, casi todas las variables están continuamente incrementando sobre el tiempo.

La razón del presente calentamiento global no puede ser explicada por el incremento en la cantidad de manchas solares; sin embargo, este podría ser explicado por el incremento de dióxido de carbono en la atmósfera. El incremento de la temperatura global es reflejado sobre la región local, donde cada isla tiene un diferente comportamiento con respecto a las otras. En adición, las variaciones de la cubierta de nube tienen un muy importante efecto en los procesos físicos atmosféricos en nuestro planeta.

Estadísticamente fue hallada una relación entre el nivel del mar y la cubierta media de nubes (desde 680 a 440 mb), durante el evento del Niño 1997/1998. En la región del Caribe, esta relación es claramente observada en el mes de Marzo. Por otro lado, el modelo de mesoscala RAMS muestra que la relación entre la cubierta de nubes medias y El Niño 1997/1998 tomo lugar debido a un muy intenso calentamiento del mar y una intensa velocidad vertical de corte. La intensa velocidad vertical de corte quebró la convección vertical, inhibiendo el transporte de calor y humedad hacia los niveles altos de la troposfera. Como consecuencia, el calor y la humedad se almacenaron en los niveles medios.

Dedication

TO MY GOD, BECAUSE I NEVER FELT ALONE, HE ALWAYS WAS WITH ME, INDICATING ME THE CORRECT WAY TO FOLLOW. TO MY WIFE GABY, WHO ALWAYS HELPED ME UNCONDITIONALLY WITH THIS PROJECT ALL THE TIME, WITH UNDERSTANDING, PATIENCE AND LOVE. TO MY LOVING DAUGHTER ARIADNA WHOM I OWE THE MOTIVATION THAT I NEEDED EACH DAY. TO MY DAD OSWALDO, WHO I THANK FOR HIS SACRIFICES. TO ALL MY SIBLINGS: ARTURO, JAVIER, NANCY, MARCO, JANNETH AND EDUAR, THANKS A LOT. AND TO MANY PEOPLE WHO ARE ALWAYS IN MY HEART AND MIND.

ACKNOWLEDGEMENTS

I would like to thank the NASA-EPSCOR program at the University of Puerto Rico – Mayagüez Campus for sponsoring this research. My sincere gratitude to my thesis adviser Dr. Nazario Ramirez for gave me the opportunity to work in this research. I also would like to thank Dr. Jorge Gonzalez. Thanks to Pieter Van Der Meer for his continuing help and collaboration; I also would like to express my gratitude to the following persons: Moises Angeles for helping me to understand the RAMS model and his valuable friendship; Joan Castro for his continuous technical support and friendship; Christian Calderon for his friendship and help in several moments; to Axel Maldonado, my best friend the best, thanks a lot; to Luis Lopes, the administrator of the Climate Master – UPRM; to the administrator of the High Performance Computer Facilities – UPR Rio Piedras.

Table of Contents

Table List

Tables **Page**

Figure List

Figures **Page**

Symbols List

Legend of Symbols (Roman)

n	total number of observed data.
$\{X_t\}$	time series, t = 1, …,n.
$E(X_t)$	mean function of $\{X_t\}$.
iid	independent and identical distributed random variables with zero mean.
AST	Air Surface Temperature.
COOP	Cooperative Station.
GHE	Greenhouse effect.
GHG's	Greenhouse gases.
IPCC	Intergovernmental Panel on Climate Change.

LW	Longwave
NCEP	The National Center for Environmental Prediction.
NOAA	National Oceanic and Atmospheric Administration
RH	Relative humidity.
RAMS	Regional Atmospheric Modeling System.
SST	Sea surface temperature.
SW	Shortwave
T	Air temperature in the specific pressure level.
U	Zonal wind.
V	Meridional wind.
VWS	Vertical Wind Shear

Legend of Symbols (Greek)

μ_t	mean function of $\{X_t\}$.
γ_t	covariance function of $\{X_t\}$.
ρ_t	autocorrelation function of $\{X_t\}$.
θ	coefficients of a moving average (MA) model.
ϕ	coefficients of a auto-regressive (AR) model.

1 INTRODUCTION

At present there are several studies that use numerical models and/or statistical techniques to detect and attribute climate changes ([17], [4], [19], [65], [67], [64], [44], [46], etc.). The detection of climate change consists of determining the time and the magnitude of the climate change. The attribution consists of determining what the physical causes have generated the climate change. The typical tools used to detect climate changes are: pattern of trend changes, Gaussian distribution, correlations techniques, and optimal detection procedures. The attribution techniques are mostly based on using numerical simulation techniques. This thesis focuses only on climate change detection problem.

The attributions explain the possible reasons by which the earth is heating. This is a controversial problem because some people consider global warming due to natural variability; however, other researchers attribute –or suggest– that global warming is due to anthropogenic sources ([27], [24], [18] and [73]), the Intergovernmental Panel on Climate Change (IPCC) in 2001 established that: "The balance of evidence suggests a discernible human influence on global climate". The anthropogenic sources are influenced by the emission of greenhouse gases (GHG) and changes in land use, such as urbanization and agriculture. It is difficult to separate GHG and land use because both tend to increase the daily mean surface temperature [32].

A statistical algorithm was proposed by Ramirez et. al [56] to detect climate changes in time series in an easier way. The improved version established that a climate change can be exhibited in the trend, in the periodicity or in the stochastic component of a given time series. As a result it was easier to identify a change, in one specific time, which can be produced by external behavior. These external behaviors can be produced by data error or by real external behavior (natural or anthropogenic). This improved version has also the capability to associate phenomena, such as El Niño or solar radiation.

In a recent publication by the IPCC 2007 [32], it is stated that: "Most of the observed increase in globally averaged temperatures since the mid-20th century is very likely due to the observed increase in anthropogenic greenhouse gas concentrations". Natural variability is another attribution found in nature as the variability of energy transported by the atmosphere, ocean and their respective circulation [5], although others include volcanic eruption and solar flux variability ([66], [4], [29]) as natural variability. The analysis presented here considers as natural variability the volcanic eruption and solar flux. However recent publications have shown that the global warming of the last 20th century can not only be explained by external forces (effects, processes, objects, or materials that are derived from human activities, as opposed to those occurring in natural environments without human influences, for example land use, ozone depletion, and mainly the greenhouse gases). It is also necessary to include in the model the natural variability and external forces to explain the present warming ([27], [28], [32]).

Current researchers are using models under different scenarios to predict the climate and environmental bahavior. Thus it is possible to predict the temperature, rain, and other climate variables [1], [24], [27], [69]. The IPCC has made very important contributions in the area by developing future scenarios that could occur. The idea of predicting exactly the temperature is considered impossible, due to the anthropogenic as well as the natural origin, which are difficult to predict. In other words, there are several uncertain variables [68]. So regardless of the attribution, natural and/or anthropogenic forces, the global warming is affecting human society and its economy. The global warming is a serious problem which may cause dramatic effects in the weather of the world. Hence, the understanding of past events is very important to estimate uncertainties and design strategies to mitigate the climate change effects.

The IPCC 2007 [31] pointed out that: "Small islands, whether located in the Tropics or higher latitudes, have characteristics which make them especially vulnerable to the effects of climate change, sea level rise and extreme events". Moreover, sea-level rise is expected to exacerbate inundation, storm surge, erosion and other coastal hazards, thus threatening vital infrastructure, settlements and facilities that support the livelihood of island communities. A reduction of water resources has been projected in many small islands, e.g., in the Caribbean and Pacific, to the point that they may become insufficient to satisfy the demand during the low rainfall periods. With higher temperatures, increased invasion by non-native species is expected to occur, particularly on middle and high-latitude islands.

The global and regional climate changes are evident and they could be extremely dangerous to each community along the world. Therefore, it is important to determine how the climate indicators are related, its impacts and the physical phenomena involved in the process. This work studies some natural and anthropogenic contribution with its effect on the atmosphere, land and ocean (for example, the temperature, clouds and sea level). This investigation presents two analyses, the first refers to the statistical technique to detect climate changes and the second is to use the regional climate model to understand the impact of the climate change over the Caribbean basin. The statistical technique refers to the global coverage and the other Caribbean area (especially the major 4 islands: Dominican Republic and Haiti, Cuba, Jamaica and Puerto Rico). In summary the statistical techniques are used to identify the time when a climate change has occurred and the regional numerical mode is used to analyze the impact of climate changes in small regions, which has consisted of downscaling global information to the regions of interest, also called dynamic downscaling. It transforms global atmospheric data to regional atmospheric information from coarse resolutions to finer resolutions. The mesoscale Regional Atmospheric Model System (RAMS) is used as a downscaling tool, coupled with National Centers for Environmental Prediction (NCEP) data.

1.1 Motivation

The global mean surface air temperature has risen about 0.5°C during the 20th century [17]. A large part of the world ocean has exhibited coherent changes of ocean heat content during the past 50 years, exhibiting a net warming [38]. In addition the sea level has increased 1.8 mm/yr from the period 1950–2000 [12]. However, by using satellite data from 1993 until 2004 a rate of 3 mm/yr was found [56], almost twice compared to the previous study. A more detailed work [21] indicates that during the second half of the 20^{th} century, the world has become both warmer and wetter for global land areas. Moreover, currently wet periods produce significantly higher rainfall than a few decades ago. In addition, heavy rainfall events have become more frequent and cold temperature extremes have become less frequent during the second half of the 20th century. These observed extremes are in line with the changes expected due to the new greenhouse conditions.

Since 1987 more than 360 weather events had been detected in the United States, with a loss greater than $5 million for each event, and with several record-setting catastrophes. The Midwest drought of the years 1988–1989, caused a loss of $39 billion. Hurricane Andrew in South Florida in 1992, originated $30 billion of loss, and the Midwest flood of 1993 $19 billion [9]. Hurricane Katrina, according to the "Financial Times", produced a total economic loss closer to $100 billion. On the other hand, the deaths number by heat wave has also increased in the last decades [9]. Geographical locations of the large loss trends further reveal that population growth and demographic redistributions are playing a major role in the losses degree for weather–climate extremes. Therefore, societal impacts from weather and climate extremes, and trends in those impacts, are a function of both climate and society.

Climate, agriculture and forestry are intrinsically linked. The mean surface air temperature of the earth can be used as a measure of the stability of the climate system. It responds to energy inputs, and cycling process such as the hydrological (water) cycle. The temperature is part of the process of the life systems [63]. Native forests take centuries to adjust their range, and agriculture would face almost impossible adaptations. On the other hand, malaria, dengue and insects, which already are endemic in tropics and sub tropics areas, could aggravate [59]. The production of cultivations could decrease significantly in countries such as Africa and Latin America and in other growing countries. Water could become scarcer in several areas of the world, which already have scarcity. The climate change also exasperates the decreasing biodiversity of species, which will increase the danger of extinction of several species, especially those with little or fragmented habitats.

Numerical experiments using general circulation model have shown changes in extreme events for future climates, such as extreme high temperatures increase, extreme low temperatures decrease, and an increase in intensity of precipitation events [18]. In addition, IPCC 2001 [29] showed that the sea level will rise of between 9 and 88 cm in 110 years, for scenarios that include rapid, probably unrealistic, growth of climate forcings.

A discernible human influence was identified in the present global warming, including ocean warming, continental-average temperatures, temperature extremes and wind patterns [32]. All events and facts described above are linked to climate changes and this reality has motivated me to do the present work. So, the concurrent and the possible future climate changes need to be understood and quantified. Hence, by using a statistical and climate modeling techniques it may be possible to explain why significant change and its relation with other climate variables occur. The analysis will include the regional climate change for the Caribbean Islands and global climate change.

1.2 Objective

The main objectives of this work are shown next:

- To understand the importance of the climate indicators such as external forcing (carbon dioxide), natural variability (sunspot which is related with the solar radiance), and their influence or relation in the development of the climate and weather (temperature, sea level, cloud cover, El Niño, etc).

- To develop a statistical test that will have the ability to determine the shifts in correlated or uncorrelated time series. Apply the statistical test to detect changes in selected observed data such as sunspot, CO_2, sea level, clouds and air temperature will also be employed.

- To identify climate changes at regional and global scale and to explain the possible relation between them by using climate modeling software (RAMS) as a tool.

1.3 Summary of Following Chapters

We first develop the necessary background theory in Chapters 2 and 3. Chapter 4 presents the sources of information and describes the variables used in this analysis. Chapter 5 describes the methodology developed for the climate change detection and the regional climate model. Monte Carlo simulation technique and real data is used to explain the statistical procedure to detecte a climate change in a single climate indicator. This chapter also describes the initialization and configuration of the numerical model. Chapter 6 presents the results and discussions of the climate change detection and the climate change impacts through the regional climate model. The last chapter presents some conclusions and recommendations. Appendices present data, computer programs and some details of the research work.

2 THEORETICAL BACKGROUND

In this chapter will be cover the principles and basic concepts with the variables and atmospheric processes that generate the climate changes. These physical concepts are necessary to understand the processes atmospheric and therefore its changes. In addition, the statistical concepts and tools are presented which will be employed to detect the climate changes.

2.1 Introduction of Climate System and its importance

2.1.1 Some Definitions

Weather and climate

Weather and climate have a profound influence on life on Earth. They are part of the daily experience of human beings and are essential for health, food production and well-being. If one wishes to understand, detect and eventually predict the human influence on climate, one needs to understand the system that determines the climate of the Earth and of the processes that lead to climate change.

There is a tremendous common confusion unrelated with the present topic about the notions of "weather" and "climate", by thinking that the two words are the same. The "weather", as we experience it, is defined as the fluctuating state (from hour-to-hour or day-to-day) of the atmosphere around us, characterized by the temperature, wind, precipitation, clouds and other weather elements. The weather systems arise mainly due to atmospheric instabilities, and their evolution is governed by non-linear chaotic dynamics. As a result the weather is not really predictable beyond a week or two into the future. *"Climate"* refers to the average weather in terms of the mean and its variability over a certain time-span and a certain area. Classical climatology provides a classification and description of the various climate regimes found on Earth. Climate varies from place to place, depending on latitude, distance to the sea, vegetation, presence or absence of mountains or other geographical factors. Climate varies also in time; from season to season, year to year, decade to decade or on much longer time-scales, such as the Ice Ages [7].

Climate change

A climate change is the significant deviation from the average state of the atmosphere over time scales ranging from decades or longer, in the Earth's global climate or in regional climates over time. These changes can be caused by processes of internal or external forces. *Internal forces* (or natural variability) are the Earth’s orbit, volcanic activity and mainly solar radiation. *External forces* (or anthropogenic effects) are effects, processes, objects, or materials that are derived from human activities, as opposed to those occurring in natural environments without human influences, for example land use, ozone depletion, and mainly the greenhouse gases [28].

Climate variables

The traditional knowledge of weather and climate focuses on those variables that affect daily life most directly: average, maximum and minimum temperature, wind near the surface of the Earth, precipitation in its various forms (snow, hail, rainfall and other forms of water falling from the sky), humidity, cloud type and amount, and solar radiation. These are the variables observed hourly by a large number of weather stations around the globe. However this is only part of the reality that determines weather and climate. The growth, movement and decay of weather systems depend also on the vertical structure of the atmosphere, the influence of the underlying land and sea and many other factors not directly experienced by human beings. Climate is determined by the atmospheric circulation and by its interactions with the large-scale ocean currents and the land with its features such as albedo, vegetation and soil moisture. The climate of the Earth as a whole depends on factors that influence the radiative balance, such as for example, the atmospheric composition, solar radiation or volcanic eruptions. To understand the climate of our planet Earth and its variations and to understand and to predict the changes of the climate brought about by human activities, one cannot ignore any of these many factors and components that determine the climate. We must understand the climate system, the complicated system consisting of various components, including the dynamics and composition of the atmosphere, the ocean, the ice and snow cover, the land surface and its features, the many mutual interactions between them, and the large variety of physical, chemical and biological processes taking place in and among these components. "Climate" in a wider sense refers to the state of the climate system as a whole, including a statistical description of its variations [26].

2.1.2 Climate system and the importance of some climatic variables

Climate System

As mentioned in the previous section, the climate system is the result of several interactions and their components are the atmosphere (including the troposphere and stratosphere), the geosphere (which includes the solid earth (lithosphere), the oceans, rivers and inland water masses (hydrosphere) and the snow, ice and permafrost (cryosphere)) and the biosphere (the transition zone between them within which most plant and animal life exists and most living and dead organic matter (biomass) is to be found). Figure 2.1 illustrates the main physical processes that take place within the climate system and thus exert an influence on it. The direct effect of human activities on the climate system is also considered an external forcing [28].

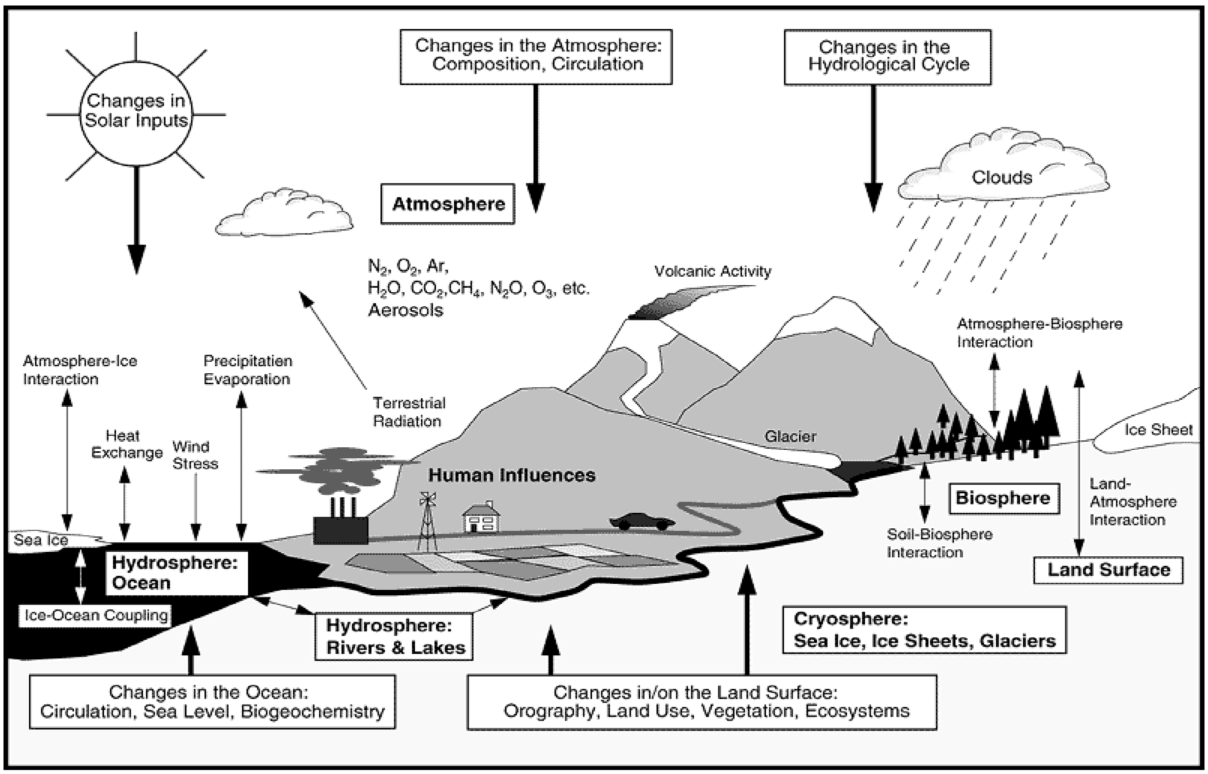

Figure 2.1 Multiscale interactions in the earth system.
Taken from IPCC 2001 [28]

Interactions among the components

Many physical, chemical and biological interaction processes occur among the various components of the climate system on a wide range of space and time scales, making the system extremely complex. Although the components of the climate system are very different in their composition, physical and chemical properties, structure and behavior, they are all linked by fluxes of mass, heat and momentum: all subsystems are considered open and interrelated [28].

As an example, the atmosphere and the oceans are strongly coupled and exchange, among others, water vapor and heat through evaporation. This is part of the hydrological cycle and leads to condensation, cloud formation, precipitation and runoff, and supplies energy to weather systems. Atmosphere and oceans also exchange, among other gases, carbon dioxide, maintaining a balance by dissolving it in cold polar water which sinks into the deep ocean and by outgassing in relatively warm upwelling water near the equator.

Some other examples: the biosphere influences the carbon dioxide concentration by photosynthesis and respiration, which in turn is influenced by climate change. The biosphere also affects the input of water in the atmosphere through evapotranspiration, the atmosphere's radiative balance through the amount of sunlight reflected back to the sky (albedo), and any change, whether natural or anthropogenic, in the components of the climate system and their interactions, or in the external forcing, may result in climate variations.

Importance of some climatic variables

Sun

The Sun is the star located at the center of the Solar System. Energy from the Sun—in the form of sunlight—supports almost all life on Earth via photosynthesis, and drives the Earth's climate and weather. The Earth's climate system constantly tries to maintain a balance between the energy that reaches the Earth from the Sun and the energy that is emitted to space. Scientists refer to this process as the Earth's "radiation budget".

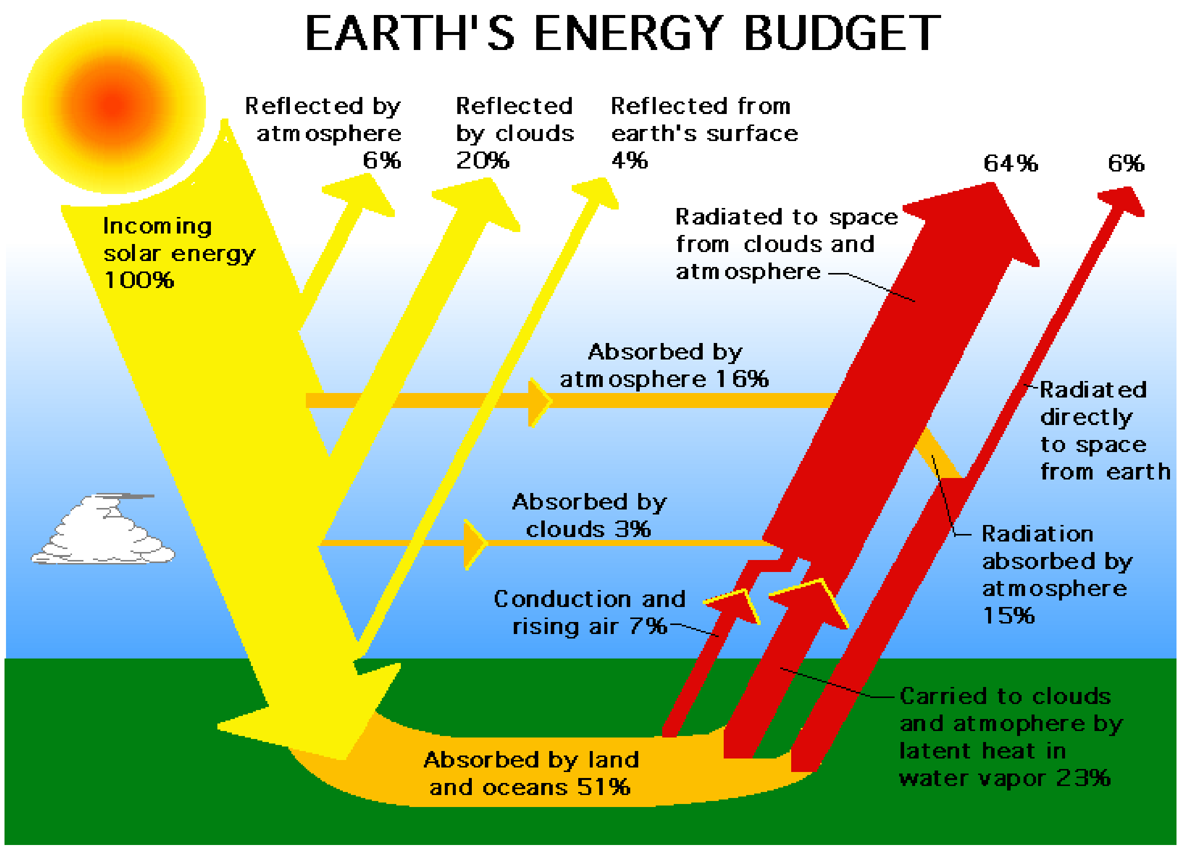

Figure 2.2 Balance of incoming solar energy above Earth.
Taken from ATMOSPHERIC SCIENCE DATA CENTER - NASA

Figure 2.2 describes the modification of solar radiation by atmospheric and surface processes for the whole Earth over a period of one year. Of all the sunlight that passes through the atmosphere annually, only 51 % is available at the Earth's surface. This energy is used to heat the Earth's surface and the lower atmosphere, melt and evaporate water, and run photosynthesis in plants. Of the other 49 %, 4 % is reflected back to space by the Earth's surface, 26 % is scattered or reflected to space by clouds and atmospheric particles, and 19 % is absorbed by atmospheric gases, particles, and clouds. Another part of the energy going back to the space from the Earth is the longwave radiation emitted by the Earth. From this: 7

% is emitted by sensible heat which is the product of conduction and rising air, and 23% is carried to clouds and to the atmosphere by latent heat of vaporization in the form of water vapor; both making a total of 30 %, from this amount only 3 % is absorbed by the clouds. 21 % is emitted by the surface in form of longwave radiation, from this 15% is absorbed by water vapor and CO_2, and 6 % is radiated directly to the space. Finally, it can be noticed that 64 % is radiated to space in the following way: 26 % from clouds and 38% from the atmosphere (water vapor, CO_2 and ozone). Thus the energy balance shows that the total incoming energy from the sun leaves completely (100% percent) the earth [16].

Comparison between Solar irradiance and Sunspot

Irradiance is the electromagnetic radiation which is incident on the surface, while ***sunspot*** is a region on the Sun's surface that is marked by a lower temperature than its surroundings and intense magnetic activity, which inhibits convection, forming areas of low surface temperature [36].

The number of sunspots has been found to correlate with the intensity of solar radiation over the period - since 1979 - when satellite measurements of radiation have become available (see Figure 2.3). Since sunspots are dark it is natural to assume that more sunspots decrease the solar radiation. However, the surrounding areas are brighter and the overall effect is that more sunspots imply a brighter sun.

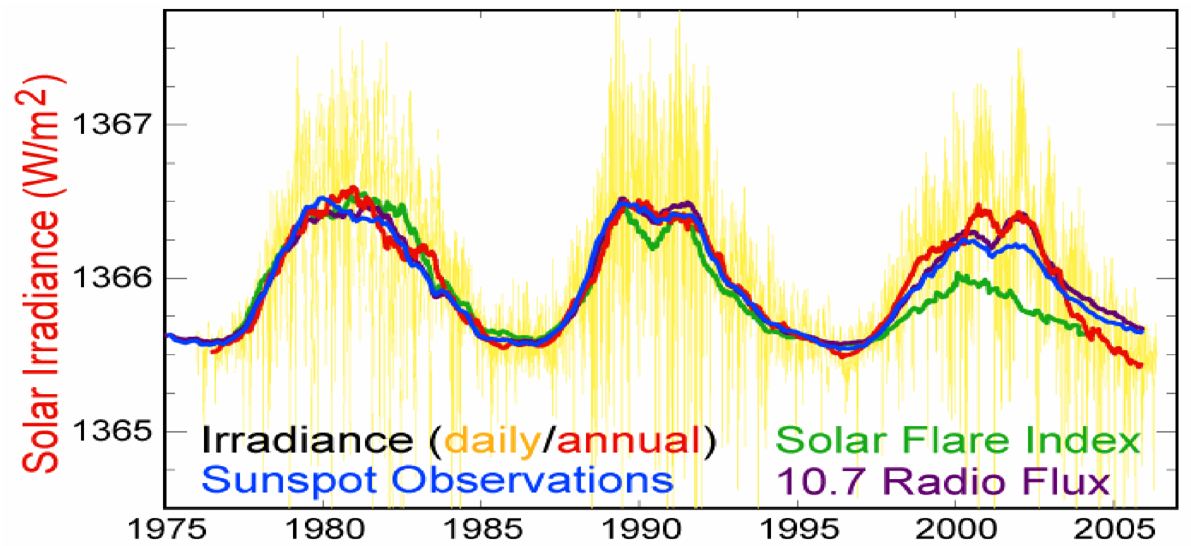

Figure 2.3 Solar Cycle Variations.
Made by PhD Robert A. Rohde - UC Berkeley.

Carbon dioxide and global warming

One of the possible causes of the global warming is due to anthropogenic greenhouse effect (GHE). Figure 2.4 shows that the amount of heat energy added to the atmosphere by the GHE is controlled by the concentration of GHG's in the Earth's atmosphere.

The concentration of the major greenhouse gases have increased since the beginning of the Industrial Revolution (about 1700 AD). As a result of these higher concentrations, scientists predict that the greenhouse effect will be *enhanced* and the Earth's climate will become warmer. Predicting the amount of warming is accomplished by computer modeling. Computer models suggest that doubling of the concentration of the main GHG, ***carbon dioxide***, may raise the average global temperature between 1º and 3° Celsius.

The concentration of carbon dioxide (CO_2) in the atmosphere has increased by about 25% in the past 100 years, mostly due to human activities, such as combustion of fossil fuels and deforestation. Its concentration at the present time is about 380 parts per million (ppm). The projections estimate that the concentrations of CO_2 will double the pre-industrial concentration (270 ppm) within the next 50 to 100 years, in the absence of any mechanism of controls [15].

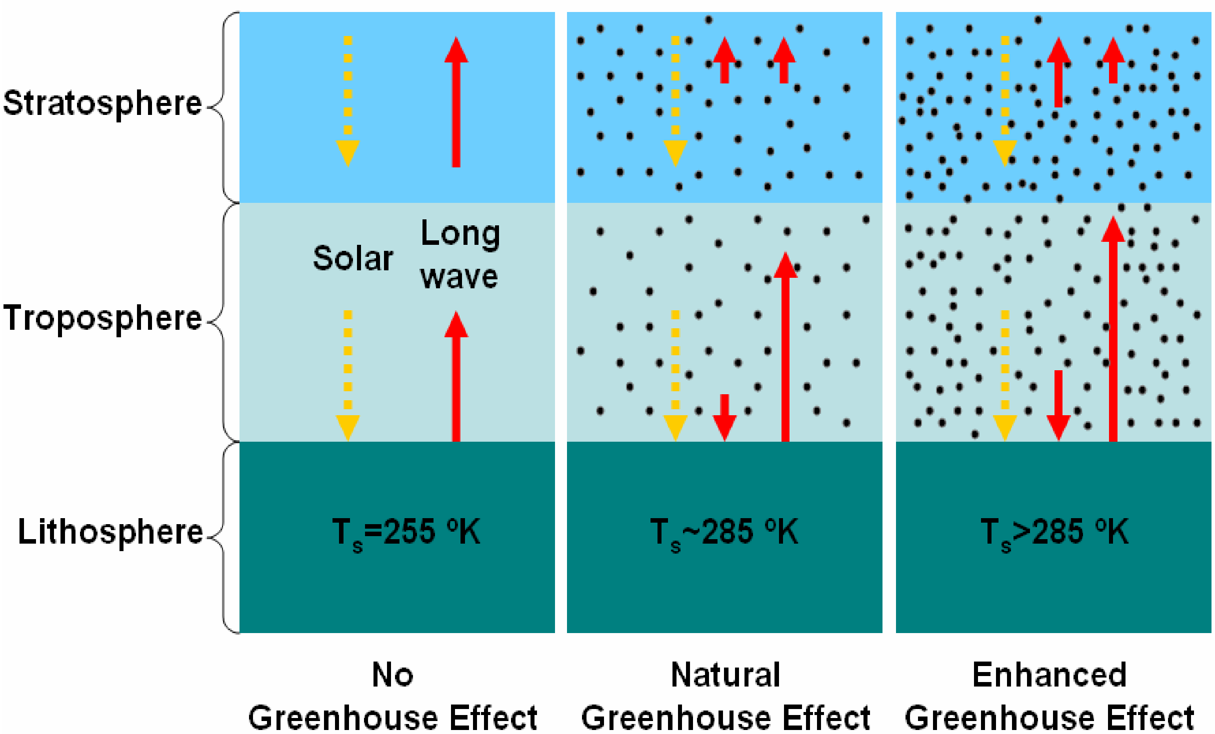

Figure 2.4 Enhanced greenhouse effects.
Taken from Commonwealth of Australia 2007, Bureau of Meteorology.

The Intergovernmental Panel on Climate Change (IPCC) concluded in 1995 that: "*the increased amount of carbon dioxide is leading to climate change, and will produce, on an average, a global warming of the Earth's surface because of its enhanced greenhouse effect* ...". The Fourth Assessment Report 2007 IPCC [32] established that it is very likely that global warming could be due to the observed increase in anthropogenic greenhouse gas concentrations.

Cloud properties

The study of cloud cover makes the analysis more aware of the dynamic nature of the atmosphere and may reveal clues to future weather investigation. Clouds are aggregates of tiny water droplets, ice crystal, or some combination of both. For example, ice crystal clouds occur at high altitudes where air temperatures and pressure are relatively low and they may have a fibrous or wispy appearance (Figure 2.5a). Water droplets clouds occur at low altitudes where temperatures are higher and their edges are more sharply defined (Figure 2.5b) [48].

Water vapor is an invisible component of air, but its condensation and deposition products (water droplets and ice crystal) are visible. A cloud is the visible product of condensation or deposition of water vapor within the atmosphere; it consists of an aggregate of minute water droplets and/or ice crystals suspended in the atmosphere. Clouds are composed of millions of water droplets that have condensed. These water droplets grow into larger droplets by colliding and coalescing with one another. Eventually, the droplets can grow large enough that they will not be able to stay suspended in the cloud. When this occurs, they fall out of the cloud as ***precipitation***. If the cloud's temperature is below freezing, it will contain ice crystals. Ice crystals collide and stick to other ice crystals and eventually fall from the cloud as snow. Precipitation is water, either liquid or solid, that falls from the atmosphere to the surface [51].

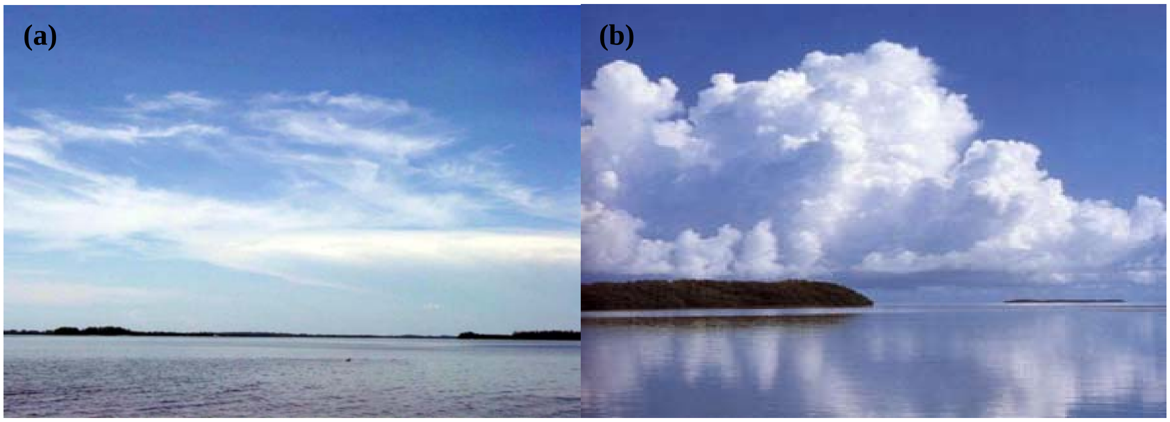

Figure 2.5 Types of clouds (a) High, thin cirrus appear fibrous because they are composed of mostly ice crystals, (b) Low, these are composed of water droplets and have sharply defined edges.

Clouds cover play an important role in the Earth's climate system by affecting the amount of heat – in the form of electromagnetic radiation – that is allowed to pass into or out of the system. Figure 2.6 depicts the relation of the cloud above incoming radiation and emitted heat. In general low, thick clouds tend to cool the Earth by reflecting the sun's radiation and preventing it from reaching the Earth's surface. In contrast, high, thin clouds tend to warm the planet by allowing solar radiation (called shortwave, SW) to pass easily through to the Earth's surface while, at the same time, trapping some of the Earth's infrared radiation (called longwave, LW) and radiating it back to the Earth surface [76]. The possibility that a given cloud will cause heating or cooling depends on several factors, such as the clouds height, its size, and the make-up of the particles that form the cloud. The balance between the cooling and warming actions of global cloud cover is very close; but in general cloud cover produces cooling on a global basis.

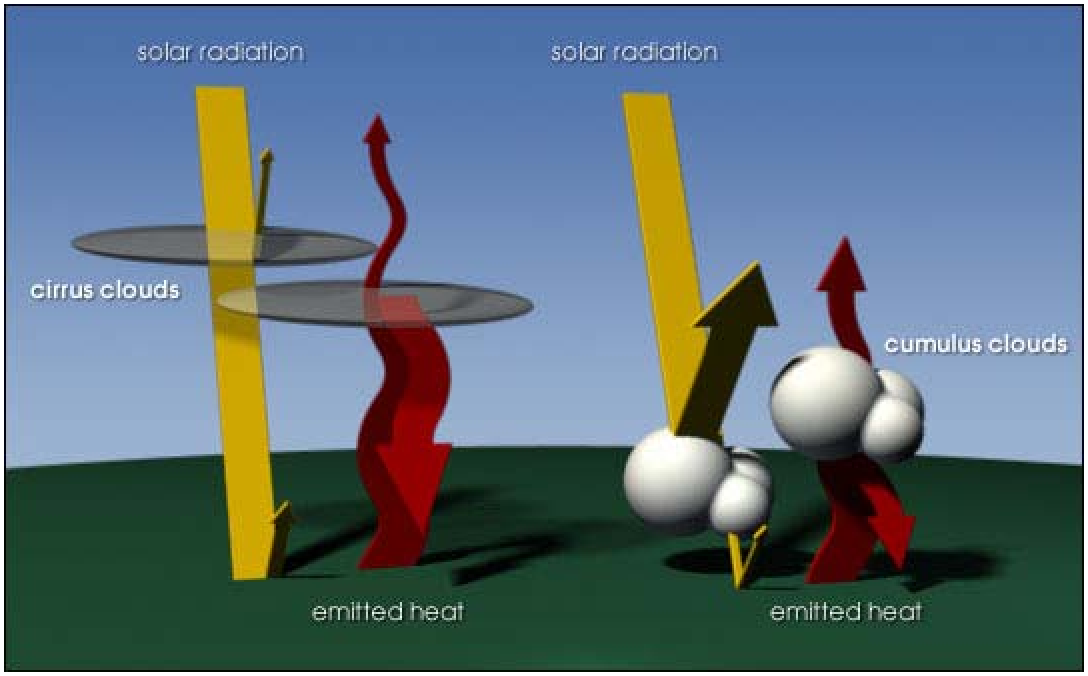

Figure 2.6 Effects of the clouds above incoming solar radiation and emitted heat.
Taken from Weier J. [76].

Sea level

The oceans cover about 70% of the Earth's surface, and through their fluid motions, high heat capacity, and ecosystems, they play a very important role in shaping the Earth's climate and its variability. Another major role of oceans in climate that has major impacts on multi-decadal time-scales is the sea level rise.

Sea level rise can be a product of global warming through two main processes: expansion of sea water as the oceans warm, and water exchange with continents as for example: melting of ice cover of Greenland, Antarctica and mountain glaciers, terrestrial water storage variations, etc. Global warming is predicted to cause a significant sea level rise over the course of the twenty-first century.

Figure 2.7 shows the change in annually averaged sea level at 23 geologically stable tide gauge sites with long-term records. The thick dark line is a three-year moving average of the instrumental records. This data indicates a sea level rise of 1.8 mm/year from 1900-2000. The problem with tide gauge records is the limited geographic coverage of these records, but satellite altimetry data from TOPEX/Poseidon since about 1992 are shown in red (Figure 2.7). It is increasing a rate of 3 mm/year of which 1.5 ±0.3 mm/year is found as product of thermosteric (from thermal expansion) sea level rise [40]. But to the last century, only 0.4 mm/year was a product of thermosteric (of the 1.8 mm/year observed sea level rise). For both time spans, the past few decades and the last decade, a contribution of 1.4 mm/year is not explained by thermal expansion, thus it needs to be of water mass origin [40].

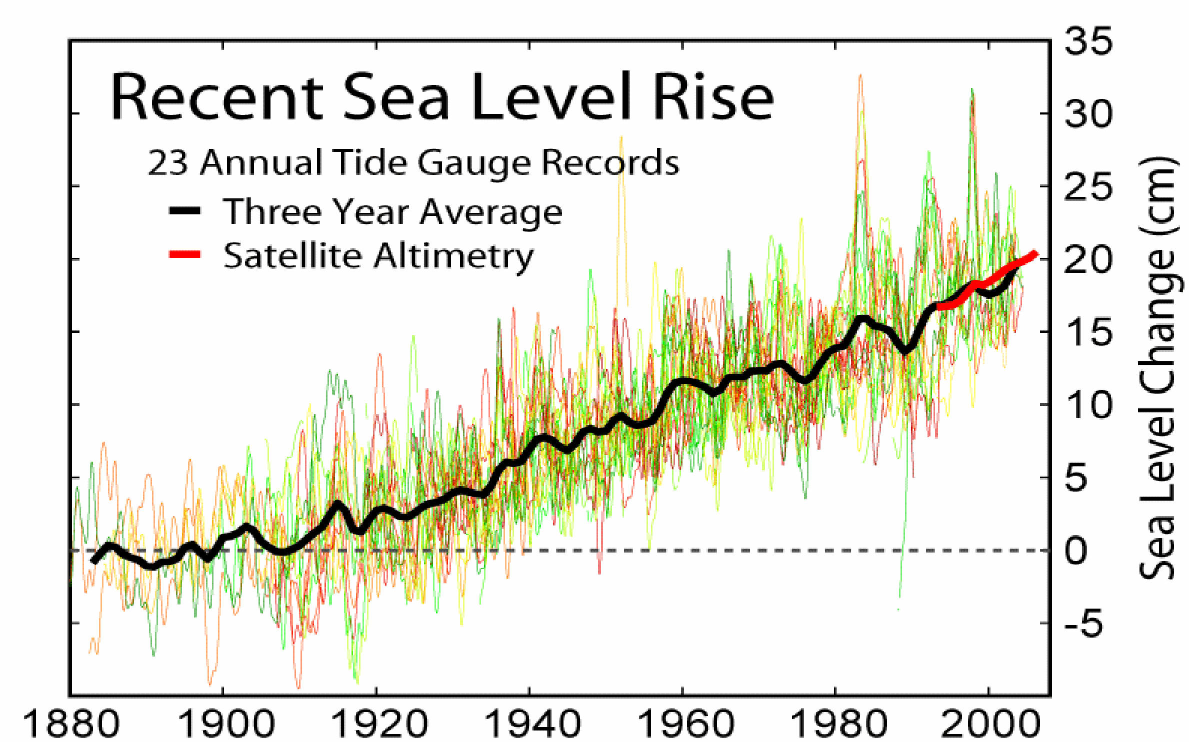

Figure 2.7 Recent Sea Level Rise about the last century
Taken from Earth System Science.

2.2 Statistical Tools

2.2.1 Time Series

A time series is a set of observations x_t, each one being recorded at equal time intervals t, many types of time series occur in the physical sciences, particularly in meteorology, marine science and geophysics. For example: rainfall, air temperature, relative humidity, sea level pressure, and wind speed. Most of these variables are measured at equal time intervals, which usually could be at every, hour, day, month, and year. Figure 2.8 shows the average carbon dioxide at Mauna Loa Observatory (Hawaii) in successive months over a 60 year period, approximately. Seasonal and tendency component can be clearly seen.

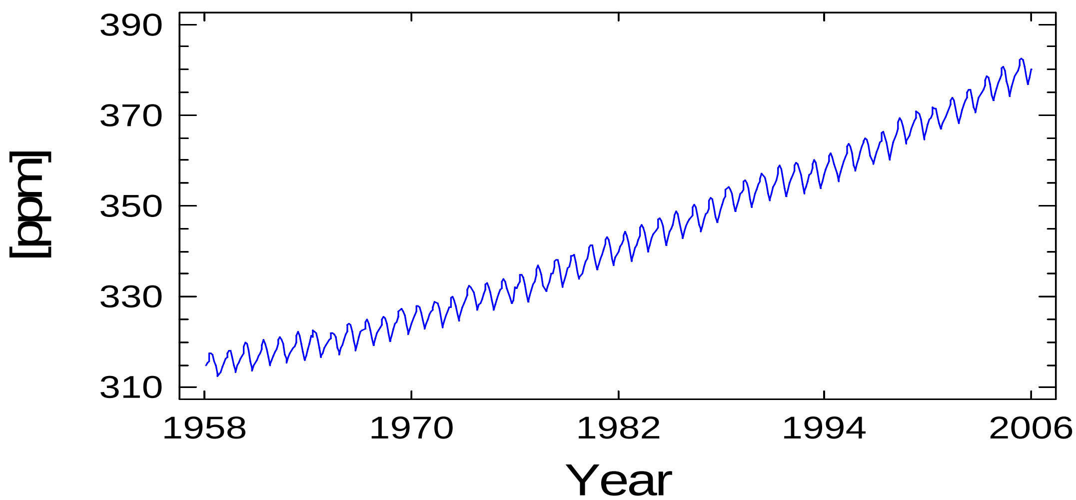

Figure 2.8 Monthly Carbon Dioxide Time Series (from 1958 until 2006)

Some data are taken in different manners: discrete or continuous. A discrete time series is one in which observations are taken only at specific times, for example, when observations are made at fixed time intervals. Continuous time series are obtained when observations are recorded continuously over some time interval, as in the Figure 2.8. The series studied in this investigation are continuous series in time, which will be called *time series*.

Box et. al [6] mentioned that is necessary to distinguish between *stochastic process* and the *time series*. Thus, a *time series* $z_1, z_2, ..., z_N$ of N successive observations is regarded as a sample realization from an infinite population of such time series that could have been generated by the stochastic process. *Stochastic process* is a statistical phenomenon that evolves in the time according to probabilistic laws is called a stochastic process. The time series to be analyzed may then be thought of as one particular realization, produced by the underlying probability mechanism, of the system under study. In other words, in analyzing a time series we regard it as a realization of a stochastic process. Hence, a stochastic process—or process—is a set of random variables $\{X_t\}$ ordered with respect to time t. And stochastic means random.

Estimation and elimination of trend and seasonal components

A time series typically has three major components: trend, periodicity and stochastic components. A practical tool to observe the components of a particular time series is to create a plot. The plot allows the analysis of time series to describe the data and to help in formulating a sensitive model. The plot will show up important components of the time series such as trend, seasonality, and the stochastic component in addition to the presence of possible outliers and discontinuities. The data can be represented as a realization of the process (the ***classical decomposition model***)

$$X_t = m_t + s_t + Y_t \qquad \textbf{2.1}$$

where m_t is a slowly changing function known as a ***trend component***, s_t is a function with known period *d* referred to as a ***seasonal component***, and Y_t is a ***stochastic*** component that is stationary (which will be explained later).

The objective of this study is to estimate and extract the deterministic component m_t and s_t in the hope that the residual or noise component Y_t will turn out to be a stationary time series. In this manner it is possible to use the theory of such processes to find a satisfactory probabilistic model for the process Y_t, to analyze its properties, and to use it in conjunction with m_t and s_t.

Another approach, developed extensively by Box and Jenkins [6], is to apply differencing operators repeatedly to the series $\{X_t\}$ until the differenced observations resemble a realization of some stationary time series $\{W_t\}$.

Definition: Classical Decomposition Model

$$X_t = m_t + s_t + Y_t,\ t = 1,\dots,n, \qquad \textbf{2.2}$$

Where $E(Y_t) = 0$, $s_{t+d} = s_t$, and $\sum_{j=1}^{d} s_j = 0$.

Elimination of the Trend Component

One technique to eliminate the trend can be to ***fit a parametric relationship***, the simplest type of trend is the familiar 'linear trend + noise', for which the observation at time t is a random variable m_t, given by

$$m_t = a + bt + e_t \qquad \textbf{2.3}$$

where a, b are constant and e_t denotes a random error term with zero mean. The mean level at time t is given by $E(m_t) = (a + bt)$; this is sometimes called 'the trend term'. Other writers prefer to describe the slope b as the trend, so that trend is the change in the mean level per unit time. Regression techniques are used to estimate the parameters a and b [10] and [8].

It can be obtained by using the minimums squares to estimate the new trend $\hat{m}_t$ (this technique is used in this work).

When there is not interest on trend parametric representation, the trend component can also be removed by using a difference operator. The use of ***difference operator*** is very practical and defined as the lag-1 difference operator ∇ by

$$\nabla X_t = X_t - X_{t-1} = (1 - B)X_t, \qquad \textbf{2.4}$$

where B is the backward shift operator,

$$BX_t = X_{t-1} \qquad \textbf{2.5}$$

Powers of the operator B and ∇ are defined in the obvious way, i.e., $B^j(X_t) = X_{t-j}$ and $\nabla^j(X_t) = \nabla(\nabla^{j-1}(X_t))$, $j \geq 1$, with $\nabla^0(X_t) = X_t$. Polynomials in B and ∇ are manipulated in precisely the same way as polynomial functions of real variables. For example,

$$\nabla^2 X_t = \nabla(\nabla(X_t) = (1 - B)(1 - B)X_t = (1 - 2B + B^2)X_t$$

$$= X_t - 2X_{t-1} + X_{t-2}$$

The principal problem with this technique is the reduction of the time series. For example, in the last exercise is shown the technique for a second order polynomial, then to resolve the equations is necessary that this series begins in the second time because there are 2 lags. Therefore, this series is reduced in two times and if series is of third order polynomial is reduced in three times, etc.

This is the reason, the difference operator is not used in our investigation, because the length of the series is reduced. Hence, the fitting of a parametric relationship is better.

Elimination of the Seasonal Component

First, it is required to determine the period d, which can be found by using the autocorrelation function and periodogram (both methods are used and explained in Chapter 4, section 4.13). There are three techniques to eliminate the seasonal component. The first technique is called ***block averaging***. The simplest way to remove seasonality is to average the observations at the same point in each repetition of the cycle (for example, for monthly data with $d = 12$, average all the January values) and subtract that average from the values at those respective points in the cycle, it is usually called ***climatology***. The second technique is to a fit a ***harmonic regression***, which uses sine and cosine functions to model the seasonal component,

$$s_t = A + B \cos\left(\frac{2.\pi.t}{d}\right) + C \sin\left(\frac{2.\pi.t}{d}\right) \qquad \textbf{2.6}$$

where the A, B and C are unknown parameters which will be estimated by using multiple regression techniques and d is the period.

The third technique is the ***seasonal differencing*** that eliminates the period of one times series in the same way that ordinary differencing will remove a polynomial trend.

$$\nabla_d X_t = X_t - X_{t-d} = (1 - B^d) X_t \qquad \textbf{2.7}$$

For example if $d = 12$,

$$\nabla_{12} X_t = X_t - X_{t-12} = (1 - B^{12}) X_t$$

Out of the three methods explained in this section, the harmonic regression is selected because it is a parametric method, because it does not decrease the length of the series and with the harmonic function can fit a periodic function regardless of the size of the period.

Stationary models, sample autocorrelation function and partial autocorrelation function

Once all the apparent deterministic components have been removed, we want to model the resulting residuals $\{Y_t\}$ as an ARMA model (the ARMA model will be defined in the following paragraphs). If there's no evidence of dependence among the residuals, they can be treated as independent and identically distributed (IID), which is the simplest model for time series, where there is no trend or seasonal component. But, we need to understand and to determine when a process is stationary or not.

Stationary Models

A time series $\{X_t, t = 0, \pm 1, ...\}$ is said to be stationary if it has statistical properties similar to those of the 'time-shifted' series $\{X_{t+h}, t = 0, \pm 1, ...\}$, for each integer h.

Definition:
Let $\{X_t\}$ be a time series with $E(X_t^2) < \infty$. The **mean function** of $\{X_t\}$ is defined as flows:

$$\mu_x(t) = E(X_t)$$

The **covariance function** of $\{X_t\}$ is given by the expression:

$$\gamma_x(r,s) = Cov(X_r, X_s) = E[(X_r - \mu_x(r))(X_s - \mu_x(s))]$$

for all integers r and s.

Definition:
$\{X_t\}$ is (**weakly**) **stationary** if

i. $\mu_x(t)$ is independent of t.

ii. $\gamma_x(t+h,t)$ is independent of t for each h.

Definition:
Let $\{X_t\}$ be a stationary time series. The **autocovariance function** (ACVF) of $\{X_t\}$ at lag h is written as follows:

$$\gamma_x(h) = Cov(X_{t+h}, X_t) = \gamma_x(t+h,t).$$

The **autocorrelation function** (ACF) of $\{X_t\}$ at lag h is

$$\rho_x(h) \equiv \frac{\gamma_x(h)}{\gamma_x(0)} = Cor(X_{t+h}, X_t).$$

Same examples to stationary process are:

i. First order moving average or MA (1) process
Consider the series defined by the equation

$$X_t = Z_t + \theta Z_{t-1}, \qquad t = 0, \pm 1, \ldots, \tag{2.8}$$

where $\{Z_t\} \sim WN(0,\sigma^2)$ and θ is a real value constant. So, from (2.8) we see that $E(X_t) = 0, \quad E(X_t^2) = \sigma^2(1+\theta^2) < \infty$, and

$$\gamma_x(t+h,t) = \begin{cases} \sigma^2(1+\theta^2), & \text{if } h = 0, \\ \sigma^2\theta, & \text{if } h = \pm 1, \\ 0, & \text{if } |h| > 1. \end{cases}$$

With this result, $\{X_t\}$ is stationary, because satisfied the definition. The autocorrelation function of $\{X_t\}$ is

$$\rho_x(h) = \begin{cases} 1, & \text{if } h = 0, \\ \theta/(1+\theta^2), & \text{if } h = \pm 1, \\ 0, & \text{if } |h| > 1. \end{cases}$$

If the MA process is of order *q*, the expression will be MA (*q*) and it is represented by following equation

$$X_t = Z_t + \theta_1 Z_{t-1} + \ldots + \theta_q Z_{t-q},$$

where $\{Z_t\} \sim WN(0,\sigma^2)$ and $\theta_1,\ldots,\theta_q$ are constants.

ii. First order autoregression or AR (1) process

Let us assume now that $\{X_t\}$ is a stationary series satisfying the equations

$$X_t = \phi X_{t-1} + Z_t, \qquad t = 0, \pm 1, \ldots, \qquad \textbf{2.9}$$

where $\{Z_t\} \sim WN(0,\sigma^2)$, $|\phi| < 1$, and Z_t is uncorrelated with X_s for each $s < t$. By taking expectations on each side of (2.9) and using the fact that $E(Z_t) = 0$, we see at once that

$$E(X_t) = 0$$

It follows from the linearity of the covariance function in each of its arguments and the fact that Z_t is uncorrelated with X_{t-1} that

$$\begin{aligned}\gamma_x(0) &= Cov(X_t, X_t) \\ &= Cov(\phi X_{t-1} + Z_t, \phi X_{t-1} + Z_t) \\ &= \phi^2 \gamma_x(0) + \sigma^2\end{aligned}$$

and hence that $\gamma_x(0) = \sigma^2 / (1-\phi^2)$.

And $\gamma_x(h)$ is defined by

$$\gamma_x(h) = \frac{\sigma^2 \phi^h}{(1-\phi^2)},$$

Observing that $\gamma(h) = \gamma(-h)$ and using definition of the autocorrelation function, one finds that

$$\rho_x(h) = \frac{\gamma_x(h)}{\gamma_x(0)} = \phi^{|h|}, \qquad h = 0, \pm 1, \ldots.$$

If the AR process is of order *p*, the expression will be AR (*p*) and it is represented by following equation

$$X_t = \phi_1 X_{t-1} + \ldots + \phi_p X_{t-p} + Z_t, \qquad t = 0, \pm 1, \ldots,$$

where $\{Z_t\} \sim WN(0, \sigma^2)$ and $\phi_1, \ldots, \phi_q$ are constants.

iii. Autoregressive moving average or ARMA (*p*, *q*) process

ARMA (p, q) is formed with the combination of AR (p) and MA (q), its equation is given by

$$X_t - \phi_1 X_{t-1} - \ldots - \phi_p X_{t-p} = Z_t + \theta_1 Z_{t-1} + \ldots + \theta_q Z_{t-q},$$

where $\{Z_t\} \sim WN(0, \sigma^2)$ and the polynomials $(1 - \phi_1 z - \ldots - \phi_q z^p)$ and $(1 + \theta_1 z + \ldots + \theta_q z^q)$ have no common factors.

Sample autocorrelation function

To assess the degree of dependence and to select a model for the data (See the Figure 2.9a), one of the important tools we use is the **sample autocorrelation function** (sample ACF) of the data. If we believe that data are real values of a stationary time series $\{X_t\}$, then the sample ACF will provide the information of $\{X_t\}$. For example, a sample ACF that is close to zero for all nonzero lags suggests that an appropriate model for the data might be a stationary process, Figure 2.9b.

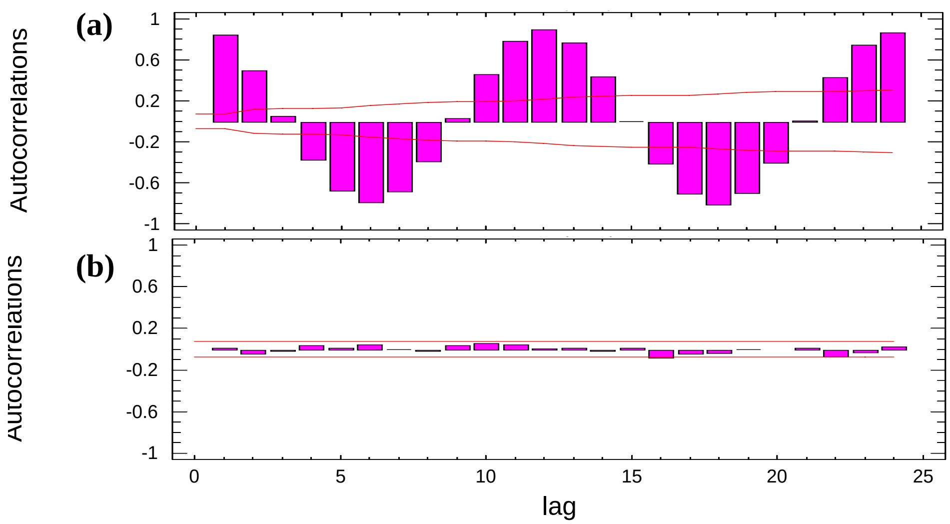

Figure 2.9 (a) shows the Sample Autocorrelation Function (SAF), this SAF shows that the series has a period of 12 and (b) Shows the SAF of stationary process, after eliminating the seasonal and trend component, and fitting a model ARMA. The data used in the figures is the monthly series of minimum air temperature in Puerto Rico from 1948 until 2005.

Definition:

Let $x_1,...,x_n$ be observations of a time series. The **sample mean** of $x_1,...,x_n$ is

$$\bar{x} = \frac{1}{n}\sum_{t=1}^{n} x_t$$

The **sample autocovariance function** is

$$\widehat{\gamma}(h) := n^{-1}\sum_{t=1}^{n-|h|}(x_{t+|h|}-\overline{x})(x_t-\overline{x}), \qquad -n < h < n$$

The **sample autocorrelation function** is

$$\widehat{\rho}(h) = \frac{\overline{\gamma}(h)}{\overline{\gamma}(0)}, \qquad -n < h < n$$

With sample ACF the sample autocorrelation coefficients $\rho_x(h)$ are plotted against the lags $h = 0,1,...,\mathrm{M}$, where M is usually smaller that N. For example if N=200, then the analysis may look at the first 20 or 30 coefficients (see the Figure 2.9). This tools is able to show whether the series is stationary or not, and the number of the period.

Partial autocorrelation function

In one time series can be present a correlation between X_t and X_{t-h}, where h is a specific lag, but it is possible to remove the intervening correlations by defining a partial autocorrelation function (PACF).

The partial autocorrelation coefficients are defined as the last coefficient of a partial autoregression equation of order h.

If $\{X_t\}$ is an ARMA (AutoRegressive Moving Average) process, the function $\alpha(\cdot)$ is defined by the equations

$$\alpha(0) = 1$$

and

$$\alpha(h) = \phi_{hh}, \quad h \geq 1,$$

where ϕ_{hh} is the last component of

$$\phi_h = \Gamma_h^{-1} \gamma_h, \tag{2.10}$$

$\Gamma_h = [\gamma(i-j)]_{i,j=1}^h$, and $\gamma_h = [\gamma(1), \gamma(2), ..., \gamma(h)]'$.

For any set of observations $\{x_1, ..., x_n\}$ with $x_i \neq x_j$ for some *i* and *j*, the sample PACF $\hat{\alpha}(h)$ is given by

$$\hat{\alpha}(0) = 1$$

and

$$\hat{\alpha}(h) = \hat{\phi}_{hh}, \quad h \geq 1,$$

where $\hat{\phi}_{hh}$ is the last component of

$$\hat{\phi}_h = \Gamma_h^{-1} \gamma_h, \tag{2.11}$$

Partial autocorrelations are useful in identifying the order of an autoregressive model. If the sample autocorrelation plot indicates that an AR model may be appropriate, then the sample partial autocorrelation plot is examined to help identify the order (see Figure 2.10). We look for the point on the plot where the partial autocorrelations essentially become zero. Placing a 95% confidence interval for statistical significance is helpful for this purpose.

Autoregressive Moving Average process or ARMA process

AutoRegressive Moving Average (ARMA) processes are an important class of time series to be generated by a linear aggregation of random shocks. They provide a flexible parametric structure to approximate the behavior of stationary processes, and lead to a prediction theory that is relatively simple and elegant.

The autoregressive process or AR Process

One of the most intuitive ways to model the behavior of a time series is to regress X_t on its past p values, say. The resulting model is called an AutoRegression of order p, or AR (p):

$$X_t = \phi_1 X_{t-1} + ... + \phi_p X_{t-p} + Z_t, \qquad \{Z_t\} \sim \text{WN}(0, \sigma^2) \qquad \textbf{2.12}$$

This is similar to linear regression, except that we are regressing the series on past values $X_{t-1}, ..., X_{t-p}$ of itself.

Defining the AR polynomial of AR (p) process

$$\phi(\text{z}) = 1 - \phi_1 \text{z} - ... - \phi_p \text{z}^\text{p} \qquad \textbf{2.13}$$

where z are the roots of the polynomial in the equation (2.13). Moreover, equation (2.12) can be represented with the backward shift operator B

$$\phi(\text{B}) X_t = Z_t$$

To ensure that a process $\{X_t\}$ satisfy the AR (p) equations is **stationary** and depends only on the past (is **causal**), all the roots of $\phi(z)$, equation (2.13), must be greater than 1 in magnitude ($\phi(\text{z}) = 0$ must lie outside the unit circle).

The moving average process or MA Process

Analogously to the AR, the Moving Average of order q, MA (q), regresses X_t on lagged values of the WN process, $\{Z_t\}$

$$X_t = Z_t + \theta_1 Z_{t-1} + ... + \theta_q Z_{q-1}, \qquad \{Z_t\} \sim \text{WN}(0, \quad \sigma^2) \quad \textbf{2.14}$$

Similar to the AR (p) process, the definition of MA polynomial is

$$\theta(\mathrm{z}) = 1 - \theta_1 \mathrm{z} - ... - \theta_q \mathrm{z}^{\mathrm{q}} \qquad \textbf{2.15}$$

It can be easily shown that MA (q) processes are always **stationary**, given that the parameters of any finite MA (q) processes always verify the conditions of $E(X_t) = 0$ and $E(X_t^2) < \infty$. For parameter **identifiability** reasons, and in analogy with the concept of causality for AR processes, we require that all roots of $\phi(z)$ be greater than 1 in magnitude. The resulting process is said to be **invertible**.

The autoregressive moving average process or ARMA Process

We can put an AR (p) and an MA (q) process together to form the more general ARMA (p,q) process

$$X_t - \phi_1 X_{t-1} - ... - \phi_p X_{t-p} = Z_t + \theta_1 Z_{t-1} + ... + \theta_q Z_{q-1},$$

where $\{Z_t\} \sim \text{WN}(0, \sigma^2)$. And using the compact AR & MA polynomial notation, we can write the ARMA (p, q) as

$$\phi(\mathrm{B}) X_t = \theta(B) Z_t,$$

which can also be written as

$$X_t = \frac{1 + \theta_1 B + \theta_2 B^2 + ... + \theta_q B^q}{\phi_1 B - \phi_2 B^2 - ... - \phi_p B^p} Z_t \qquad \textbf{2.16}$$

so, $\phi(\mathrm{z})$ and $\theta(\mathrm{z})$ have no common factors.

In ARMA (p, q) it is necessary that the series must be causal and invertible. It is required as before, that all roots of $\phi(z)$ and $\theta(z)$ must be greater than 1 in magnitude. In addition, AR and MA process are special cases: an AR (p) = ARMA (p, 0), and an MA (q) = ARMA (0, q).

Figure 2.10 shows several process of ARMA model, making it easy to identify different models with the help of ACF and PACF graphic. As mentioned above and before, an Autoregressive model is easy to identify when it is plotted in a PACF graphic, for example Figure 2.10a is an ARMA (1, 0), because the first lag is the larger than the 95% confidence limits, shown as parallel horizontal lines. The Moving Average model is easy to classify when it is plotted in a ACF graphic, for example Figure 2.10b is ARMA (0, 1), because the first lag is the larger than the 95% confidence level. The Figure 2.10c correspond an ARMA (1, 2) model; to identify this model it is required a significant experience in recognizing the patterns of the ACF and PACF functions.

2.2.2 The Exponential Weighted Moving Average (EWMA) control chart

Exponentially Weighted Moving Average (EWMA) is a statistical tool that can be used to detect small changes in the mean of a given process. The EWMA test was adopted because it is an efficient test to detect a small shift in the mean (0.5 to 2 times the standard deviations) and also because it is robust test in the senses that it is not affected by moderate deviations from the Gaussian process and because it is not affected by weakly auto-correlated time series [55]. Cumulative sum (CUSUM) test can also be used to detect climate change. Since the implementation EWMA is easier than the CUSUM and detection results are about the same, the EWMA test is recommended. An excellent discussion of the implementation of these tests can be found in Montgomery [47].

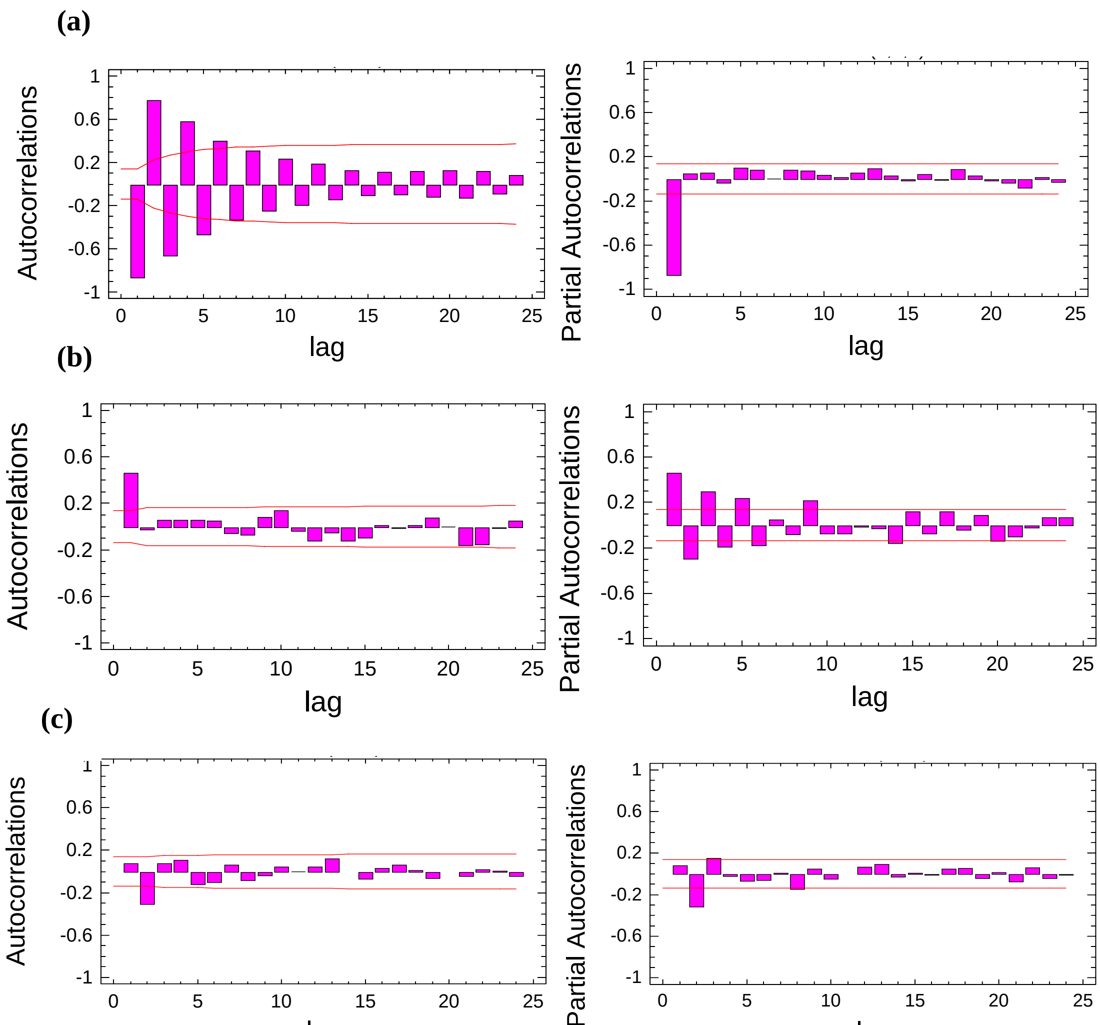

Figure 2.10 Simulation of (a) AutoRegressive model with p=1, ARMA (1, 0), (b) Moving Average model with q=1, ARMA (0, 1), and (c) AutoRegressive Moving Average model with p=1 and q=2, ARMA (1, 2).

EWMA control chart for monitoring the process mean

The EWMA control chart was proposed in 1959 by Roberts [60]. The Exponentially Weighted Moving Average is defined as follows [47]:

$$z_i = \lambda x_i + (1 - \lambda) z_{i-1} \qquad \textbf{2.17}$$

where x_i is the actual observations at time i, z_i is the weighted average of the process, and lambda is constant in range of $0 < \lambda \leq 1$. It is recommended to initialize equation 2.17 with

$$z_0 = \mu_0$$

Ussually, the average of preliminary data is used as the starting value of the EWMA, that is $z_0 = \bar{x}$.

It should be noted that z_i is a weighted average of all previous sample means, we may substitute for z_{i-1} on the right hand side of the equation (2.16) to obtain

$$\begin{aligned} z_i &= \lambda x_i + (1 - \lambda)[\lambda x_{i-1} + (1 - \lambda) z_{i-2}] \\ &= \lambda x_i + \lambda (1 - \lambda) x_{i-1} + (1 - \lambda)^2 z_{i-2} \end{aligned}$$

Continuing to substitute recursively for z_{i-1}, j = 2, 3, ..., t , we obtain

$$z_i = \lambda \sum_{j=0}^{i-1} (1 - \lambda)^j x_{i-j} + (1 - \lambda)^i z_0 \qquad \textbf{2.18}$$

The weights $\lambda(1-\lambda)^j$ decrease geometrically with the age of the sample mean. Furthermore, the weights sum to unity, since

$$\lambda \sum_{j=0}^{i-1} (1 - \lambda)^j = \lambda \left[\frac{1 - (1 - \lambda)^i}{1 - (1 - \lambda)} \right] = 1 - (1 - \lambda)^i$$

If the observations x_i are independent random variables with variance σ^2, then the variance of z_i is

$$\sigma_{z_i}^2 = \sigma^2\left(\frac{\lambda}{2-\lambda}\right)[1-(1-\lambda)^{2i}] \quad \mathbf{2.19}$$

Therefore, the EWMA control chart would be constructed by plotting z_i versus the sample number i (or time). The center line and control limits for the EWMA control charts are expressed in the chapter 5.

EWMA control chart with autocorrelated process data

Standard control charts require that observations come from an independent process and follows a normally distribution with mean μ and standard deviation σ. A point that falls outside of the control limits indicates the presence of an abnormal behavior. If the underlying process is a climate indicator, then a point the falls outside of the control limits may indicated a possible climate change. The EWMA control chart usually detects changes in the mean of the process and the magnitude of the change is usually given in terms of the variability of the process.

The most important assumptions made concerning the control charts is about the independence of the observations. For conventional control charts it does not work well if the quality characteristic exhibits even low levels of autocorrelation. Specifically, these control charts will give misleading results in form of too many false alarms if the data are autocorrelated. Therefore, the control chart will indicate a process has shifted when in reality the process has NOT been shifted (a false alarm).

Unfortunately, the assumption of uncorrelated or independent observations is not even approximately satisfied in several processed data. For example the series studied in the concurrent thesis as: temperature, sunspot, carbon dioxide, sea level and cloud cover where consecutive measurements on process characteristics were often highly autocorrelated. Therefore, these time series should not be analyzed by using the conventional technique of control chart. Thus, the suggested approach to analyze autocorrelated data is described in chapter 5.

3 NUMERICAL PHYSICAL MODEL

At the present chapter is developed the basic concepts of an atmospheric model, the different scales to which any simulation could be fitted. This depends on the physical phenomenon that is desired to study. The analysis will be made in the Caribbean region and then a mesoscale model must be selected as RAMS.

This chapter is in relation with the statistical analysis, because depending of the statistical result that shown the studied variables, RAMS is simulated in the same date where the changes is detected. Then, it will be explained if there are any relation between the statistical result and the atmospheric variables in the selected region. In addition, the configuration and basic concept of RAMS are presented to simulate the selected date.

3.1 Atmospheric Models and Modeling Local-Scale Meteorology

3.1.1 Atmospheric Models

A scientific model is an approximate representation or simulation of real system. A system could be the atmospheric components that interact between them and that are described by fundamental physics principles. The models can provide important insights about how the variables interact among them, or they may allow to understand and to predict the behavior of complex phenomena. Depending on their particular function, scientific models are classified as conceptual, graphical, physical, or numerical.

A conceptual model is an abstract idea that represents some fundamental law or relationship. While, a graphical model compiles and displays data in format that readily conveys meaning. The physical model is a miniaturized representation of some system.

Currently atmospheric scientists usually depend on numerical models rather than physical models for investigating the atmosphere, weather and climate. A numerical model consists of one or more mathematical equations that describe the relationship among variables of a system. Numerical models are usually programmed in a computer that can process and storing enormous quantities of data and perform calculations with high speed.

3.1.2 Modeling Local-Scale Meteorology

The atmosphere is considered as continuous fluid flow and it is studied using fluid mechanics law for external flow, thermodynamic properties, transport phenomena among others. In order to analyze specific phenomena, the atmospheric circulation is divided in different spatial and temporal scale, Moran [48]. The large-scale wind belts encircling the planet (polar easterlies, midlatitude westerlies, and trade winds) are global or planetary-scale systems. Synoptic-scale systems comprise continental or oceanic events, cyclones migrating, hurricanes and air mass advection. Mesoscale systems consist of thunderstorm, sea and lake breezes, and small circulation systems able to influence the weather in only a portion of a large city or county. A weather system covering a very small area (e.g. a weak tornado) corresponds to the smallest spatial subdivision of atmospheric motion, microscale systems [51] (see TABLE 3.1).

TABLE 3.1 Scales of Atmospheric Circulation.

Circulation	Space Scale	Time Scale
Planetary scale	10,000 to 40,000 Km	Weeks to months
Synoptic scale	100 to 10,000 Km	Days to week
Mesoscale	1 to 100 Km	Hours to day
Microscale	1 m to 1 Km	Seconds to hour

Patterns in the planetary-scale circulation may persist for weeks or even months. Synoptic-scale systems typically have a life from several days to weeks. Mesoscale systems usually complete their life cycles in hours and in same case in a day, whereas microscale systems might persist for minutes or less. Vertical wind speeds may be comparable in magnitude to horizontal wind speeds and Coriolis effect is neglected in mesoscale and microscale events. Synoptic and planetary scales have as characteristic that horizontal winds are considerably stronger than vertical motions and the Coriolis effect play a important role.

Small scale weather system depends of larger scale atmospheric motion. For instance, extreme nocturnal radiational cooling requires a synoptic weather pattern that favors clear skies and light or calm winds. At microscale, theses weather conditions may be accompanied by formation of frost or radiation fog in a river valley.

3.2 Mesoscale atmospheric model

3.2.1 RAMS History

The Regional Atmospheric Model System (RAMS) is a mesoscale model highly versatile developed for simulating and forecasting regional phenomena. The numerical model uses the full set of the primitive non-hydrostatic compressible fluid dynamic equations along with the thermodynamic and continuity equation of the water vapor, liquid and ice hydrometeor mixing ratios [1], [13].

RAMS was developed at Colorado State University (CSU) and by scientists of the *ASTeR division of Mission Research Corporation. Currently RAMS is being developed by the Atmospheric, Meteorological, and Environmental Technology (ATMET). Colorado State University and Mission Research Corporation (MRC) developed the Regional Atmospheric Model System in the 1980s.

3.2.2 General Model Structure of the Computational Process

The RAMS procedure for pre-processing and post processing is showed in Figure 3.1.The input is divided in two major components. The first component is the transient data (1a, 1b, 1c) and the second component to the non-transient data (2a, 2b, 2c and 2d). The spatial data introduced in the model are vegetation type (LAND, 2a), sea surface temperature (SST, 2b), terrain height (TOPO, 2c) and miscellaneous (MISC, 2d). Miscellaneous comprises the soil type, soil surface roughness length, soil temperature, vegetation temperature and vegetation moisture (input for Land Ecosystem Atmosphere Feedback version2 (LEAF2) submodel). Although the sea surface temperature is transient data, observational data has revealed slowly changes and for three consecutive days it remains almost constant. On the other hand, the transient data at 2.5 degree of resolution corresponds to the pressure level: air temperature, zonal and meridional wind, geopotential height and relative humidity, provided by National Center of Environmental Prediction (NCEP, 1c).

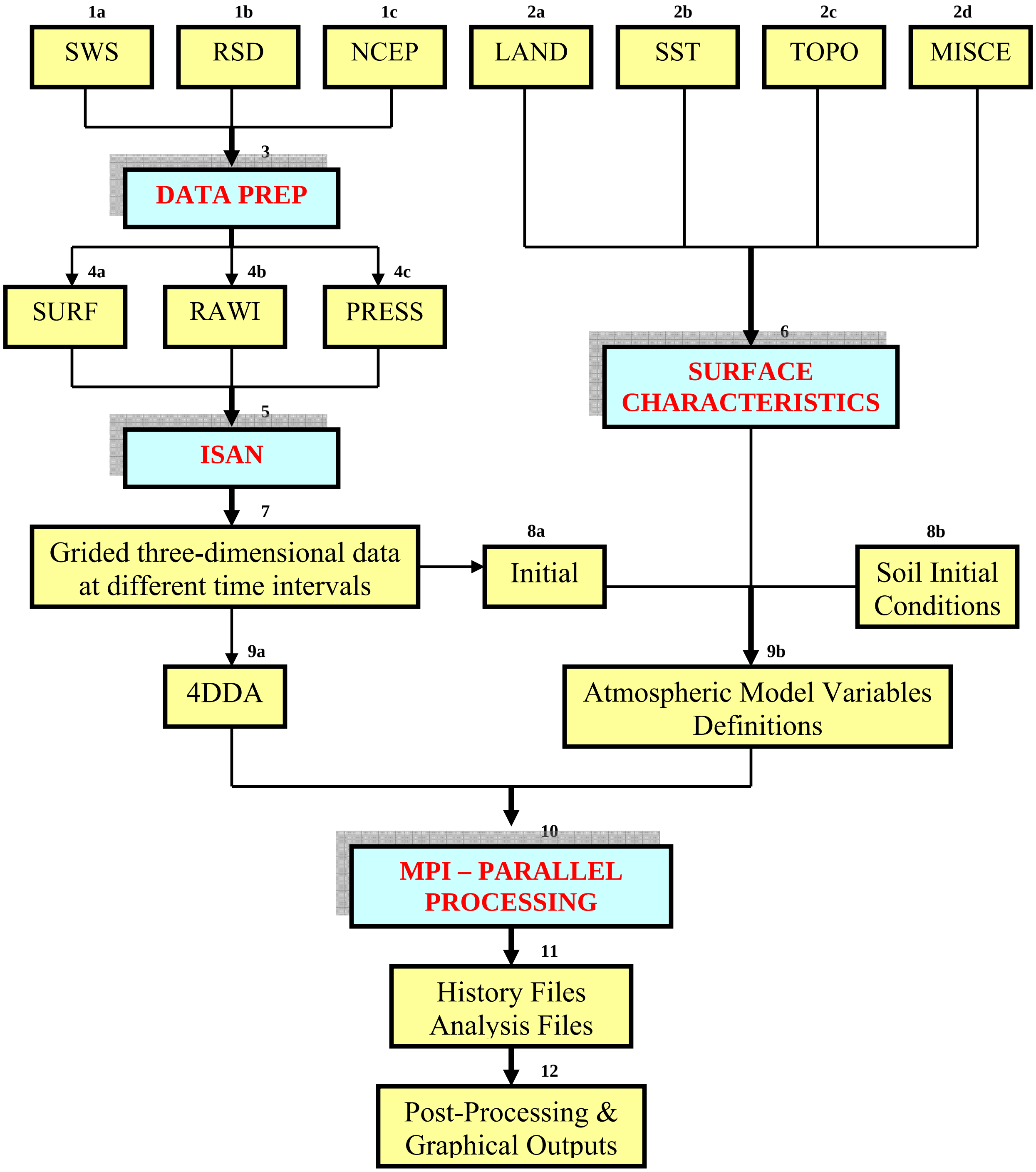

Figure 3.1 General Model Structure Flow Diagram of the Computational Process.

This data can be combined with other transient observational data such as COOP surface weather stations (SWS, 1a) and radiosondes data (RSD, 1b). The pre-processing input data can be divided in three basics steps. The first step consists in read GRIB file containing the NCEP reanalysis data and turn on in RALPH2 format. This pre-processing is performed by the code called DATa PREP (3). The second step allows us to process the surface data and located in the mesh grid made during the ISAN (5) process. The thermo-mechanical properties and conditions of the soil are very important to initialize the model. This non-transient input is pre-processed in the Surface Characteristics step. The third, and last step, identified as ISAN (5) performs the four-dimensional mesh grid, place it over a specific area of the earth and process all atmospheric and surface data, locating them over each grid point. The resultant gridded fields are used by the model as initial fields and boundary conditions. In addition, the time-dependent fields could be used for the Newton relaxation scheme (4D Data Assimilation, 9a). The Computational Parallel Processing (MPI, 10) was designed for distributed memory computer architectures and it uses the method of domain decomposition. The final output is a set of “analysis and history files” that contains all results of the prognostic numerical solutions. The post-processing routine is the RAMS Evaluation and Visualization Utility (REVU), which generates several gridded fields in GRADS, VI5D, among others. In addition, REVU can display atmospheric fields using NCAR GRAPHICS tools [71], [74].

3.2.3 Physical and Numerical Options

RAMS, is a numerical tool that solves the coupled quasi-Boussinesq nonhydrostatic equations set. The regional model is able to have a better representation of the topography and microphysics, which are very important in the sub-grid scale phenomena. RAMS has a nesting grid scheme which solves simultaneously the prognostic equations. RAMS needs to specify the grid size and geographic locations of the nested grids to be able to solve these equations; in addition the cloud microphysics, radiation, among other physical features are solved by means of parameterizations. RAMS usually uses the six-hour NCEP reanalysis data as an initial and variable lateral boundary conditions (4DDA). The boundary conditions (BC) along with the kind of turbulent mixing parameterization to solve the closure problem of the turbulence need to be specified.

High vertical resolution near the ground is necessary to study mesoscale phenomena into the boundary layer and to consider the strong influence of the topography and convective development. The horizontal and vertical mesh has a nested grid where the coarse resolution corresponds to the parent grid (PG), while the nested grid (NG) to the finer resolution.

The nudging technique is a type of four-dimensional data assimilation (4DDA) scheme, and through this process the model solutions are nudged toward the observed conditions. In addition, the non-homogeneous initialization options use the nudging condition for the top model as absorbing layer. On the other hand, RAMS computes surface layer fluxes of heat, momentum, and water vapor from the land to the atmosphere (surface layer parameterization). The grid cells of RAMS have three different surfaces, water, bare soil, and vegetated surface.

For the water surfaces, in the surface layer parameterization the temperature is held constant over time, but spatially variable, while the moisture values are defined as the saturation mixing ratio at the surface pressure and water temperature. For bare soil, RAMS uses the multi-layer soil model, which considers a finite depth soil/atmosphere interface layer. The soil surface temperature and the mixing ratio on the ground surface are calculated using prognostic equations in LEAF2 sub-model. The vegetation surface and the effective moisture vegetation are computed in RAMS through the big-leaf approach, where prognostic equations are solved [1].

4 DATA ACQUISITION

Five data sets were studied in this research. Two data sets are associated with possible causes of climate change, which are called attribution variables and three climate indicators. The attribution variables are the solar radiation and CO_2 emissions. The data climate indicators are surface temperature, sea level and cloud cover.

4.1 Attribution variables

Attribution is the identification of causes that are responsible of generating climate changes over the Earth. Meehl et al. [42], used global climate model to reconstruct the historical temperature record. In this model, he incorporated the effects of five predetermined forcing factors: greenhouse gases, man-made sulfate emissions, solar variability, ozone changes (both stratospheric and tropospheric), and volcanic emissions (including natural sulfates). He concluded that the signature of globally averaged temperature during time in the twentieth century is a direct consequence of the sum of the forcings factors.

The predetermined forcing factors are important if we would like to understand the phenomena occurring in a recent climate change event.

One of the typical limitations is the lack of historical data records. This study is based on observed sunspots and carbon dioxide (as one of the fundamental components of greenhouse gases).

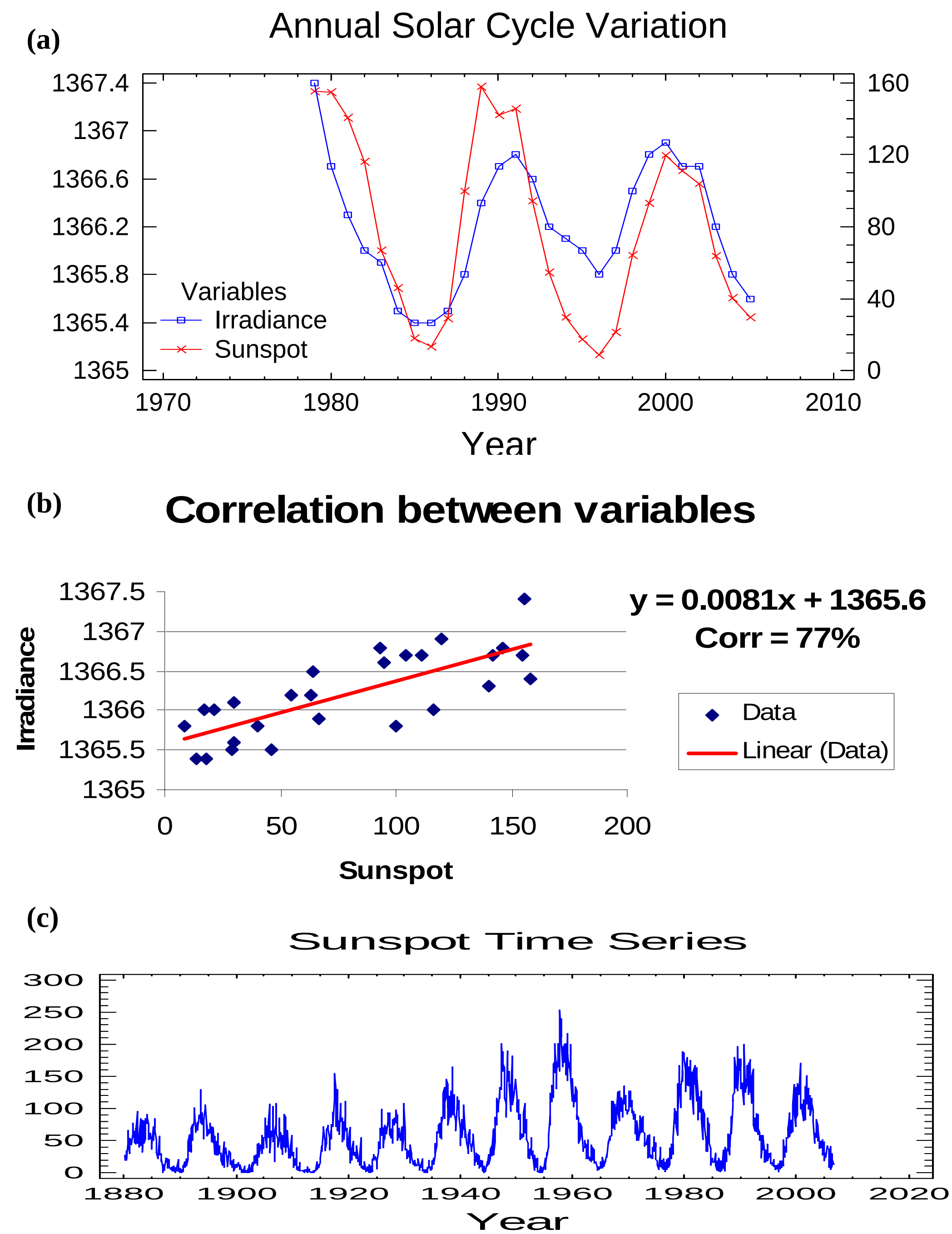

Figure 4.1 Solar behavior, (a) Annual Irradiance and Sunspot Time Series from 1979 – 2005, (b) Correlation between Annual Irradiance and Sunspot Time Series, and (c) Monthly Sunspot Time Series (1880 - 2005).

4.1.1 Sunspots

The Earth is continuously receiving the radiation from the sun and, consequently any changes, even small ones, can have widespread effects on climate change such as the Earth surface temperature [36]. Sun emits approximately 1365 W/m^2*year which delivers, a globally averaged, 341 W/m^2 to Earth. Satellite data has been used to prove that solar radiation can be measured by studying the behavior of sunspots. Figure 4.1.a shows the observed sunspot and solar irradiance during the period 1979-2005, while Figure 4.1.b shows that there is 77% correlation between irradiance solar and sunspot. Then the solar activity can be studied by analyzing the behavior of sunspots.

Sunspots are dark holes in the sun creating larger increment of sun brightness in the surrounding areas, and the overall effect is the more sunspots the more solar radiation. The time series of sunspots was obtained from the Royal Observatory of Belgium (http://sidc.oma.be/sunspot-data/). The selected period dates from Jan 1880 until Aug 2006 (see Figure 4.1.c). This period was selected because the available global air surface time series contained exactly this period. Using the periodogram, to monthly data, a period of approximately 138 months which is equal 11.5 years was found. This time series shows 12 periods along the total time series.

4.1.2 Carbon Dioxide

The carbon dioxide time series was obtained from Mauna Loa station Hawaii. This data set includes the period from Jan 1958 – Aug 2006. Figure 2.8 shows the behavior of the CO_2. This data constitute the longest continuous record of CO_2 concentrations available in the world. This climate indicator is considered as one of the most favorable locations for measuring undisturbed air because the local influences of vegetation and human activities are minimal over CO_2 concentrations. It should be noted that the volcanic events are excluded from the records [35]. The CO_2 time series was obtained from the following web site: http://cdiac.ornl.gov/ftp/trends /co2/maunaloa.co2.

4.2 Climate indicators

In the recent report IPCC 2007 [32], it was reported that eleven of the last twelve years (1995 -2006) were the 12 warmest years in the instrumental record of global surface temperature (since 1850). The cryosphere – Earth's frozen water on land, in the soil and on top of the ocean – is also changing rapidly in response to a warming planet [20], thus, at most, of the order of 5–10% of the planetary energy imbalance went into melting of ice. The calculated sea level rise is mainly due to thermal expansion of ocean water, and secondarily to melting alpine glaciers [24]. The thermal expansion is a reaction of the warming of the ocean; the upper layers of the ocean are storing enormous amounts of additional heat from the atmosphere and this is a consequence of the reaction of the variability of Earth's heat balance [39].

Solar forcing is spatially heterogeneous (i.e., acting most strongly in areas where sunlight reaches the surface) while GHG forcing is more spatially uniform. Thus over relatively cloud-free oceanic regions, the enhanced solar forcing produces greater evaporation [42]. Therefore, the cloud cover is an important factor relation in the world climate.

4.2.1 Global Surface Temperature

The global surface temperatures were provided by the Goddard Institute for Space Studies (GISS) [25]. The anomalies of global surface temperature data were acquired from the web site http://data.giss.nasa.gov/gistemp/. Figure 4.2.a shows the anomalies of the global land surface temperature. Figure 4.2.b shows the anomalies of land and ocean surface temperature, and Figure 4.2.c shows the land surface temperature over the North Hemisphere. These data sets include the period from Jan 1880 to Aug 2006.

The surface data set was developed based on the Global Historical Climatology Network (GHCN), and the development and analysis of this data set was described by Hansen et. al [25].

4.2.2 Caribbean Air Temperature

Air temperatures for the major Caribbean islands (Cuba (CU), Jamaica (JA), Puerto Rico (PR), and La Espanola, which includes Dominican Republic (DR) and Haiti (HA)) were obtained from GHCN 2, available at http://www.ncdc.noaa.gov/oa/climate/ghcn-monthly/index.php. PR is the Caribbean island with a large amount of meteorological stations, and has 14 stations that belong to GHCN, and 39 additional stations that are administered by the National Weather Services (COOP stations, http://www.dnr.state.sc.us/pls/cirrus/cirrus.login) and makes a total of 53 stations. APPENDIX B shows the location of the Caribbean stations. TABLE 4.1 depicts all the available stations used in this work. The monthly air temperature includes the period from 1948 to 2006.

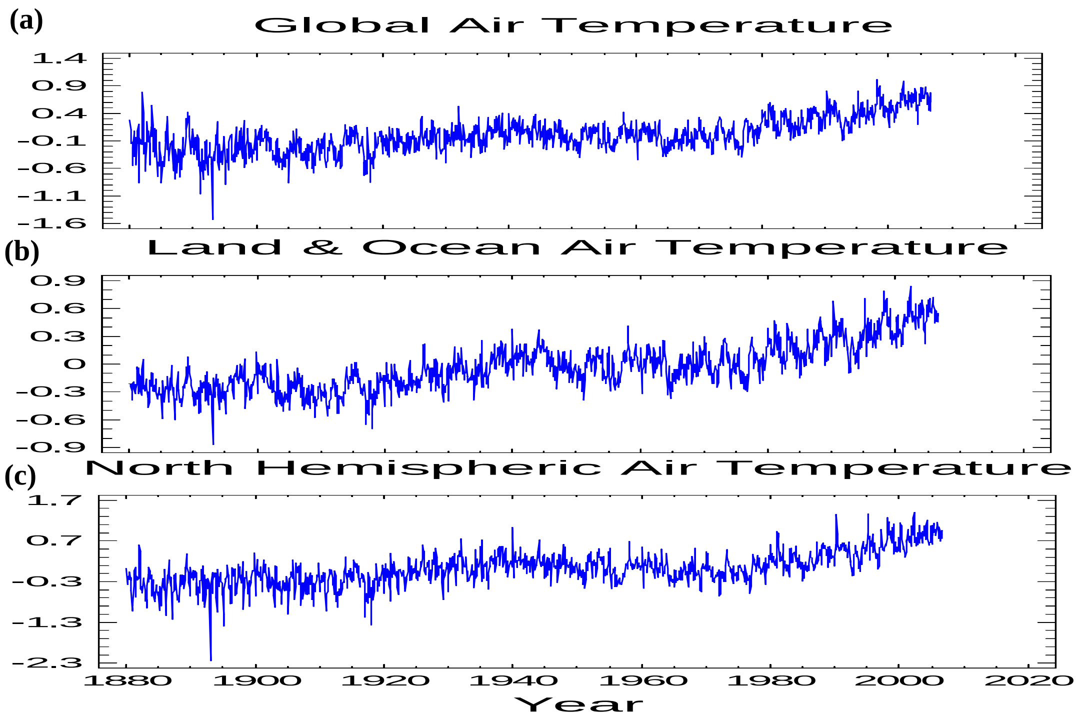

Figure 4.2 Anomalies of the surface temperature, (a) global land surface temperature, (b) global land and ocean surface temperature, and (c) north hemispheric land surface temperature.

TABLE 4.1 The number of stations in the Caribbean area.

Country	**Cuba**	**Dominican Republic**	**Haiti**	**Jamaica**	**Puerto Rico**
Number of stations	14	28	1	5	53

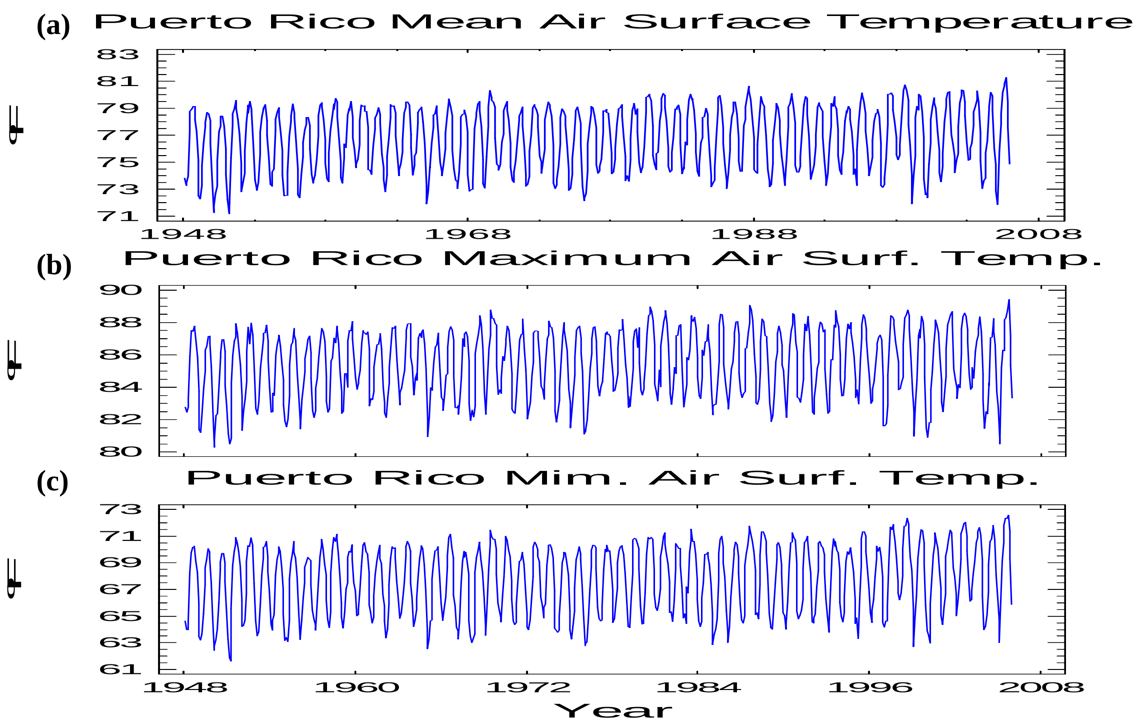

Figure 4.3 Monthly air temperature (AT) of Puerto Rico from Jan 1948 until Dec 2005, (a) The mean AT was obtained from 53 stations data, (b) The maximum AT was calculated from 42 stations, and (c) The minimum AT was computed from 42 stations. This data was extracted from COOP and GHCN 2 stations.

Figure 4.3 shows the monthly average, maximum and minimum monthly air temperature corresponding to PR. Figure 4.4 shows the mean air temperatures of CU based on 14 stations, and maximum and minimum air temperature for Guantanamo station - CU. Figure 4.5 illustrates the air temperature corresponding to DR, HA, and JA.

The surface air temperature of the NCEP/NCAR reanalysis data were used as a proxy variable to estimate some of the missing values that were encountered in the mean, maximum or minimum air surface temperature from the stations. The nearest grid points to each island were used to derive a regression equation between the observed air temperature by the stations and the NCEP temperature (minimum at 6 GMT (Greenwich-Mean-Time), maximum at 18 GMT and mean as the average of 0, 6, 12 and 18 GMT). The regression equations exhibit a correlation of 0.92 on average (See Appendix C).

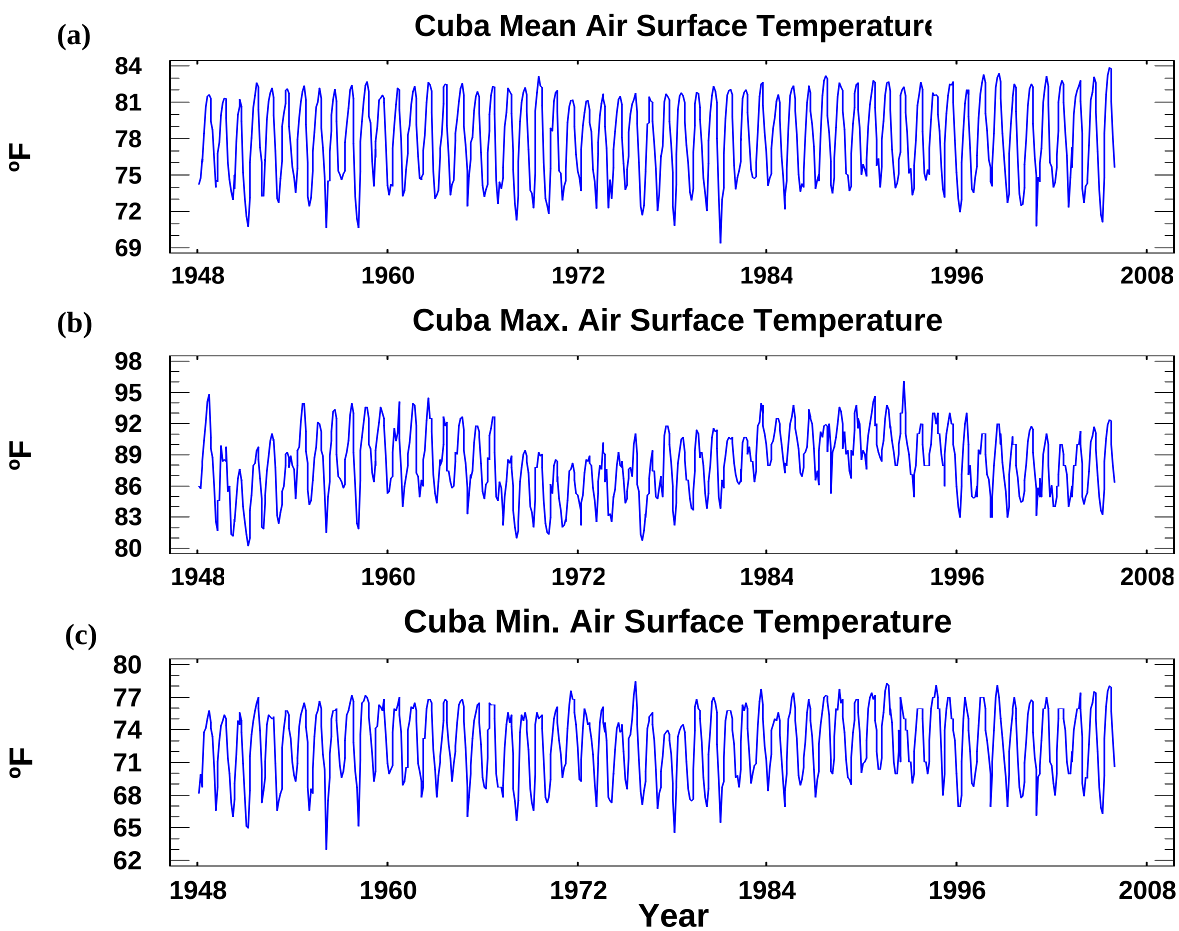

Figure 4.4 The average AT for Cuba from Jan 1948 until Dec 2005, (a) The mean AT was computed from 14 stations, (b) the maximum AT for Guantanamo station, and (c) the minimum AT for Guantanamo station. Figures (b) and (c) are based on one station data. Data included in (a), (b) and (c) were was extracted from GHCN 2.

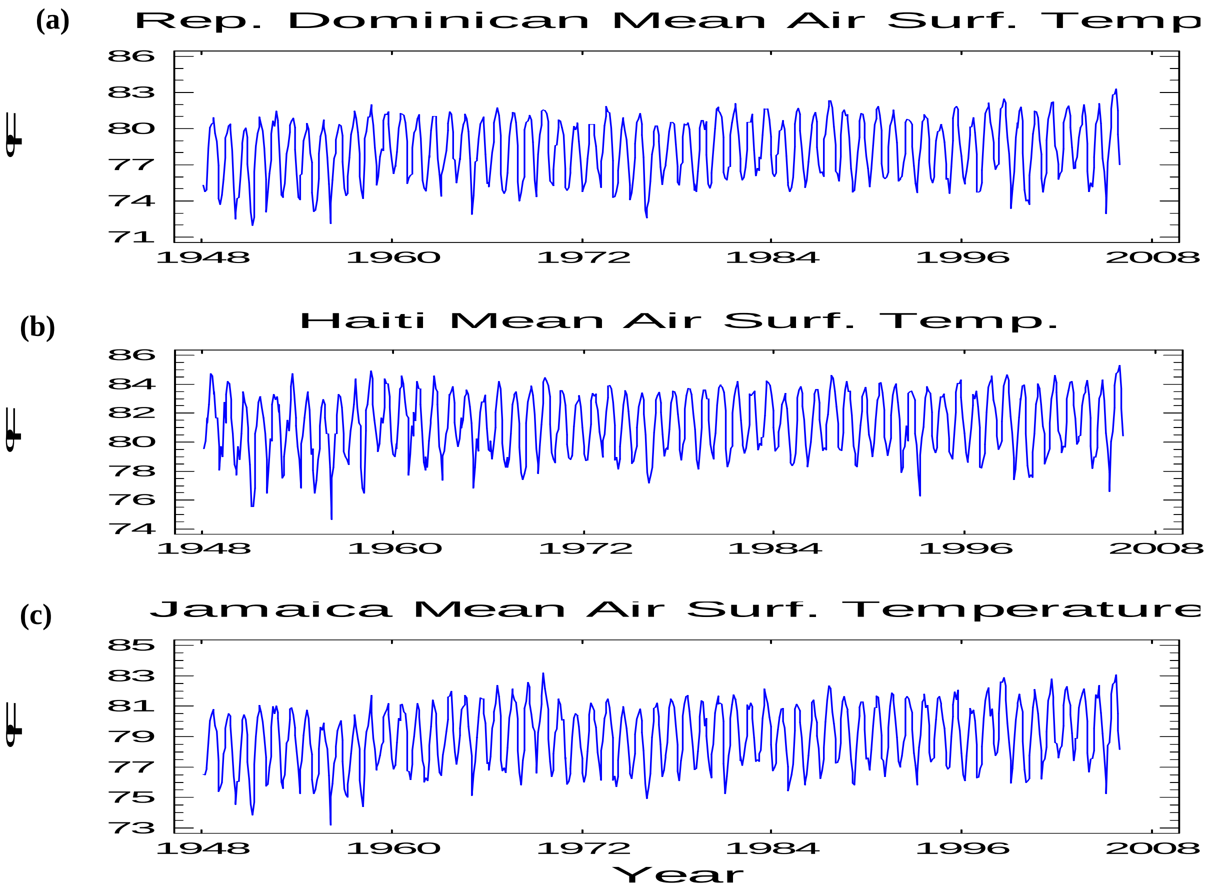

Figure 4.5 The average AT from Jan 1948 until Dec 2005, (a) The average AT for Dominican Republic was computed with 28 stations, (b) The average AT for Haiti was based on a single station, and (c) the average AT was computed from 5 stations. These data were extracted from GHCN 2.

4.2.3 Global and Caribbean Cloud Cover

The cloud cover monthly time series was obtained from the International Satellite Cloud Climatology Project (ISCCP). The D2 product provides the properties of the clouds observed at every three hours and presented in monthly time series during the period from July 1983 to June 2005. Some of the included variables in this data set are: cloud cover, top-cloud temperature, top-cloud pressure, optical thickness, and water path [62], [56]. The clouds are classified based on optical thickness and top pressure. The cloud products were generated from sensors located on 7 satellites. More information can be found in the following web site: http://iridl.ldeo.columbia.edu/SOURCES/.NASA/.ISCCP/.D2/. Quispe [54] developed a user friendly computer program to read and manage the cloud data files.

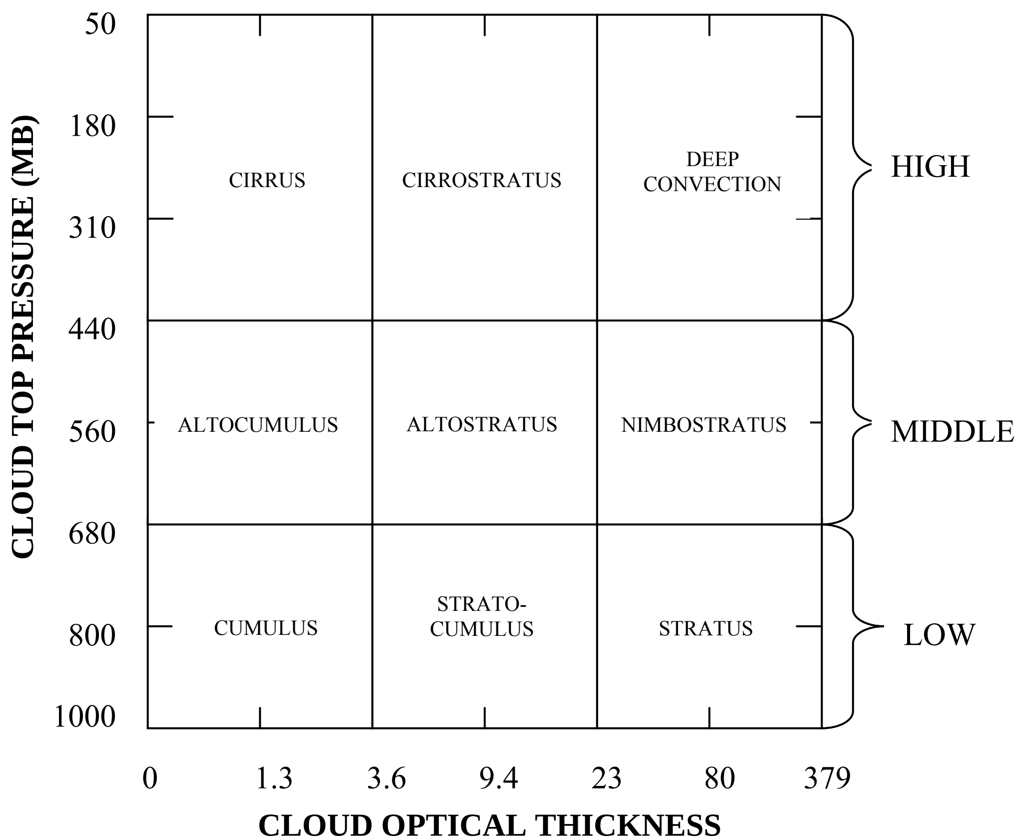

Figure 4.6 ISCCP Cloud Classification.

The global cloud cover file includes 6,596 grids and the cloud cover was obtained for each type of cloud according to its elevation: low, middle, and high (see Figure 4.6). The Caribbean area includes the following geographical location: latitude from 17N to 24N and longitude from 87W to 64W. Figure 4.7 shows the average Global and Caribbean cloud cover, from July 1983 until June 2005.

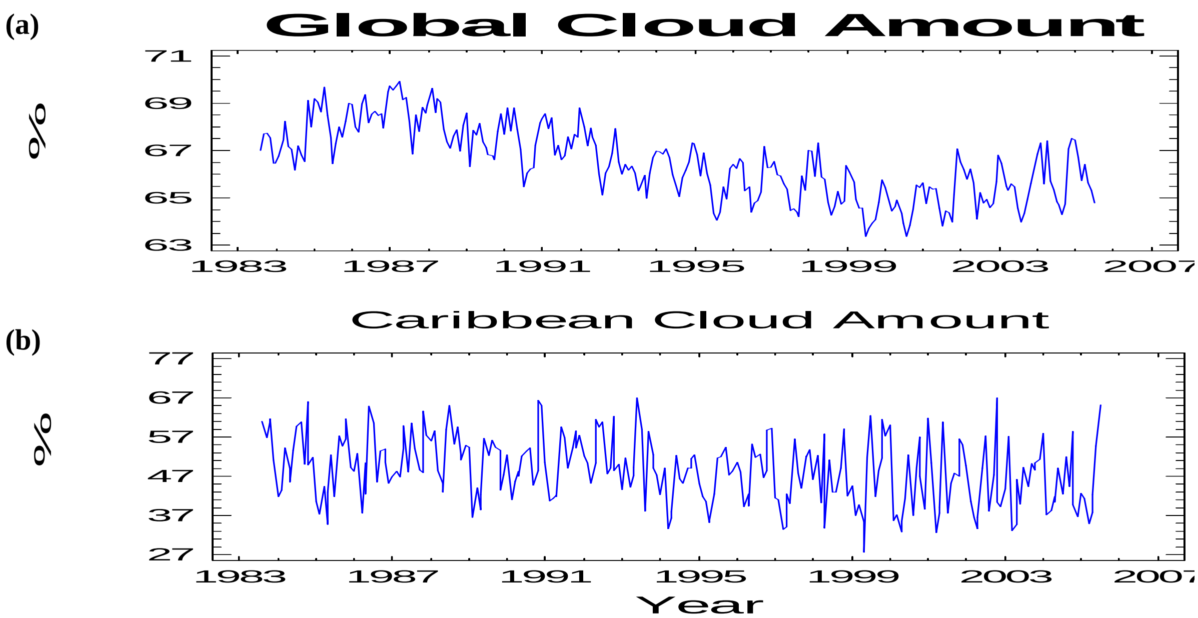

Figure 4.7 The average cloud amount from July 1983 until June 2005, (a) Global and (b) Caribbean. These data were extracted from ISCCP D2.

4.2.4 Global and Caribbean Sea Level

The sea level data set were obtained from two satellites Topex and Jason. Leuliette et al [37] show the calibration, procedure, technique and validation of this data. This data set is used as reference to several works about the sea level [12], [38], [45] and indirect relations with the ocean [41]. The global data includes monthly observations from 1992 to 2005 and the Caribbean data covers only from 1992 to 2002. The data can be obtained from the following web site: http://sealevel.colorado.edu/results.Php. Figure 4.8 shows the global and Caribbean sea level measured in mm.

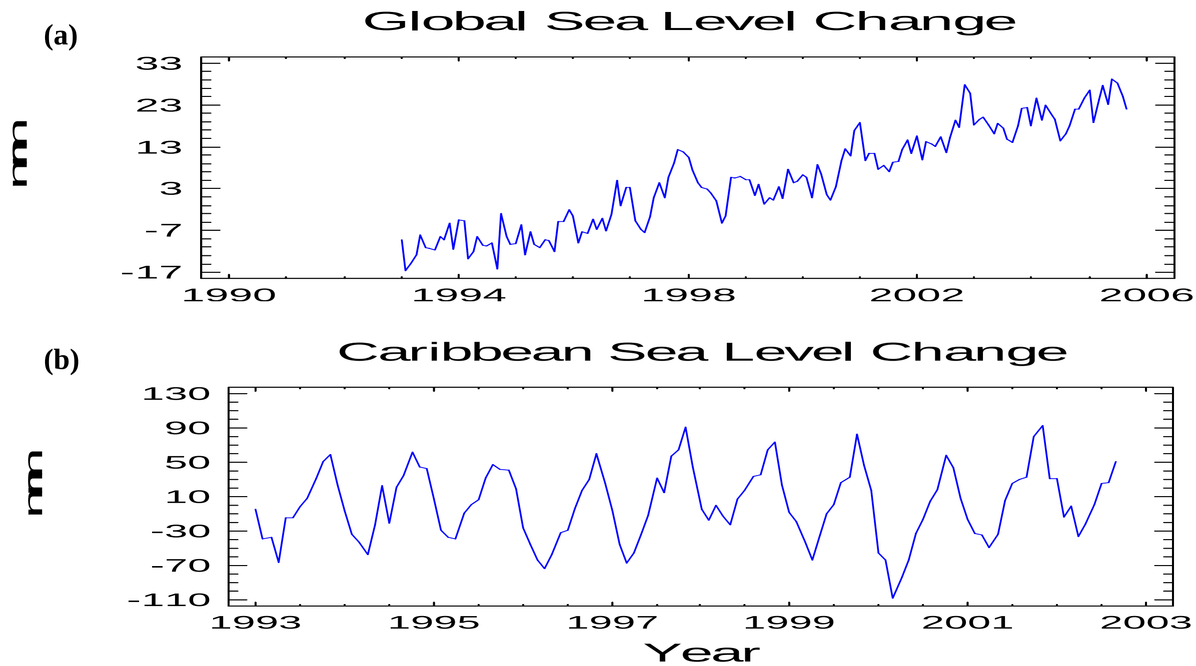

Figure 4.8 The average of sea level, (a) Global from Dec 1992 until Aug 2005. (b) Caribbean from Dec/1992 until Aug/2002. This data set was obtained from Topex/Jason.

5 METHODOLOGY

The present chapter describes the methodology used in this investigation which contains two sections. The first section describes the procedure of the statistical tools used in the technique of detection of climate changes. In addition simulation details are presented. The second section focuses on demonstrating the methodology used to analyze the impact of the climate change in the local area. The election of the year without effects of the El Niño or La Niña event is explained. Moreover, mesoscale model called RAMS is used to analyze the impact of the climate change in the local area. RAMS configuration is also described in this section too.

5.1 Methodology of Climate Change Detection

5.1.1 Climate change detection test

A climate indicator is a time series which exhibits three major components: trend, period, and stochastic component. A climate change is defined as any change that can occur either on the trend, the period or the stochastic component of the underlying climate indicator. This thesis deals only with climate changes that are exhibited on the stochastic component. The proposed detection algorithm consists of removing trend, periodicity, and the autocorrelation structure of a climate indicator and determines whether or not the mean of the process changes over time (see Figure 5.1). The algorithm consists of determining when the process changes from being a stationary to nonstationary stage and includes five major steps [56].

Step 1: Sequence of a climate indicator

It is assumed that climate properties of a given part of the world are expressed by a sequence of climate indicators. A climate indicator can be expressed as a time series of air temperature, sea level, pressure, etc. It is required that the selected time series has no missing values and it has at equal time intervals. It is desirable that the time series will be large enough to identify the autocorrelation structure and leave a significant part of the series in the testing side. The minimum length of the time sequence must be at least 50 observations.

Step 2: Compute anomalies

Each time series is processed by deleting the tendency and seasonal component. The procedure employed to remove the tendency component is computed using the Eq. (2.3) and to eliminate the seasonal component with the Eq. (2.6), where regression techniques are used to determine if each coefficient *a, b, …, A, B, C,…*is significant or not, to the respective equation. Coefficients are estimated using conventional statistical software, for instance: Stat Graphics, mintab, SAS, etc.

Step 3: Identifying the Auto-Regressive Moving Average (ARMA) model

Most of the climate indicators and meteorological variables are a sequence of autocorrelated time series. For instance, the anomalies of air temperature, sea level pressure, sun radiation, CO_2, and cloud cover are autocorrelated processes and can be represented by an ARMA model. The time series will be tested first to determine whether or not it is an autocorrelated or a white noise process. If the underlying process is a white noise the ARMA model is not required. On the other hand, if the series is autocorrelated, it will be used to identify an

ARMA model. It should be noted that the series must be a stationary process. Stationary in the sense that the mean and the autocorrelation function will not change over time. This assumption is satisfied because the climate with internal natural variability will exhibit a process with constant mean and autocorrelation function independent of time. The main purpose of identifying an ARMA model is to remove the autocorrelation structure. The identification of an ARMA model can be easily accomplished by using the methodology described in Chapter 2.

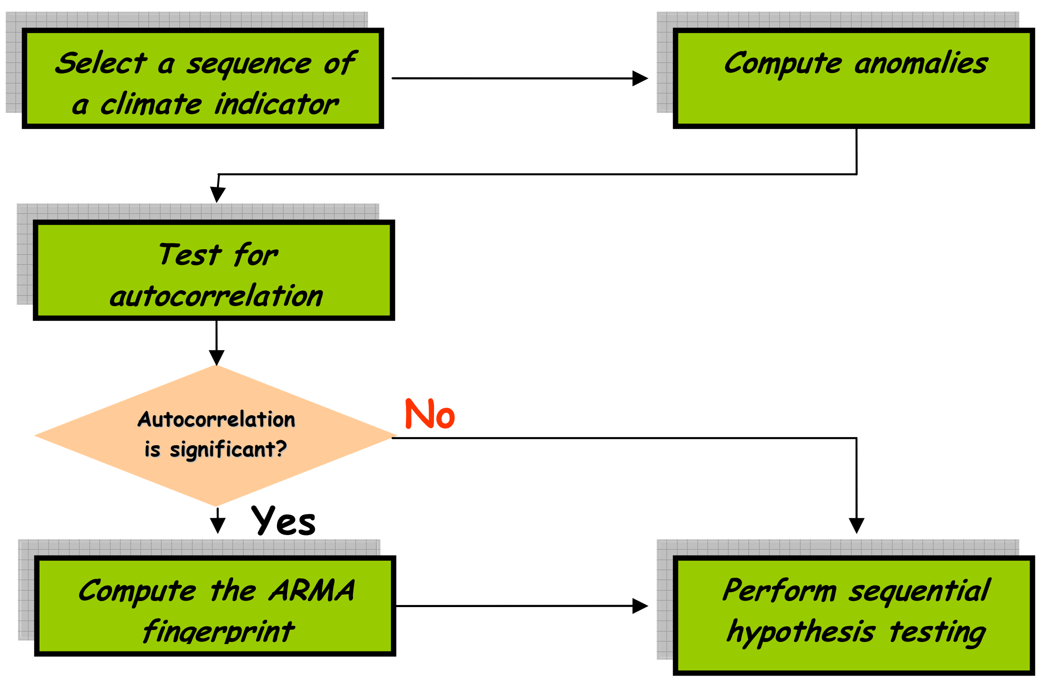

Figure 5.1 Flowchart showing the statistical methodology employed.

Several statistical softwares are available to perform an automatic identification of the ARMA model: for instance: Statgraphics, ITMS2000 and Econometric. Another alternative is to use Matlab 7.0 which includes the system identification toolbox that provides an excellent tool to identify the ARMA model. A typical representation of an ARMA model is shown in the Eq. (2.16).

Step 4: Computing the ARMA fingerprint

The time series will be divided into two parts. The first part will be called the baseline and the second part will be called the testing part. The baseline will be used as a reference point to measure the change with respect to the baseline. The baseline will be located on the left and the testing part on the right hand side of the series. Typically, the baseline may be located at the beginning of the series; however, it could be placed in almost any part of the series as long as enough testing observations are available. The testing part will be at least 20 observations and will be used to measure whether or not there exists a significant change with respect to the baseline.

It should be noted that the change detection test may be relative and may depend on the selected baseline. The baseline and the testing sequence can be expressed as follows:

Baseline sequence: X_t for $t = 1,2,\cdots,m$

Testing sequence: X_t for $t = m+1, m+2,\cdots,n$

For $m \geq 30$ and $n - m \geq 20$

where X_t represents the anomalies of the underlying climate indicator at time t; m is the sample size of the baseline, and n is the total number of available observations of the climate indicator.

The ARMA fingerprint is the sequence created by the difference at each point in time between the estimated from the ARMA model and the observed value.

The ARMA fingerprint can be computed as follows:

$$f_t = X_t - \hat{X}_t \quad \text{for } t = 1, 2, ..., \text{ n} \qquad \textbf{5.1}$$

$$\hat{X}_t = \frac{1 + \hat{\theta}_1 B + \hat{\theta}_2 B^2 + \cdots + \hat{\theta}_q B^q}{\hat{\phi}_1 B - \hat{\phi}_2 B^2 + \cdots + \hat{\phi}_p B^p} \hat{Z}_t \qquad \textbf{5.2}$$

where f_t is the ARMA fingerprint; $\hat{Z}_t$ are the residuals for the baseline sequence; $\hat{\theta}$'s and $\hat{\phi}$'s are the parameter estimates that must be computed with the baseline sequence and must maintained unchanged for $t = 1,2,\cdots,n$. Convenient software to perform this calculation is Matlab 7.0.

Thus, if no change has occurred in the underlying process then the fingerprint will reduce to residual values $\left(f_t = \hat{Z}_t\right)$, and will behave as a white noise sequence. However, if the process exhibits a significant change, the ARMA model will show a unique characteristic which will be exhibited either in the mean or in the autocovariance function of the given sequence and this special sequence will be called the ARMA fingerprint. When a significant change occurs in the mean of the process, the ARMA fingerprint will also exhibit a significant change in the mean. On the other hand, when change occurs in the second moment of the process, the fingerprint will exhibit significant change in the autocorrelation function [56].

Step 5: Sequential Hypothesis Testing

If the climate indicator is driven by external forces, its ARMA fingerprint will present a trend in the mean or a significant change in the autocorrelation structure. Thus to detect these changes two sequential tests are needed. Since the climate changes are represented by a small variation either in the mean or in the autocovariance, the tests must be very sensitive. In addition since the decision of the hypothesis testing is at each point in time, the exponentially weighted moving average (EWMA) is adopted to detect the climate change [47].

The exponential weighted moving average test is described by the Eq. (2.17), and modified as follows:

$$z_t = \lambda f_t + (1 - \lambda) z_{t-1} \qquad \textbf{5.3}$$

Therefore, f_t is the ARMA fingerprint at time t, μ and σ are the mean and the standard deviation of the baseline sequence of f_t for t=1,2,…,m; z_t is the exponentially weighted moving average of the fingerprint, and the initial value of z_t can be estimated by averaging the fingerprint during the baseline (t=1,2,…,m).

The control limits for the EWMA control charts are upper control limit (UCL) and lower control limit (LCL). These are described by

$$UCL = z_0 + L\sigma\sqrt{\left(\frac{\lambda}{2-\lambda}\right)[1-(1-\lambda)^{2t}]} \qquad \textbf{5.4}$$

Center line = z_0

$$LCL = z_0 - L\sigma\sqrt{\left(\frac{\lambda}{2-\lambda}\right)[1-(1-\lambda)^{2t}]} \qquad \textbf{5.5}$$

Montgomery [47] discussed the λ and L values by mentioning that the values of λ could change from 0.05 to 0.25; being λ= 0.05, λ= 0.10 and λ= 0.20 the most popular choices. Moreover mentioned that L = 3 (the usual three-sigma limits) works reasonably well, particularly with the larger value of λ, for example λ=0.20. However, the software used in our work StatGraphic uses $L = 3$ and $\lambda = 0.2$ in its confirmation in the EWMA analysis. Therefore, the values proposed by the analysis are: $L = 3$ and $\lambda = 0.2$.

In relation to the Eq. (5.4), a significant increment occurs in the mean at time t under the condition: $z_t > UCL_t$; and the Eq. (5.5) produces a significant decrement in the mean at time t if $z_t < LCL_t$.

5.1.2 Simulation for the Statistical Test

Monte Carlo simulation technique is used to determine if there is enough evidence to declare a change in a synthetic time series. The simulations were applied to 4 cases: i) by step, ii) pulse, iii) tendency and iv) tendency plus pulse; the procedure was applied to each time series as shown in Figure 5.1.

The simulated time series represents the monthly time series from January 1880 until December 2005 with 1512 points. These series may have the two (seasonal and stochastic component) or 3 components (seasonal, tendency and stochastic component) of any time series (Equation 2.1).

i. By Step

A time series was simulated with a period equal to 12, an ARMA (1, 2) model and with a step change was input at the beginning of year 1970 and size of the change was 1 standard deviation (see Figure 5.2). The periodogram, the ACF and the PACF of the simulated time series are shown in Figure 5.4. These tools affirm that the series has a seasonal component, specially the Figure 5.4.a, with a period equal to 12 (the bigger ordinate is in the frequency equal to 0.0833 and the period is equal to 1/0.0833 = 12). Figure 5.4.b and Figure 5.4.c show that this series has a period component and probably an ARMA model, but it is necessary to eliminate the seasonal component first.

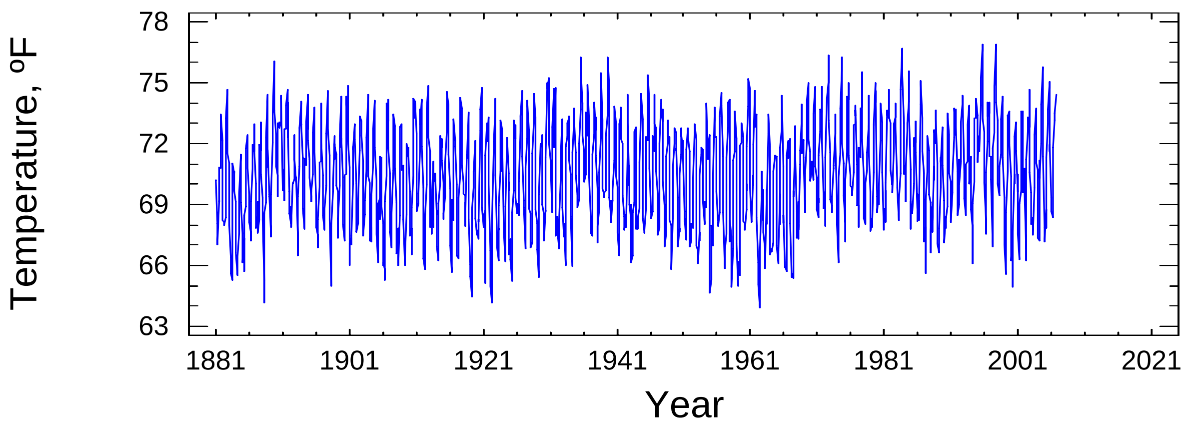

Figure 5.2 Simulated time series with a seasonal component equal to 12, ARMA (1, 2) model and a step of 1 unit in the standard deviation beginning in year 1970.

To remove the seasonal component it is required to build a sinusoidal function Eq. (2.6). A multiple regression analysis is used to estimate the parameters.

$$s_t = A + B\cos\left(\frac{2.\pi.t}{d}\right) + C\sin\left(\frac{2.\pi.t}{d}\right)$$

Parameter estimation results are presented in TABLE 5.1

TABLE 5.1 Parameter Estimation of harmonic regression with d = 12.

Parameter	**Estimate**	**p-value**
CONSTANT	70.4354	0.0000
Sine (2.π.t/d)*	0.3709	0.0000
Cosine (2.π.t/d)*	-0.7373	0.0000

* Sine (2.π.t/d) or Cosine (2.π.t/d) indicates that the unit is in degrees with a period equal to 12 to and time "*t*".

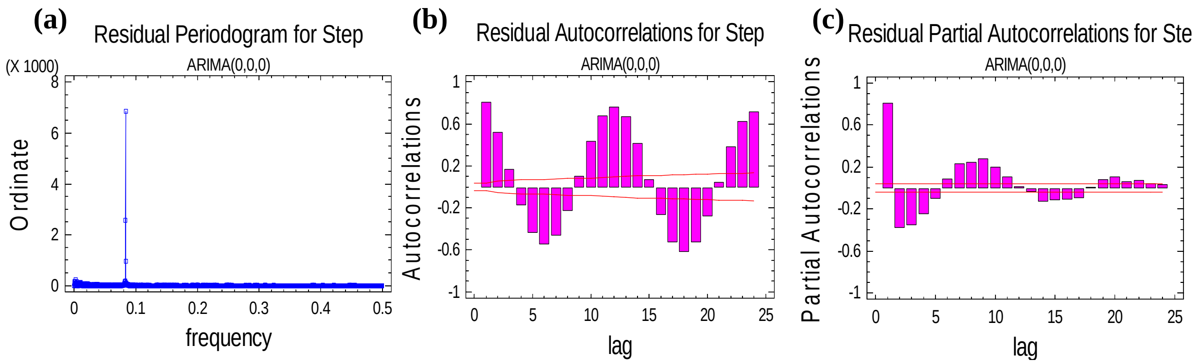

Figure 5.3 Time series analysis for the simulated series, (a) the periodogram, (b) the autocorrelation function, and (c) the partial autocorrelation function.

The p-values indicates that all the parameters are significant at the 95%. It should be noted that when the p-value of any coefficient is smaller than 0.025, it is significant at the 95%; however, if any p-value is larger than 0.025 the associated parameter is not significant and it should be removed from the regression model Eq (2.6). Once the periodic component is removed the residuals are again submitted for the analysis of the time series. Figure 5.4 indicates that one structure of ARMA (1, 2) model could be considered appropriate. To remove this autocorrelation, an ARMA (1, 2) model is fitted. Figure 5.5 shows that the autocorrelation structure is removed since the periodgram behaves as a random process and the autocorrelation are inside of the confidence limits as shown Figure 5.5. The anomalies of the time series is created after removing the periodicity and the autocorrelation components, this time series is called R1.

At this point the step 3 is completed, while step 4 and 5 are computed by a program made in Matlab (APPENDIX A). Results are shown in Figure 5.6.a and Figure 5.6.b, where the annual time series is given in (b) and detects the induced change in 1985, but monthly time series (a) has detected a change in the end of year 1983.

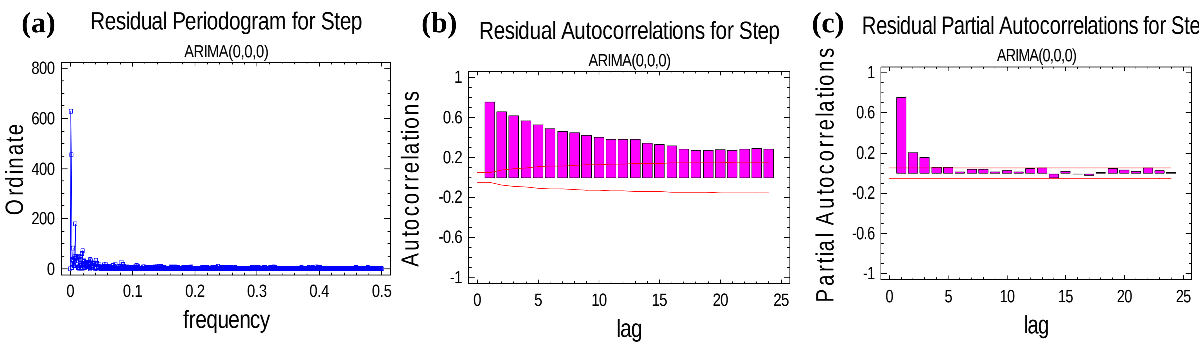

Figure 5.4 Time series analysis for the simulated series without seasonal component (called R1) and an ARMA (2, 1) model is observed, (a) the periodogram, (b) the autocorrelation function, and (c) the partial autocorrelation function.

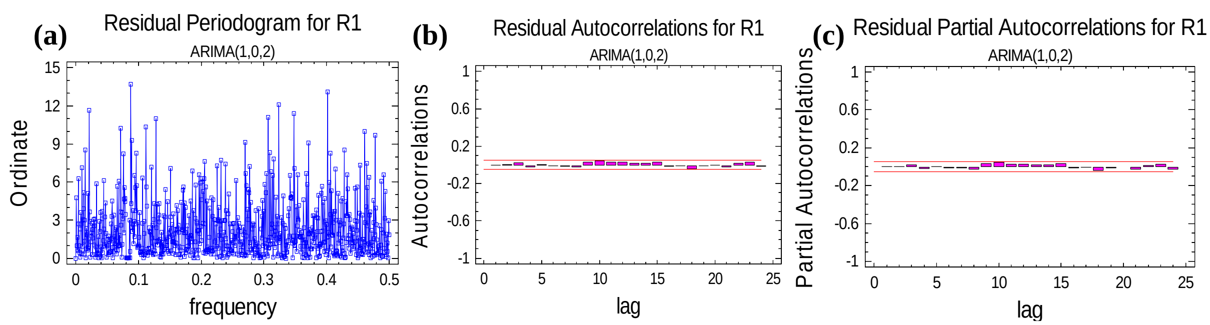

Figure 5.5 Time series analysis for the simulated series without seasonal component (called R1) and an ARMA model fitted, (a) the periodogram, (b) the autocorrelation function, and (c) the partial autocorrelation function.

ii. By Pulse

Similar to section (i), a time series was simulated with a period equal to 12, an ARMA (1, 2) model and with pulse of 1 unit of increase in specific points as 1983, 1993 and 1998 (Figure 5.7.a). The steps 1, 2 and 3 are made similarly as (i) until the ARMA model is identified. The elimination of seasonal and stochastic component is similar to the case (i) and it is now called

R2. Next, the R2 time series was submitted to the program to detect change in the series. The annual analysis (Figure 5.7.c) detects clearly the change in 1983, but the monthly analysis (Figure 5.7.b) detects more interference in the analysis.

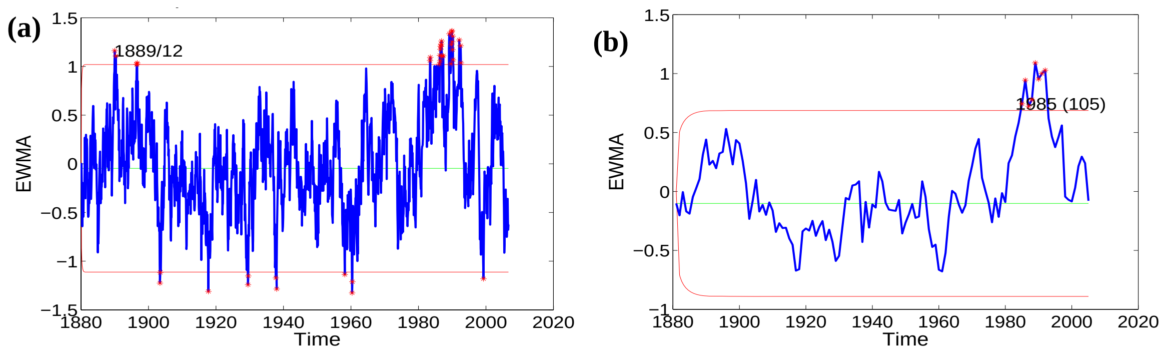

Figure 5.6 The sequential hypothesis testing to the simulated time series with step, (a) monthly analysis, and (b) annual analysis.

iii. By Tendency

Time series with a period equal to 12, an ARMA (1, 2) model and with a tendency from 1970 until 2005. The implemented slope is 0.0138 per year and corresponds to the identified slope in the NH time series. To apply the statistical test to detect a climate change first is necessary to eliminate the tendency. The tendency is eliminated by using the Eq. (2.3). The residuals of the parametric relationship are processed as case (i). Then, the new series in which have been eliminated the tendency, seasonal and auto-correlated component is called R3. The statistical test was applied to R3, and the annual analysis detected a change in 2000, nevertheless the monthly analysis also detects the change but with more noise (Figure 5.8).

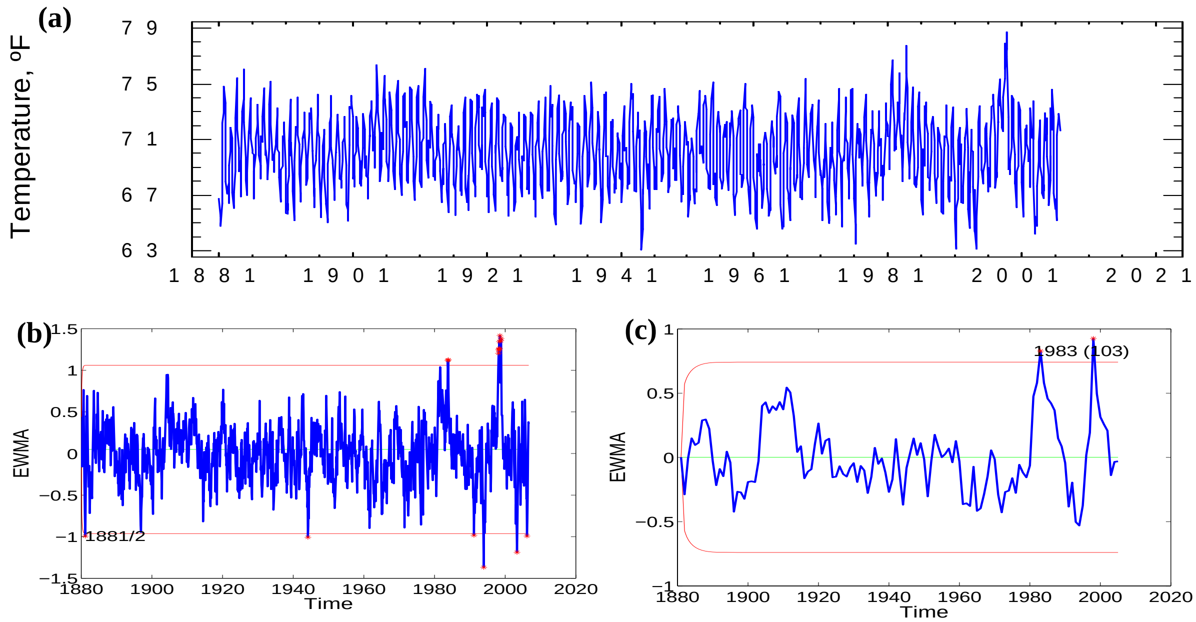

Figure 5.7 Simulated time series with pulses, (a) simulated time series, (b) monthly sequential hypothesis testing, and (c) annual sequential hypothesis testing.

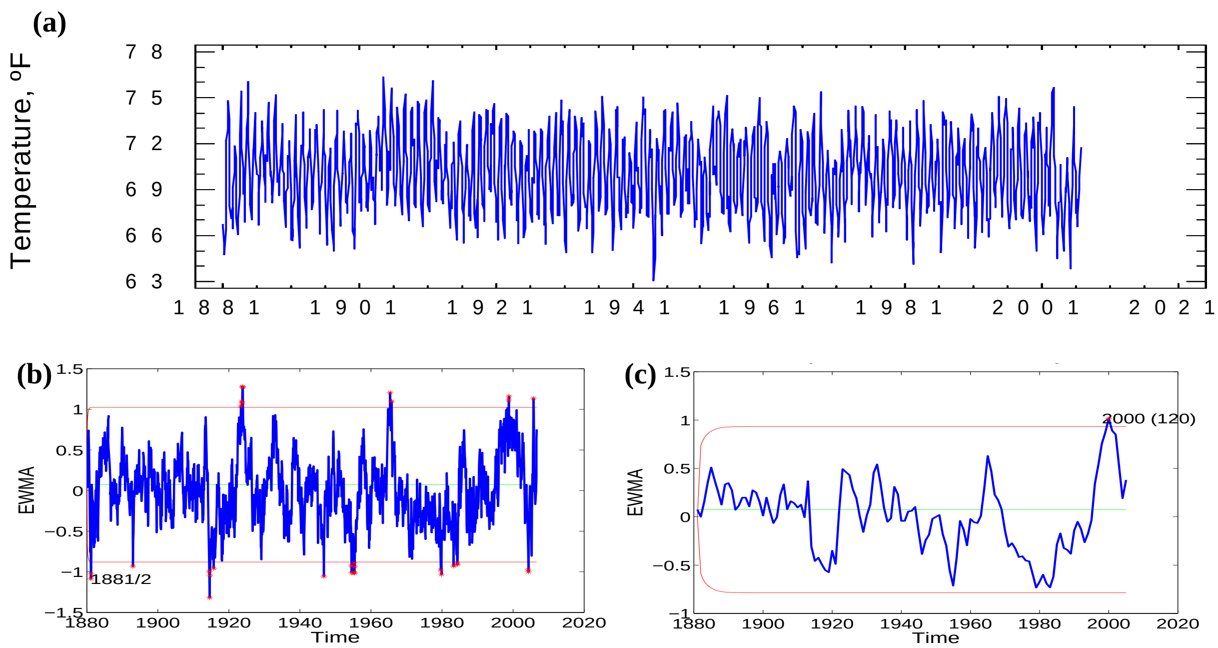

Figure 5.8 Simulated time series with tendency, (a) simulated time series, (b) monthly sequential hypothesis testing, and (c) annual sequential hypothesis testing.

iv. By Tendency plus pulses

This time series has a period equal to 12, an ARMA (1, 2) model and two tendencies first from 1880 until 1970 (slope equal to 0.02 ºF per year) and the last from 1970 until 2005 (slope equal to 0.04 ºF per year). Moreover, a pulse of one increase was added in 1998. The analysis was made similar than R3 and it is renamed as R4; the annual analysis detected a change in 1998 and the monthly analysis also detected the same change but with some interferences (see Figure 5.9).

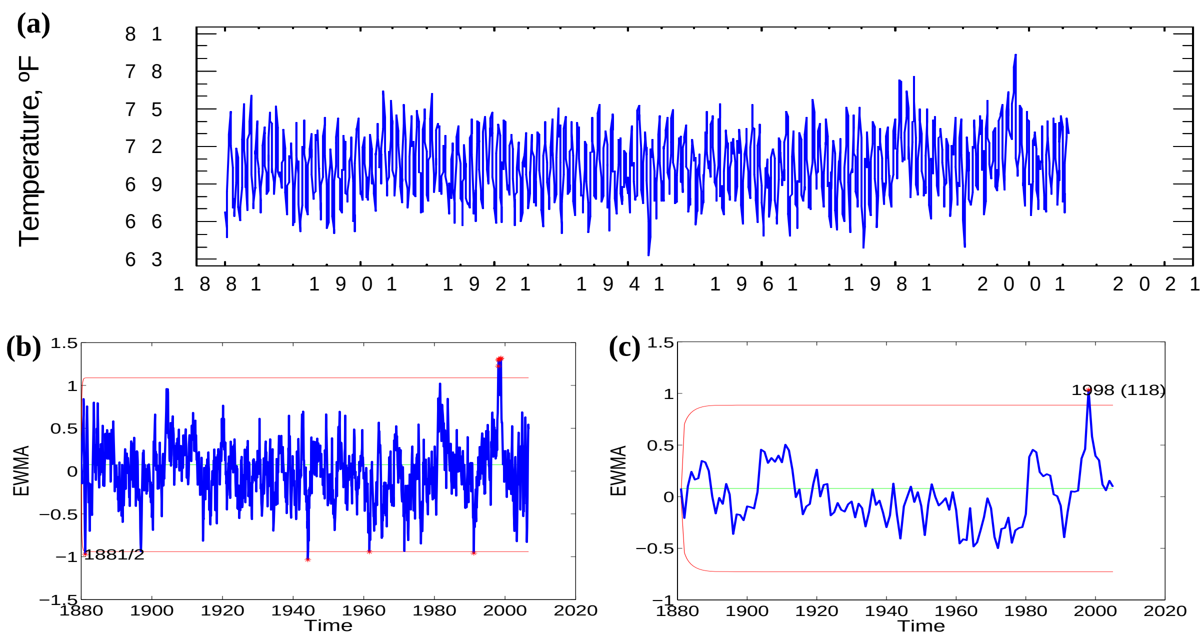

Figure 5.9 Simulated time series with two tendencies and one increase, (a) simulated time series, (b) monthly sequential hypothesis testing, and (c) annual sequential hypothesis testing.

5.1.3 Application of the Test to the Sea Level

In section 5.1.2 the statistical test has shown that it is an excellent tool to detect changes, especially when they are pulses, moreover by using this technique it is possible to appreciate the behavior of the series studied as tendency for example.

Now, it will be shown as the statistical test is applied to a real time series as the global sea level which is from December 1992 until August 2005 the Figure 5.10.a with a slope of 3 mm per year. Hence, the slope must be eliminated by fitting a linear regression and by finding if p-values are significant, the Eq. (2.3) was applied. TABLE 5.2 shows the results.

TABLE 5.2 Parameter Estimation of Linear Regression.

Parameter	Estimate	p-value
CONSTANT	-14.2055	0.0000
t	0.25359	0.0000

Where a was equal to -14.2055, b to 0.25359. After removing the trend the residuals are used to fit the periodicity component. Figure 5.10.b and Figure 5.10.c show the analysis mentioned in the section 5.1.2 part (i) to help to determine the period of Residual1 series. So, the period found is of 12, then the Eq. (2.6) is applied and the results are:

$$s_t = A + B\cos\left(\frac{2.\pi.t}{d_1}\right) + C\sin\left(\frac{2.\pi.t}{d_1}\right) + D\cos\left(\frac{2.\pi.t}{d_2}\right) + E\sin\left(\frac{2.\pi.t}{d_2}\right)$$

Where, A is equal to zero, B equal to -1.526, C equal to -1.378, D equal to 1.37 and E equal to 1.474 (see TABLE 5.3), next the new residuals are found and they are called Residual2. So from the Eq. (2.1), the trend and seasonal component are eliminated, and this is shown in Figure 5.11. The stochastic part is analyzed to determine their autocorrelated and moving average part, which is concluded from the Figure 5.11.b.c.

TABLE 5.3 Parameter Estimation of harmonic regression with d_1=12.75 & d_2=11.7692.

Parameter	Estimate	p-value
Cosine $(2.\pi.t/d_1)$	-1.52604	0.0003
Sine $(2.\pi.t/d_1)$	-1.37763	0.0009
Cosine $(2.\pi.t/d_2)$	1.37012	0.0010
Sine $(2.\pi.t/d_2)$	1.47425	0.0004

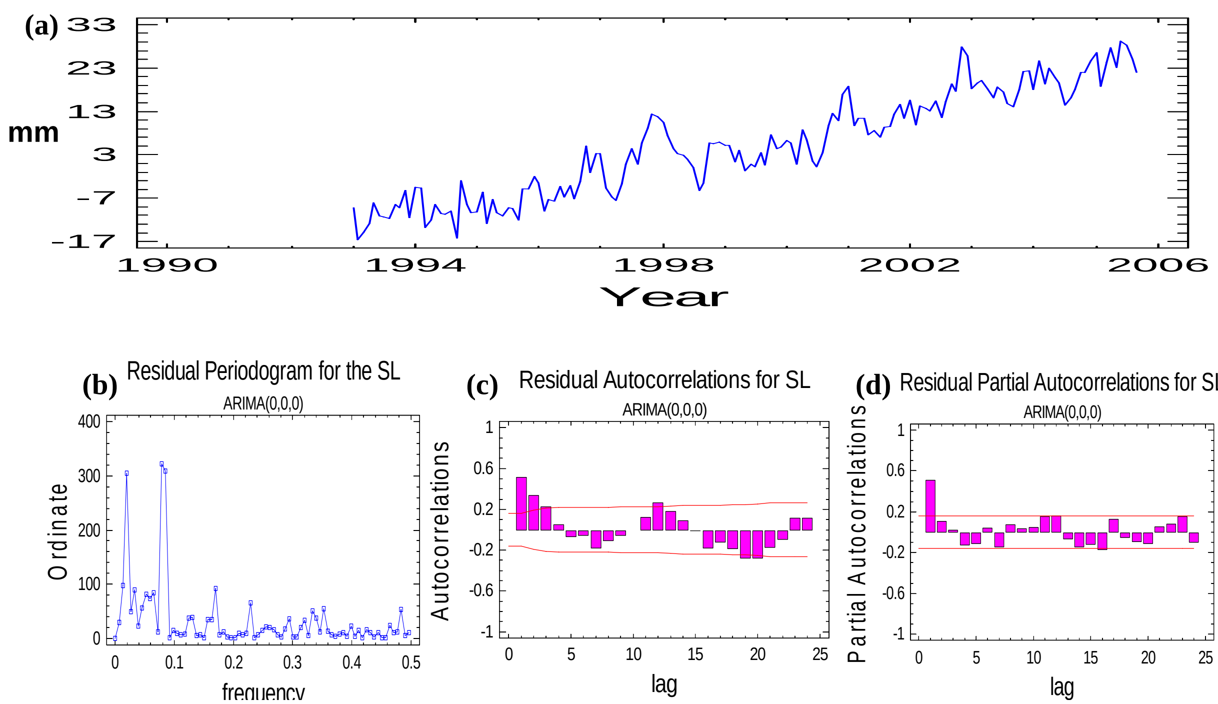

Figure 5.10 Climate indicator variable, (a) Global Sea Level Amount, (b) the periodogram, (c) the autocorrelation function, and (d) the partial autocorrelation function.

Residual2 time series is processed to fit the better coefficients of ARMA model (see equation 2.16), using the Stat Graphic software, and the results were in TABLE 5.4.

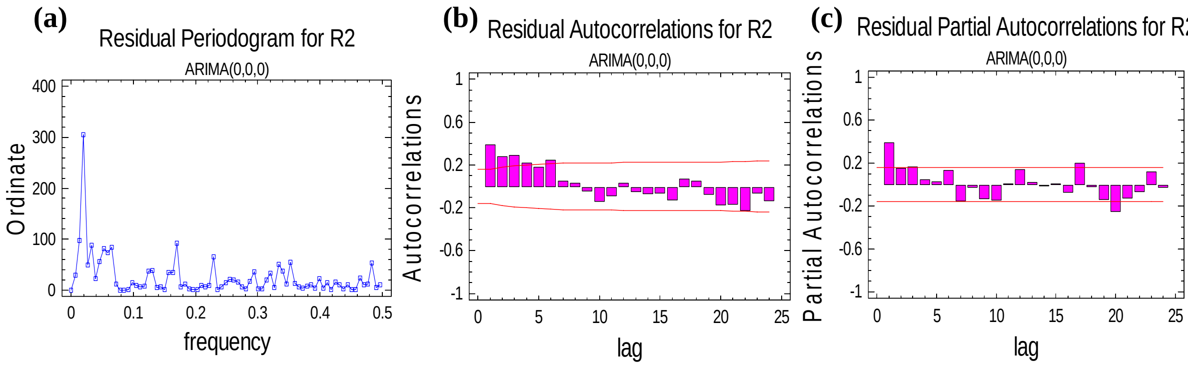

Figure 5.11 Time series analysis for the Residual2 time series, with ARMA (1, 1) model , (a) the periodogram, (b) the autocorrelation function, and (c) the partial autocorrelation function.

TABLE 5.4 Parameter Estimation of ARMA (1, 1) model.

Parameter	Estimate	p-value
AR(1)	0.815158	0.0000
MA(1)	0.531773	0.000217

Figure 5.12 shows the model fit to the ARMA (1, 1), each figure is inside limits to determine that the model presents good results.

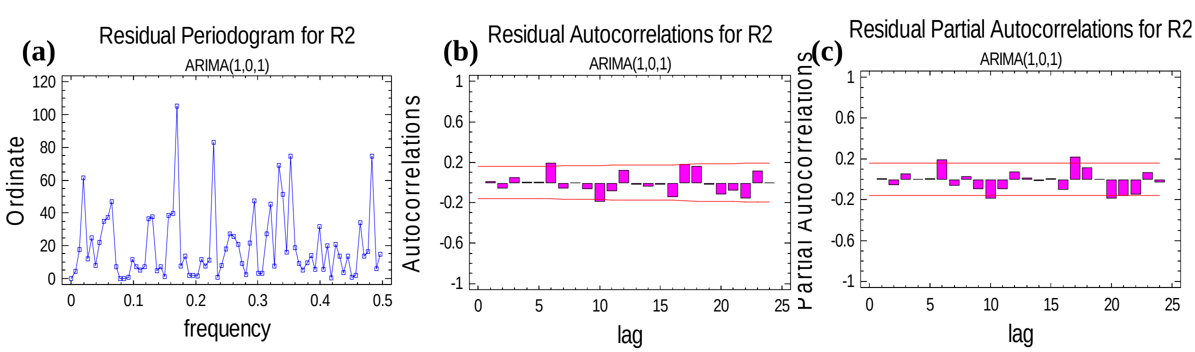

Figure 5.12 Fit of ARMA model to R2 time series, (a) the periodogram, (b) the autocorrelation function, and (c) the partial autocorrelation function.

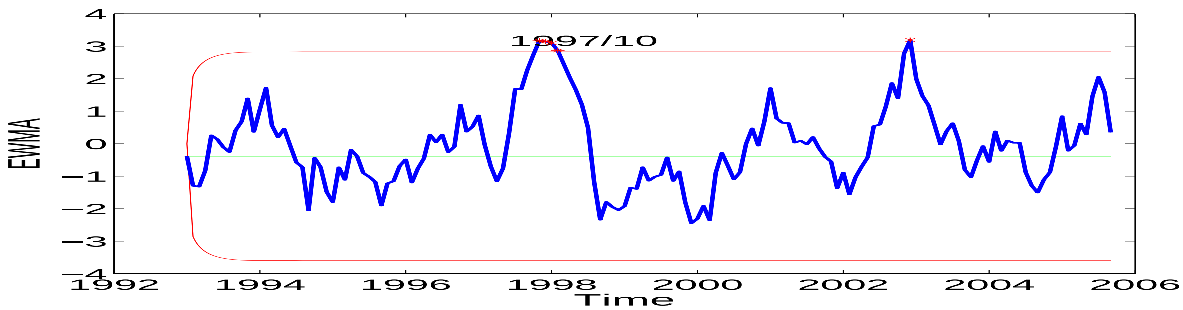

Figure 5.13 Monthly sequential statistical testing.

With the ARMA model identified, the next step is to apply the statistical test to the Residual2 time series which is fitted as ARMA (1, 1) model. Figure 5.13 shows the monthly results of the global sea level changes. Two events are detected at different times, the first one between Oct/1997 until Mar/1998. The second change registered in Nov/2001. The annual analysis is not applied because the numbers of observations along the time is small.

The described procedure was applied to the following variables: Sunspot, Carbon Dioxide, Global and Caribbean air temperature, Global and Caribbean cloud cover, and Global and Caribbean sea level. Analyses and results are shown in chapter 6.

5.2 Numerical Experiment Methodology

This section describes the statistical analysis and how RAMS will be connected. In addition, the concept of Neutral year, defined as one year without effects of the El Niño or La Niña event, is introduced.

5.2.1 Selection of a Neutral Year

In the simulation exercise made for RAMS, it is of interest to observe the behavior of a data in which a change occurred and another one in which it did not occur, for example without any influences of an external phenomenon such as El Niño. This phenomenon affects global climate patterns. Therefore, it is necessary to compare the event outside the normal range with another one in normal conditions. The date with normal conditions is selected when a neutral event is found.

El Niño and Southern Oscillation

El Niño is the name given to the occasional return of an unusually warm water in the normally cold water [upwelling] region along the Peruvian coast. This phenomena is ‘‘a Pacific basin-wide increase in sea surface temperatures in the central and/or eastern equatorial Pacific Ocean’’. The Southern Oscillation (SO) is ‘‘the global-scale phenomenon characterized by a change in the atmospheric pressure field difference between the eastern and western tropical Pacific’’. El Niño and the Southern Oscillation are now known to be part of a coupled atmosphere–ocean system commonly known as ENSO. ENSO has three phases: warm tropical Pacific SSTs (El Niño), cold tropical Pacific SSTs (La Niña), and near neutral conditions. ENSO is a complex system and many aspects of its development are still not well understood [23].

Selection of the neutral year

Figure E.1 shows the classification made by the Australia Government Bureau of Meteorology [3] as: La Niña, neutral and El Niño events, where

El Niño = SOI $\leq$ -5.5

Neutral = -5.5 $>$ SOI $<$ +5.5

La Niña = SOI $\geq$ +5.5

This classification uses June-November average SOI.

To identify the neutral months, several monthly ENSO index were applied such as: Multivariate ENSO Index (MEI) [49], the Oceanic Niño Index (ONI) [50] and monthly SOI [2]. Based on the classification made by the Australia Government Bureau of Meteorology in Appendix E (see Figure E.1) were chosen more of 20 year where a neutral year was observed. Next of to plot the three ENSO indicators, the most Neutral year is the one close to zero. So, it was found that 1990 is a neutral year because it is closer to the zero. Figure E.2 (Appendix E) illustrates the results; the years 1958, 1961 and 1990 were selected.

5.2.2 Numerical analysis

The numerical analysis will be done if two or more climate variables, analyzed with the statistical test, converge in the same point where a change is registered. This month in a specific year will be called *simulation 1*. On the other hand, the *test control* is selected in the same month of *simulation 1* but in the Neutral year. Therefore, two runs, the *test control* and *simulation 1*, will be made.

Besides trying to understand the detected change RAMS will study the impact of that change in the climate of the studied area. Chen et. al. [11] has said that the equilibrium of Earth's climate requires that the global annual mean net radiation flux at the atmosphere be approximately zero. That is why he suggests to study these variables: relative humidity, air temperature, cloud cover, energy incoming (SW) and outputting (LW), an analysis of upward air. To be more robust the precipitation will be added to the analysis to validate the model and the amount of latent and sensible heat, which are indicators of the vapor generated and of the existing heat in the atmosphere.

With respect to the analysis of upward air, the vertical wind shear (VWS) will be studied. VWS is defined as a difference in wind speed (U, V) and/or direction between two levels in the atmosphere: 850 and 200 mb [14]. This is a critical factor in determining whether severe thunderstorms will develop. When VWS, in the tropic North Atlantic, have low values ($|VWS| < \sim 8$ m/s) and warm SST's exist, an interchange of circulations between the upper and lower level feeds on vapor of any storms or hurricane. And, positive Pacific SST anomalies associated with warm-phase ENSO have been linked to increase VWS over the tropical North Atlantic and Caribbean Sea, primarily between 10º and 20º [22].

All variables selected in the analysis are output of RAMS and these are configured in REVU. In the following sections the selected area, the configuration of RAMS, the months that have been chosen, and main namelist in RAMS are shown.

NCEP/NCAR Reanalysis data Initialization

In NCEP/NCAR reanalysis there are several atmospheric data are available for each six hours from 1948 to 2006, covering the entire planet in a mesh with 2.5 degree of resolution in latitude and longitude direction. Seventeen standard pressure levels complete these set of data [34]. All data sets of data are processed from surface weather station, ship, rawinsonde, pibal (the measurement and computation of the speed and direction of winds), aircraft, satellite and other data of interest.

To initialize RAMS, five atmospheric variables are selected: zonal wind (U), meridional wind (V), relative humid (RH), geopotential high (GH) and air temperature (AT), at 17 pressure levels. These data are transforming from regular coordinates to polar-stereographic and from standard pressure levels to terrain-following sigma-z coordinate during the ISAN process.

Numerical Configuration of RAMS

Two nested grids were selected to take into account the synoptic scale and mesoscale phenomena. The parent grid encloses the Central America, Caribbean and North of South America, extending exactly from 5.18ºN to 27.22ºN and from 104.37ºW to 55.77ºW with 50Km of resolution (sees Figure 5.14.a). The nested grid has a resolution of 12.5 Km, covering the four major island of the Caribbean: Cuba, La Española, Jamaica and Puerto Rico. The latitude extends from 16.99ºN to 23.52ºN, while the longitude from 85.70ºW to 65.99ºW (see Figure 5.14.b).

For the vertical coordinate, both grids have the same resolution beginning with 100 meters near the surface and stretching with a ratio of 1.1 until 1000m. Both grids have ten soil layers to be used in the LEAF2 sub model as shown in TABLE 5.5 (NZG command).

The Newton relaxation (nudging) is activated in the horizontal direction and center. In this way, the atmospheric model solution is relaxed toward the observed data during the integration time. According to the resolution selected, the cumulus parameterization is used for the parent grid [74].

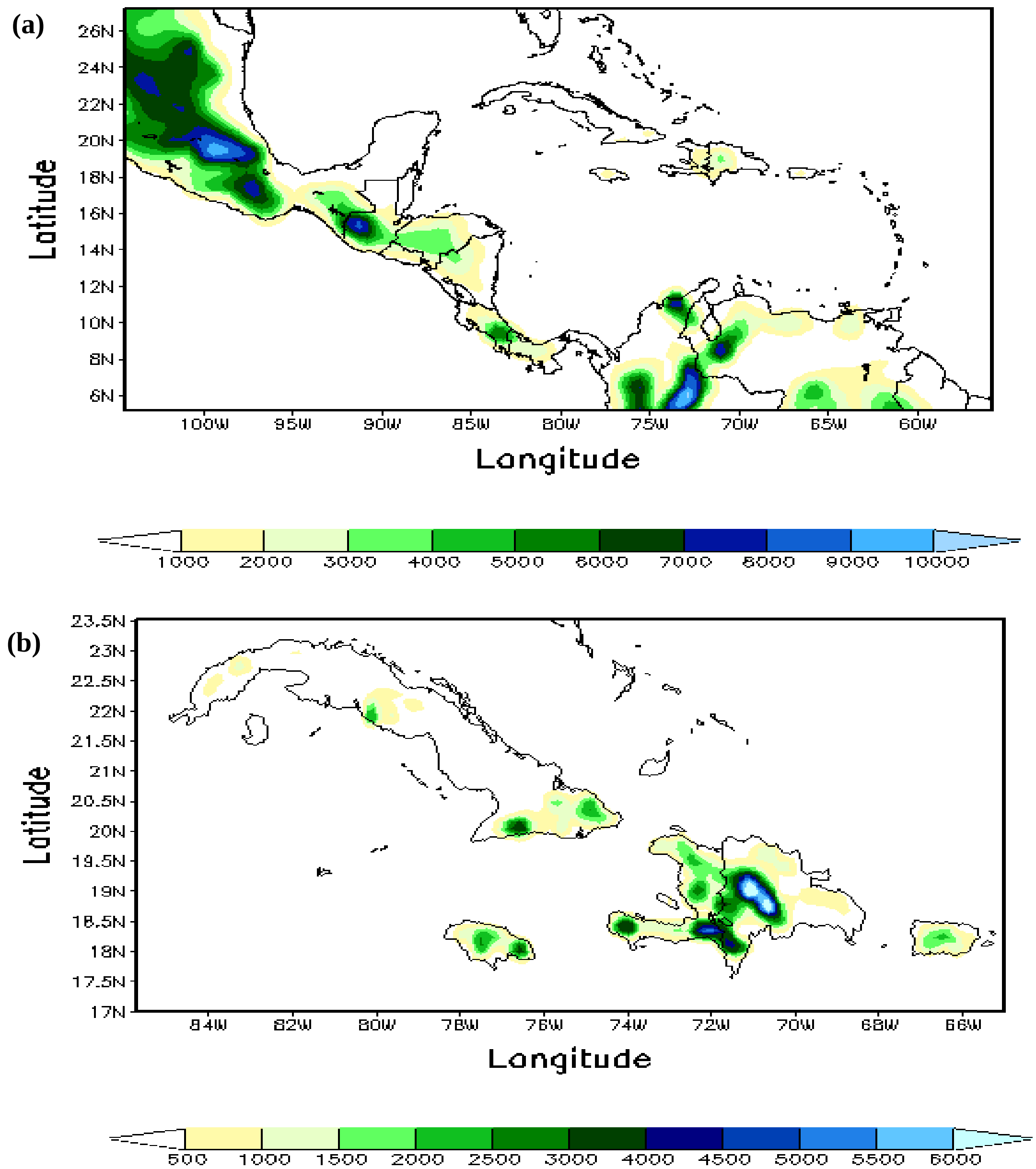

Figure 5.14 Topography in feet for a) Grid 1, and b) Grid 2.

TABLE 5.5 More Relevant Namelist to Configure RAMS.

Variable Name	**Option**	**Description**
NGRIDS	2	Number of grids
NNXP NNYP NNZP NZG	112, 178 56, 66 40, 40 10, 10	Number of x grid points Number of y grid points Number of z grid points Number of soil layers
DELTAX DELTAY DELTZ DZRAT	50000 50000 100 1.1	x grid spacing of the PG y grid spacing of the PG z grid spacing of the PG vertical grid stretch ratio
NSTRATX NSTRATY	1, 4 1, 4	x grid spacing of the NG equivalent to 12.5 Km y grid spacing of the NG equivalent to 12.5 Km
CENTLAT CENTLON	17.5, 20.8 -80, -75.25	Center latitude of grids Center longitude of grids
NUDLAT TNUDLAT TNUDCENT TNUDTOP	5 3600 21600 0	Activated nudging approach, with 5 points in lateral boundary. 3600 seconds as nudging time scale. Central nudging has 21600 time scale and top nudging is not active.
ITOPSFLG	3,3	Reflected envelope orographic topography scheme
IBND	2	Klemp/Lilly lateral boundary condition

JBND	2	
ISWRTYP, ILWRTYP	2 2	Mahrer/Pielke radiation scheme
ISFCL	1	Actives the LEAF2
NSLCON	11	Clay type of soil texture
IDIFFK	2, 1	Turbulent kinetic energy in the PG and anisotropic deformation in the NG

6 RESULTS AND DISCUSSIONS

6.1 Climate Change Detection

6.1.1 Attribution variables

A. Sunspot number

The sunspots reveal a positive significant trend with an increasing rate of 0.39 sunspots per year. After removing the trend and the seasonal component the ARMA fingerprint technique was implemented and the monthly stochastic component showed a significant increment during 1940 to 1960 and especially in December 1957. The annual time series also indicate a significant sunspot increment in 1957. Figure 6.1 shows results for the monthly and annually time series.

Finding of extremes behavior of the sun were reported in 1859 when a solar sunspot induced ground currents that burned the telegraphic lines of US. In March 1989, a major solar storm attacked the northeast part of the US triggering a blackout and disrupted spacecraft orbits and operations. Although no relations were found with the large sunspot event reported in 1957, but, the concurrent tendency was found that there was a relation with the temperatures observed in mesopause [66]. Besides, the volcanic eruption also affects the mesopause region temperatures.

B. Carbon Dioxide

Figure 2.8 demonstrates a strong trend and seasonality component, with a rate of increment of 0.79 ppm per year. But researchers by using archaeological and paleoclimate records (from 1000 to the present year), have found that carbon dioxide concentrate has increased in approximately 36 % from 1750 until 2005 year [70]. Figure 6.2 shows that after removing trend and seasonal components the annual stochastic behavior did not exhibit any change. But between 1985 until 1989 are observed several positive values which do not have the normal behavior of the rest.

Carbon dioxide in the atmosphere has two principal sources the volcanic eruptions and anthropogenic. The eruptions introduce a lot of particles and gases in the atmosphere which are transported by tropospheric and stratospheric winds to vast zones of the globe.

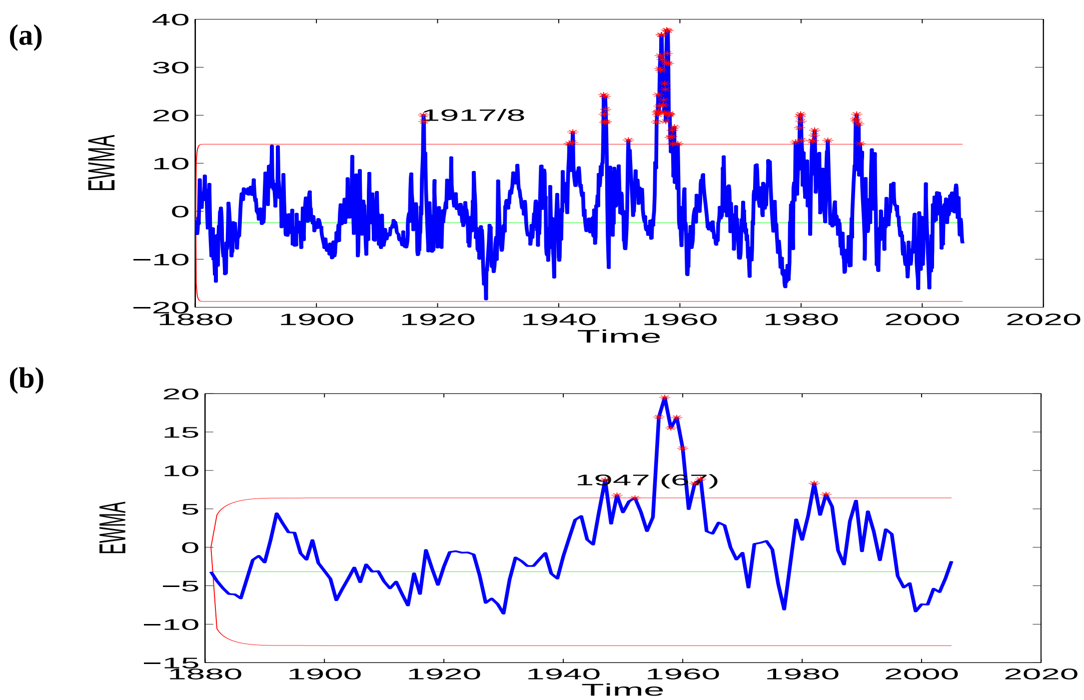

Figure 6.1 EWMA analysis for the sunspot number in, (a) Monthly time series detected a change of a stronger event in December 1957, and (b) The annual time series shows a significant change. The first increment of solar activity started 1947 and finished on 1960. The second increment started on 1982 and finished on 1984 and the second increment was smaller than the first one.

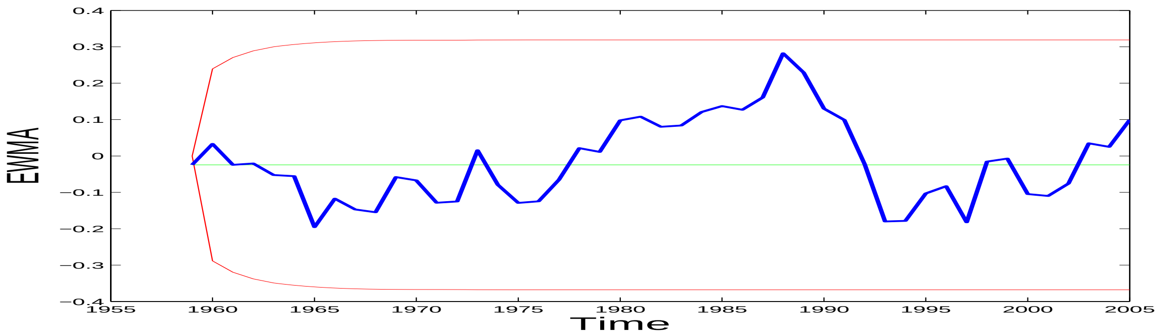

Figure 6.2 The EWMA analysis to annual carbon dioxide time series, no significant change was detected.

TABLE 6.1 illustrates the principal eruptions in the last two centuries and between the years of 1985 to 1989. It can be noticed that there were no significant eruptions; the nearest ones were registered in 1980, 1982 and 1991. It has been pointed out that H_2O and CO_2 are important greenhouse gases and its corresponding atmospheric concentrations are so large that individual eruptions have a negligible effect on their concentrations and do not directly impact the greenhouse effect [61].

TABLE 6.1 Major Volcanic Eruptions of the Past 250 Years.

Volcano	***Year of Eruption***	***VEI****
Grimsvotn [Lakagigar], Iceland	1783	4
Tambora, Sumbawa, Indonesia	1815	7
Cosiguina, Nicaragua	1835	5
Askja, Iceland	1875	5
Krakatau, Indonesia	1883	6
Okataina [Tarawera], North Island, New Zealand	1886	5
Santa Maria, Guatemala	1902	6
Ksudach, Kamchatka, Russia	1907	5
Novarupta [Katmai], Alaska, United States	1912	6
Agung, Bali, Indonesia	1963	4
Mount St. Helens, Washington, United States	1980	5
El Chichón, Chiapas, Mexico	1982	5
Mount Pinatubo, Luzon, Philippines	1991	6

VOLCANIC ERUPTIONS AND CLIMATE (Robock, 2000)
(*) volcanic explosivity index (VEI)

The sunspots and CO_2 exhibited a significant trend during the evaluated period. Lean [36] has said that, a doubling of GHG concentrations is projected to warm Earth's surface by 4.2 K and that a solar-driven surface temperature changes are substantially less, unlikely to exceed 0.5 K and maybe as small as 0.1 K. In addition, the climate model also suggests that the global warming only can be explained by applying the GHG as input in the model [29] [32] [43].

6.1.2 Effect variables

A. Air Surface Temperature (AST)

Global Air Surface Temperature

The anomaly surface temperatures show an increasing trend of 0.106, 0.099 and 0.138 ºF per decade for the global land, the global ocean and land and the north hemisphere land temperature, respectively. After, to each variable was fitted and eliminated its linear trend, then this was submitted to the statistical analysis. Figure 6.4.a shows that the global air temperature shows that the cold period started in 1964 and finished on 1979 where begins quickly to increase and the hottest period started on 2002 up. Figure 6.4.b and Figure 6.4.c indicate similar results where persistent increments are exhibited in 2002. Independently of internal changes, the Earth is heating specially in the NH where the principal countries with large sources of emissions of carbon dioxide are located in North America (midwest and eastern USA), Europe (northwest region), East Asia (eastern coast of China) and South Asia (Indian subcontinent) [30]. Vinnikov et. al [73], has said that the increasing NH temperature is the possible reason that ice sea is melting in this area.

Some people argue that the Earth warming is produced by a small number of eruptions in the last century, this is because several eruptions can produce a cooling effect [61]. However, for example from 1913 to 1962 there was no a major eruption (TABLE 6.1), but during this supposedly warm period, the Earth exhibited low temperatures. Therefore, other external forces created the cooling period.

Another analysis compared the relation between the global air temperature and the CO_2 time series (see Figure 6.4.a). This analysis was made by using the annual anomaly time series because the random was reduced. It was found that the entire correlation between both series is of 29 % (1958-2005), but if the analysis is divided in two parts the result are different. The results show that there is a correlation of 72% in the period 1958-1983 and 12% between 1984-2005. Figure 6.4.b compares the annual anomaly of the global air temperature and sunspot with poor correlation (19%).

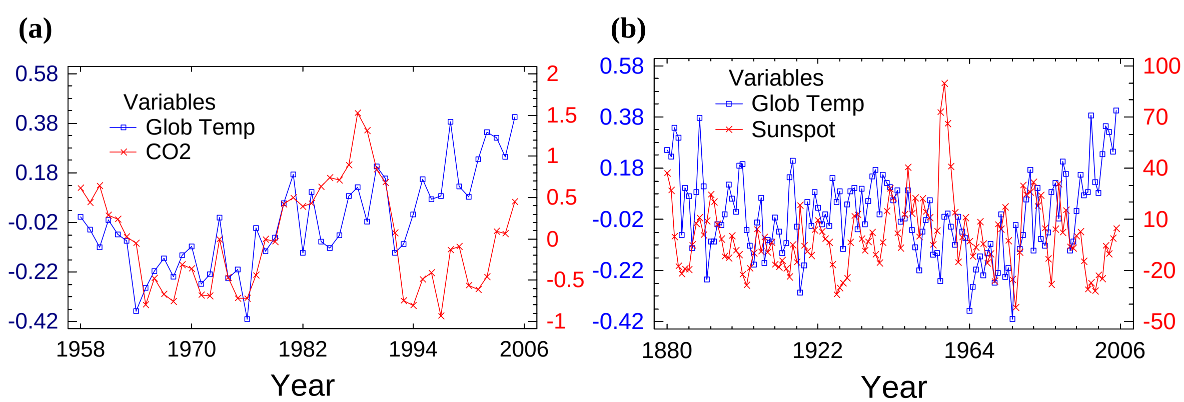

Figure 6.3 Annual anomaly for (a) Global air temperature and carbon dioxide, and (b) Global air temperature and sunspot.

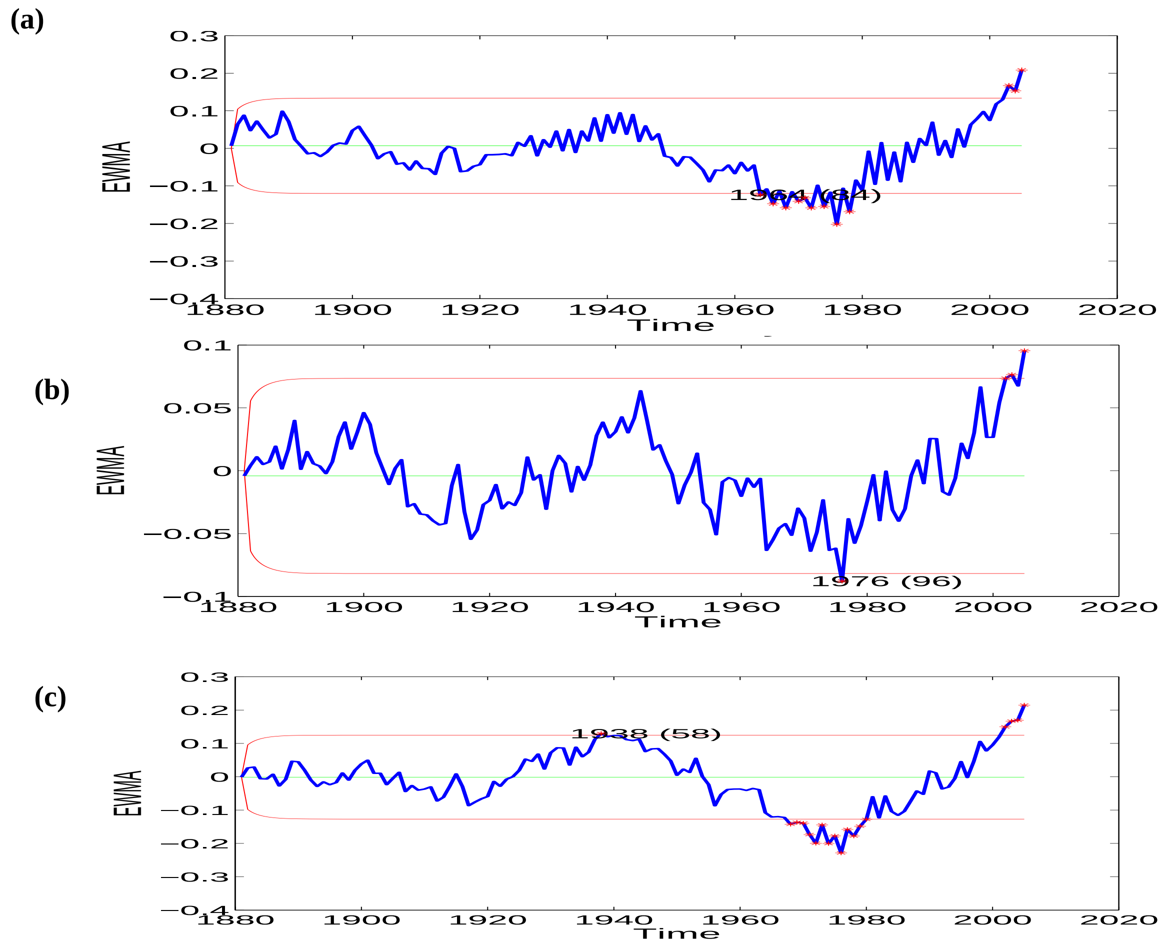

Figure 6.4 The EWMA analysis to annual mean air surface temperature (AST), (a) The global data show that the cooling period started in 1964 and finished in 1979 and the warming period started in 2002 up to present time (2006), (b) The land and ocean data exhibit a punctual cold time in 1976 and the warming period from 2002 to present and (c) the north hemisphere data shows that cooling period from 1968 to 1979 and a more intense warming period started in 2002 until present.

Caribbean Air Surface Temperature

Puerto Rico monthly time series exhibit an increasing rate of AST of about 0.193, 0.147 and 0.254 ºF per decade in the mean, maximum, and minimum air temperature, respectively. Thus, the minimum air temperature is increasing faster than the maximum air temperature (Figure 6.6.a), for this reason the nights are being hotter during the recent decades, this result is in agreement with other investigations made in the Caribbean [53] and the world [17] [21] [52]. One explanation was developed by Kalnay [33], who worked with the effect of agricultural and land use in the evolution of the temperature and concluded that both urbanization and agriculture effects could be consistent with the general increase in the minimum temperature and slight decrease in the maximum temperature, and contribute to the reduction in the diurnal temperature range. In Puerto Rico for example the increment of evaporation during the day (due to rain), would also tend to decrease the maximum temperature; this water would increase the heat capacity of the soil, thus increasing the minimum temperature.

Section 4.1.2 discussed that a climate change can best be detected using annual time series. Although the monthly time series can be more precise on change detection process and may also involve several false alarms. In spite of this, the test for PR includes monthly time series (Figure 6.5). For the mean AST (Figure 6.5.a) three changes were detected of which the strongest was in March 1983. Thereafter, for the maximum AST several changes were identified before 1985, one of these was detected in March 1983 (Figure 6.5.b). Figure 6.5.c shows the minimum AST and the statistical test detects several temperature increments that occur after 1985 and especially in March 1998. It can be noted that the minimum AST was sensitive to the El Niño 1997/1998, since a temperature increment was detected in March 1998. Similarly, the maximum AST was sensitive to the El Niño 1982/1983 because a rising temperature was detected in March 1983.

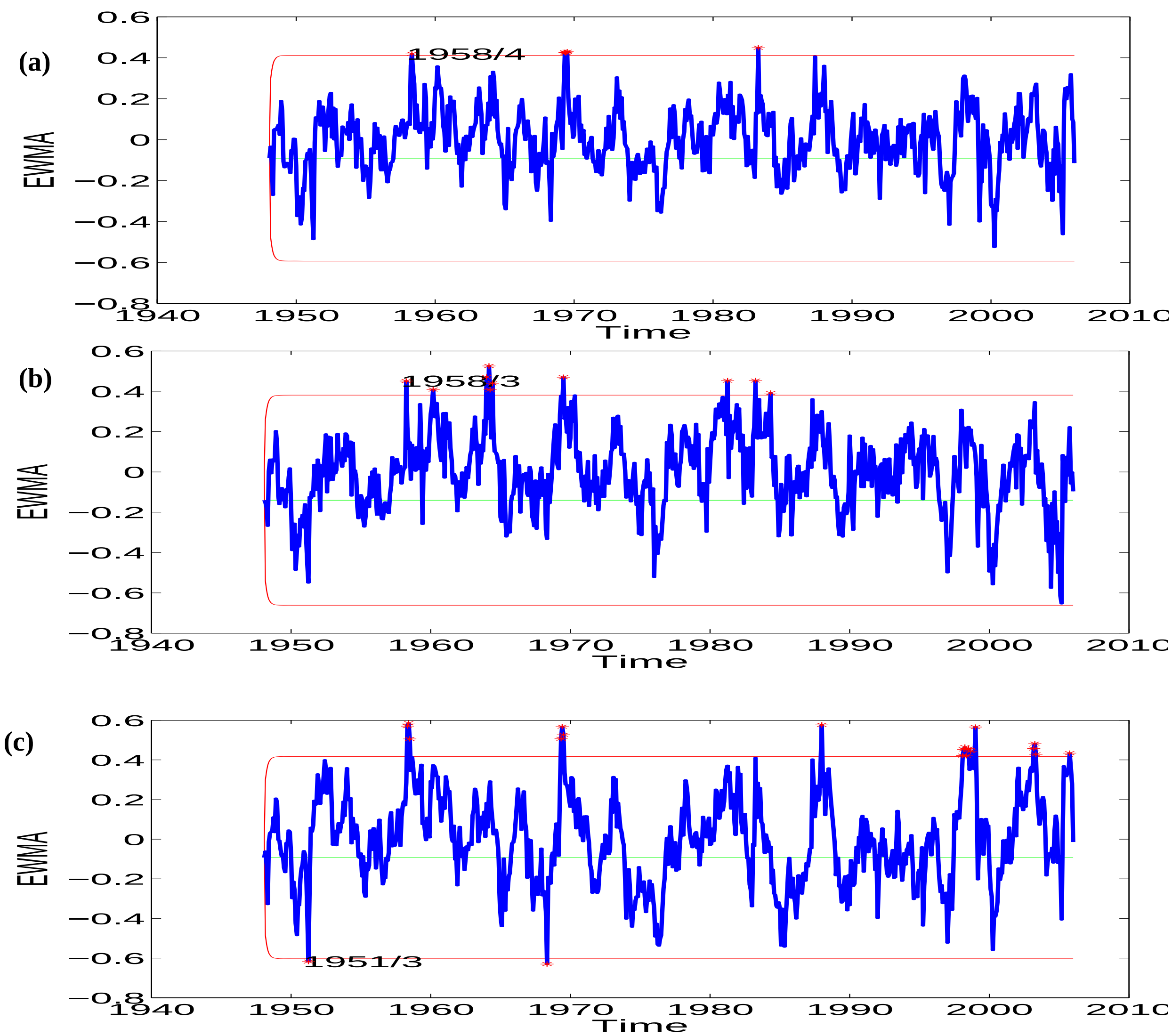

Figure 6.5 The EWMA analysis to the PR monthly time series of, (a) The mean AST, (b) The maximum AST and (c) The minimum AST.

The statistical test was implemented to detect changes over the difference between the maximum and the minimum air temperature and it was found that in Puerto Rico a significant increment was identified in 2004 (Figure 6.6.b). The minimum temperature is increasing and has become more evident from 1996 to 2005, as shown in Figure 6.6.b.

(a)

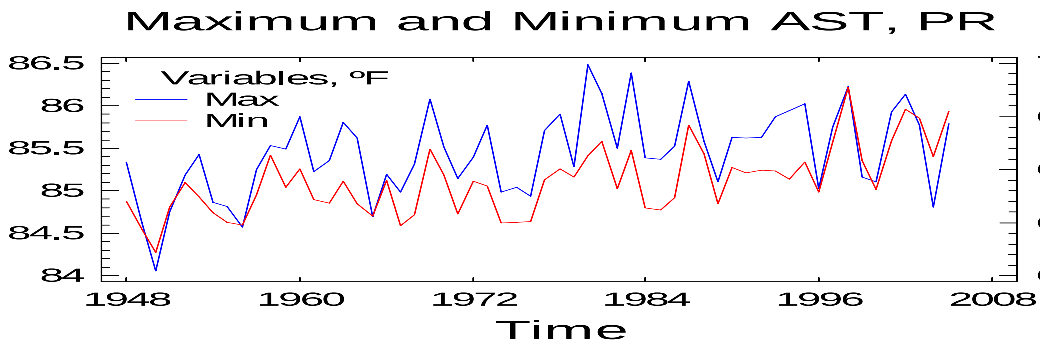

(b)

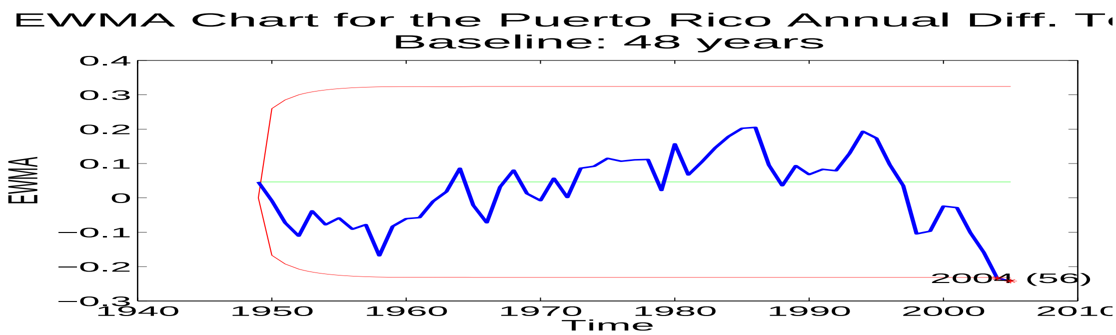

Figure 6.6 (a) The maximum and the minimum air temperatures for Puerto Rico. The scale on the left is for the maximum and on the right is for the minimum air temperature, (b) The EWMA analysis to the maximum minus the minimum air temperature shows a significant change that occurring in 2004.

Cuba (CU) time series have a different behavior of the PR data set, the mean AST did not show a tendency, but the maximum AST of Guantanamo (OR) station has a rate of increasing of 0.254 ºF per decade and the minimum was 0.162 ºF per decade. Therefore, the maximum AST is increasing faster than the minimum AST. Figure 6.7.a shows that the mean AST exhibited a change that occurred in 1998. Although, Figure 6.7.b shows that no change on the difference of temperatures, there is an increasing trend on mean air temperature.

The Caribbean islands DR, HA and JA exhibited a slope of 0.198, 0.128 and 0.249 ºF per decade, respectively. It was observed that the statistical test did not detect any additional change on air temperature on these islands (see Figure 6.8).

In summary the Caribbean islands: PR, DR, HA & JA have an increasing trend on air temperature with the exception of CU, which has no trend. This analysis indicates that each island has a different AST behavior. Appendix D provides more information about this subject indicating that AST in the west area of the Caribbean is increasing faster than the rest of the Caribbean.

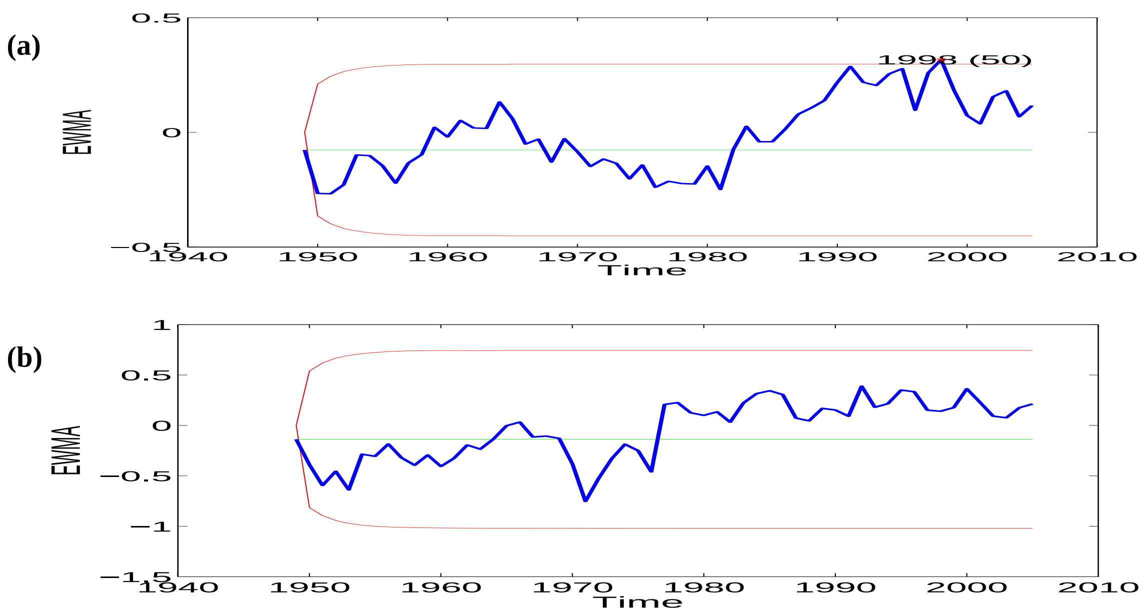

Figure 6.7 The EWMA analysis applied to CU annual stations, (a) The mean AST shows the warmest temperature occurred in 1998 and (b) difference of air temperature do not detect any significant change.

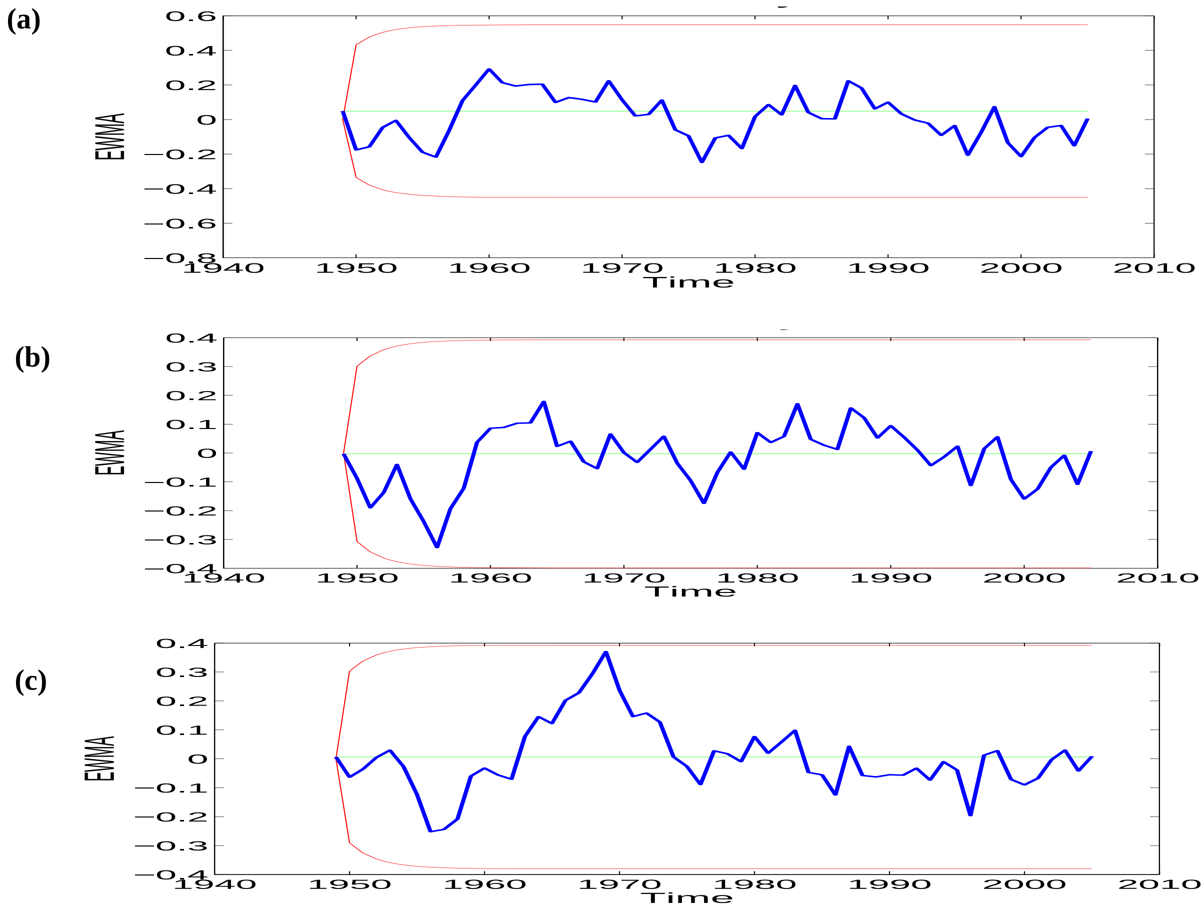

Figure 6.8 The EWMA analysis applied to (a) RD mean AST, (b) HA mean AST and (c) JA mean AST.

Global temperatures studies show that not all the regions of the world display signs of recent warming. The mean temperature has been increasing in 67% of the world area, with 55% experiencing a period of cooling followed by warming and 12% showing continuous warming, but some 20% of the world area, including the eastern tropics and South Pacific, the South Atlantic and part of the Indian Ocean, have first warmed up and are recently experiencing cooling [46]. However, the regional scales can have different results [43].

B. Cloud Cover

Figure 6.9 shows cloud amount time series with the data separated for the global (in the first column) and Caribbean time series (second column).

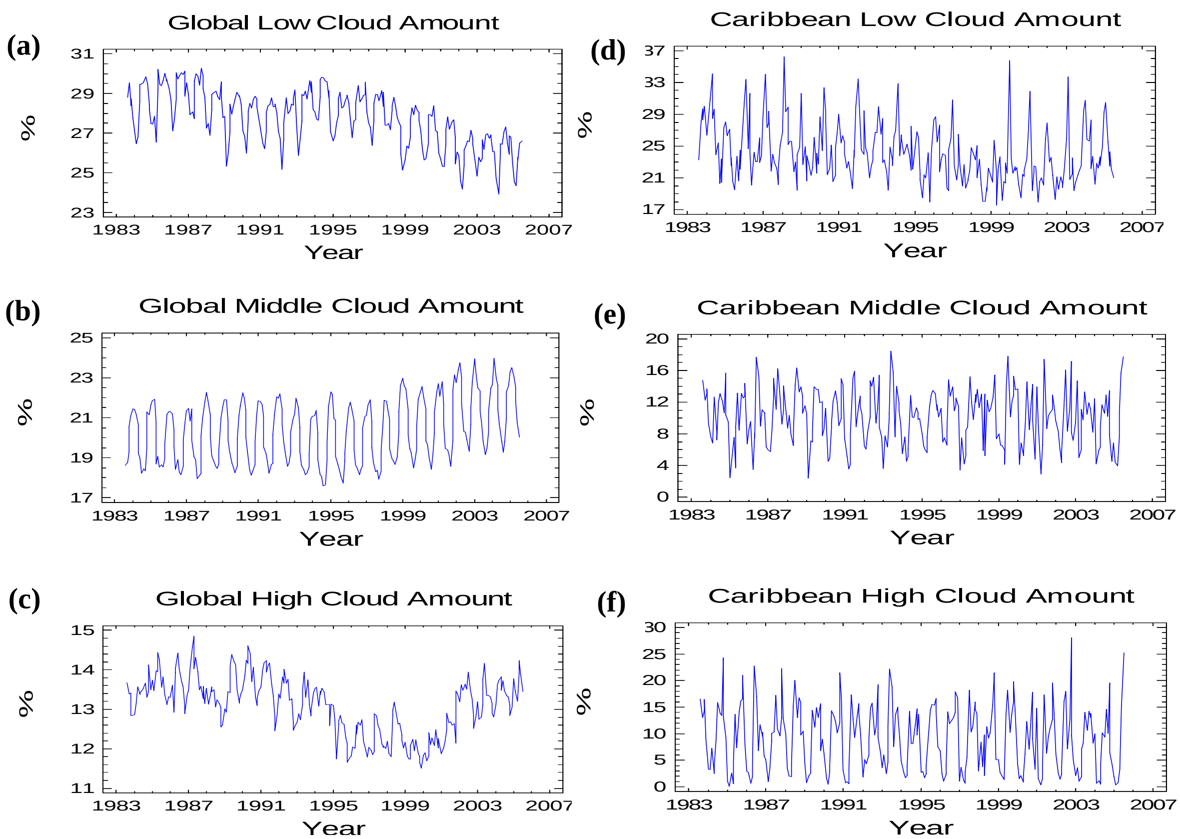

Figure 6.9 Cloud amount time series from July 1983 until June 2005 from ISCCP D2. Figures a, b, and c are at global scale (a) Low, (b) Middle and (c) High Cloud Amount. Figures d, e, and f are at Caribbean scale (d) Low, (e) Middle and (f) High Cloud Amount.

Global Cloud Cover

It was found that the global cloud amount is decreasing at the rate of -0.17 % per year. Low cloud amount has a rate of -0.13 % per year, middle cloud amount is slowly increasing with 0.08 % per year and high cloud amount is decreasing at the rate -0.05 % per year (see Figure

6.9.abc). It is clear that the low cloud amount is decreasing faster than the others. If we analyze that the incident radiation from the Sun is partly reflected from clouds (30%), partly absorbed in the atmosphere (25%) and the remainder (45%) is absorbed by or reflected from the vegetation and ground or the oceans on which it falls. Then the lower cloud cover amount contributes to a lower incident radiation reflection resulting in an increment of the incoming energy. The decreasing cloud cover contributes to the imbalance of the energy on the earth.

It has been pointed out that high cloud tended to warm the planet and low cloud cools the Earth (Figure 2.6). The decreasing trend of low cloud is contributing to the global warming (Figure 6.9.a). This result is related to satellite observations, which suggest that the thermal radiation emitted by Earth (LW) to space has increased by more than 5 watts per square meter, while reflected sunlight (SW) has decreased by less than 2 watts per square meter, over the period 1985 – 2000, with most of the increase occurring after 1990 [11]. Thus, if low cloud cover is decreasing, the percent reflected of LW will also decrease and then LW will go to space. Similarly, the percent reflected of SW will also decrease, and then SW is going to fall in the land.

Then, the global warming will be stronger when high cloud will increase and low cloud will decrease, this is a possible future scenario proposed by Weier [76]. However, cloud data show that global low and high clouds are decreasing.

After applying the test (Figure 6.10.abc) to each series, it was found that middle cloud amount has ***likely*** relation with El Niño 1997/1998, because changes were detected from October 1997 to February 1998.

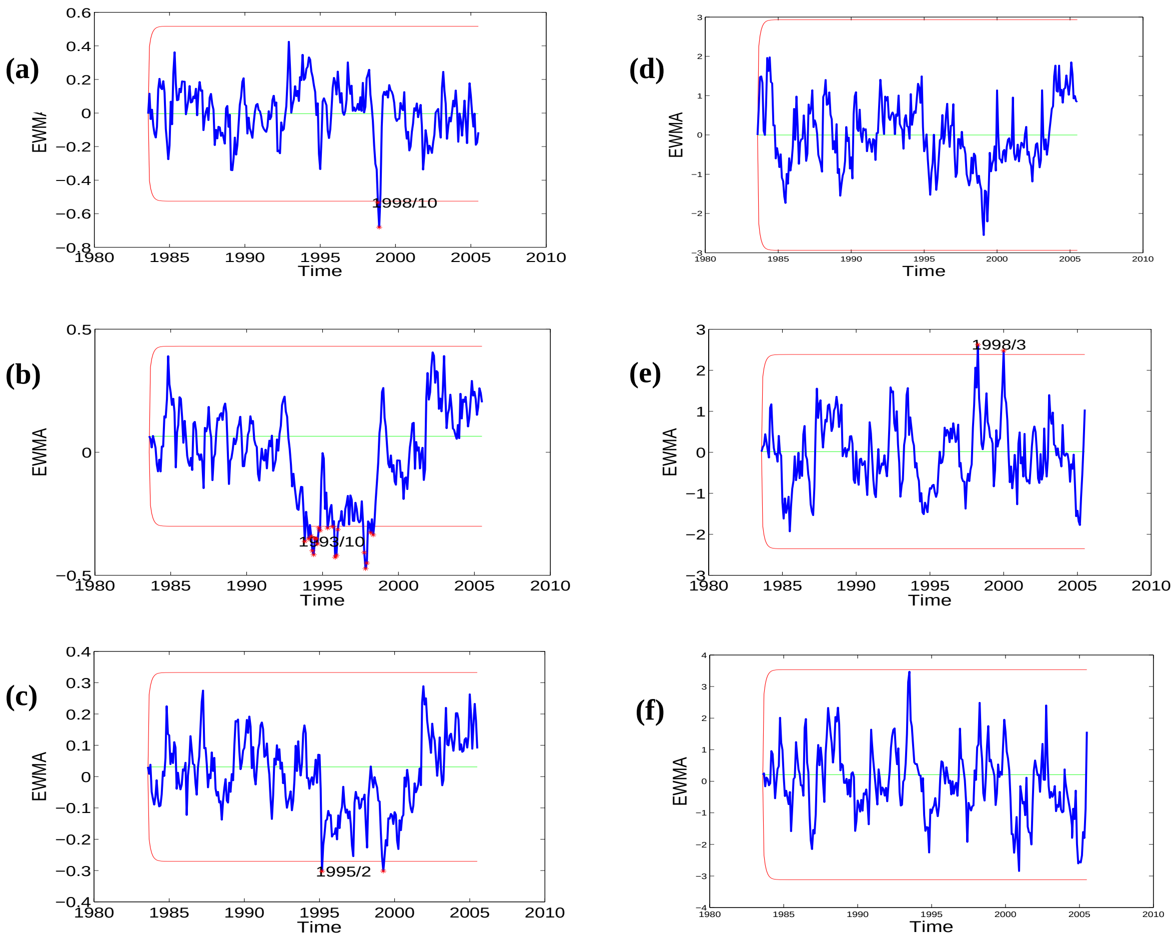

Figure 6.10 The EWMA analysis to the global climate change detection over cloud, amount (a) Low cloud amount, (b) Middle cloud amount, (c) High cloud amount. The EWMA analysis to the Caribbean climate change detection over cloud amount, (d) Low cloud amount, (e) Middle cloud amount, (f) High cloud amount.

Caribbean Cloud Cover

The Caribbean cloud cover shows a significant reduction of about -0.38 % per year. Figure 6.10.def show that the low cloud cover is decreasing at the rate of -0.17% per year, the middle cloud has a slower reduction of -0.03% per year, while the high cloud does not show any tendency, because the slope is not statistically significant.

Then, the percent of decreasing Caribbean low cloud cover is higher than global low cloud cover; in addition, the Caribbean high cloud cover is constant over the time. With these characteristics the effects of the energy imbalance are considerable; more energy will fall over the Caribbean.

Figure 6.10.d-f show that low, middle and high cloud cover have a similar result than the global clouds; where the middle cloud cover reveals a relation with the stronger El Niño phenomena 1997/1998, but with a lag of 3 months, March 1998. Hence, there may be a relation between the middle cloud amount and the El Niño phenomena. Although, Angeles [1] mentioned that, there is a strong relationship between the early season (rain present from April until July in the Caribbean area) and the El Niño event. Comarazamy [13] found that April 1998 was an unusual wet month inside the dry season and probably because of El Niño 1997/1998. Thus, there is a direct relation between El Niño and the rainfall and consequently between the rainfall and clouds.

Weier [76] pointed out that, short-term El Niño and La Niña cycles, occuring every three to seven years, show dominate cloud patterns across the tropics. This work has detected that middle cloud amount may have some relation with El Niño 1997/1998 event, and this interaction is consistent at global and at Caribbean scale.

C. Sea level

Global Sea level

It has been found that the global sea level is increasing at the rate of 3 mm per year. In addition the stochastic component shows two significant increments beginning in October

1997 until January 1998 (Figure 6.11.a). Hansen [24] affirmed that during this period the sea level rises due to unstable energy balance. In addition, the Earth is now out of energy balance by close to +1 W/m^2, i.e., more energy is absorbed from sunlight than is emitted to the outer space as thermal radiation. This large growing planetary energy imbalance has no registered precedent, greatly exceeding the global mean energy imbalance associated with changes of the Earth's orbital elements that has paced the natural building and decay of ice sheets. And based on the physical properties and mass of the world ocean as compared to other components of Earth's climate system, ocean heat content might be the dominant component of the variability of Earth's heat balance [39].

Caribbean Sea level

The Caribbean Sea level has no trend and the stochastic component shows a significant increment in March 1998 (Figure 6.11.b). This event may be associated with the El Nino event that occurred in 1997.

Apparently, the global and Caribbean Sea level exhibit some climate change that may be related to El Niño event in 1997. During El Niño 1997/1998 event the sea surface temperature anomalies (SSTAs) exceeded 4°C [72]. It is known that when the water is warm, the volume increases. This phenomenon is called thermal expansion. Lombard et al. [40] have found that the mean rate of thermal expansion sea level rise over the past decade is 1.5±0.3 mm/year, i.e. 50% of the observed 3 mm/year by satellite altimetry.

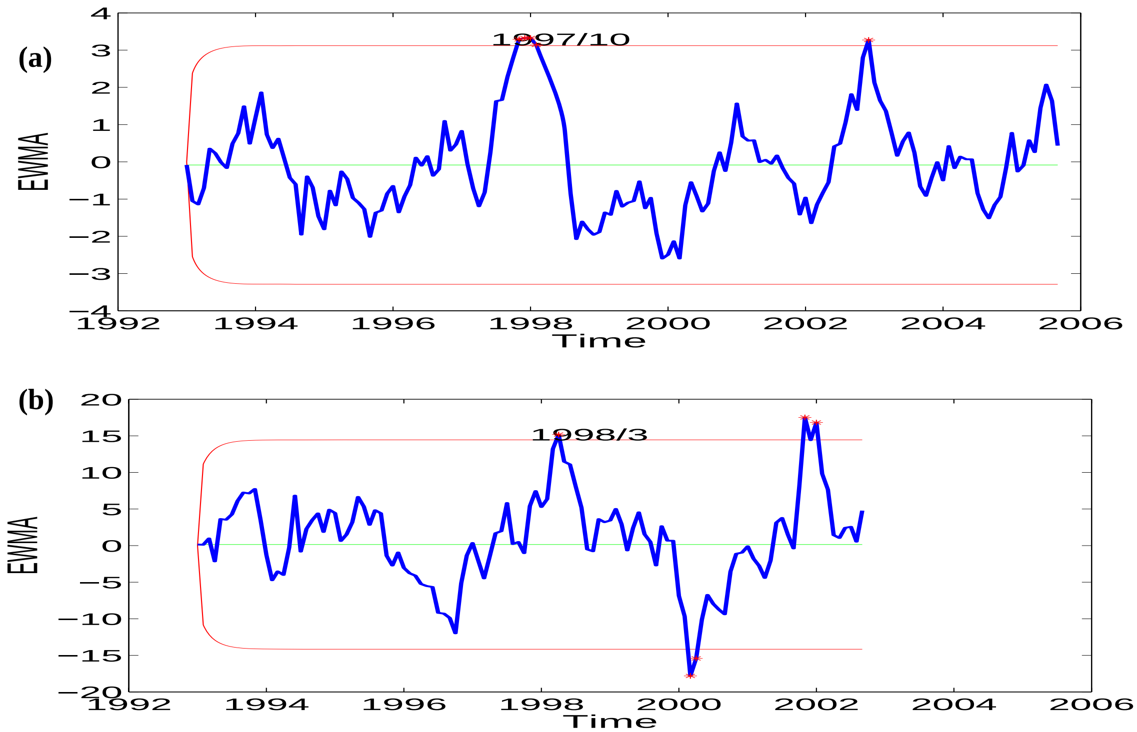

Figure 6.11 The EWMA analysis to the sea level climate change detection, (a) Global and (b) Caribbean.

Therefore, changes in the cloud cover will change the rate of incoming radiation world wide. If the radiation increase in the ocean, the sea surface temperature will change, which in turn changes the atmospheric circulation and the amount of moisture evaporated from the oceans with a resulting change in cloudiness [58].

TABLE 6.2 present the summary of all results of each variable studied by indicating the tendency per decade.

TABLE 6.2 Summary of the results to each variable analyzed in the present project.

Variable			Trend	Detected climate change
Sunspot			3.9 ss /decade	All 1957
Carbon Dioxide			13.8 ppm/decade	NO
AST	*Global*	*Global*	0.11 ºF/ decade	March/2002
		Land & Ocean	0.1 ºF/ decade	March/2002
		North Hemp.	0.14 ºF/ decade	2002 & 2005
	Caribbean	*PR Min.*	0.25 ºF/ decade	March/1998
		PR Max.	0.15 ºF/ decade	March/1983
		PR Mean.	0.19 ºF/ decade	March/1983
		CU Mean.	NO	NO
		RD Mean.	0.20 ºF/ decade	January/1998
		HA Mean.	0.13 ºF/ decade	March/1964
		JA Mean.	0.25 ºF/ decade	March/1964 & January/1998
Sea Level	*Global*		30.4 mm/ decade	October/1997
	Caribbean		NO	March/1998
Cloud Cover	*Global*	*CA*	-1.7 %/ decade	NO
		Low	-1.3 %/ decade	October/1998
		Middle	0.8 %/ decade	October/1997 - January/1998
		High	-0.5 %/ decade	February/1995
	Caribbean	*CA*	-3.8 %/ decade	June/1985
		Low	-1.7 %/ decade	January/1999
		Middle	-0.3 %/ decade	March/1998
		High	NO	April/1992

6.2 Regional Climate Modeling

Previous results show that there may be some connection between middle clouds cover and sea level with the El Niño event that occurred in 1997/1998. This relation was observed at the global and Caribbean scale. To obtain a better understanding of the causes of this relation over the Caribbean region, RAMS was run using 1990 as a neutral year for the test control. The simulation 1 (March 1998) is compared with the test control. Appendix F shows the comparison between observed and simulated data for March 1998.

Simulation results show that the incident surface flux of longwave radiation (Figure 6.12), vertical wind shear (Figure 6.13) and cloud cover fraction (Figure 6.14) indicate an increment in March 1998 with respect to March 1990. In addition, the SST anomalies (see Figure 6.15, taken from website http://iridl.ldeo.columbia.edu/SOURCES/.IGOSS/.nmc/.Reyn_SmithOIv2/.monthly/.ssta/) put in evidence the presence of El Niño event in the area.

Vertical wind shear (VWS) is closely associated with the vertical flux of momentum, heat, and water vapor.

The warm-phase ENSO caused VWS intensification along with water warming inhibiting the vertical convection between the lower and upper troposphere. In addition, the mesoscale model was able to capture the cloud cover and LW radiation intensification. The increment of the cloud cover fraction can be explained by the SST increase. Greater amount of water is evaporated, but at the same time, this water vapor is obstructed to ascend to the upper level due to the intense VWS, and accumulating in the middle levels.

With respect to the increase the LW radiation Chen et. al [11] studied the tropical area and indicated that, in 1998 both the ENSO index and the tropical mean LW flux anomalies reach their maximum, but they showed that both data are uncorrelated. This implies that the mechanism behind the long term average LW flux increase is distinct from the ENSO phenomenon.

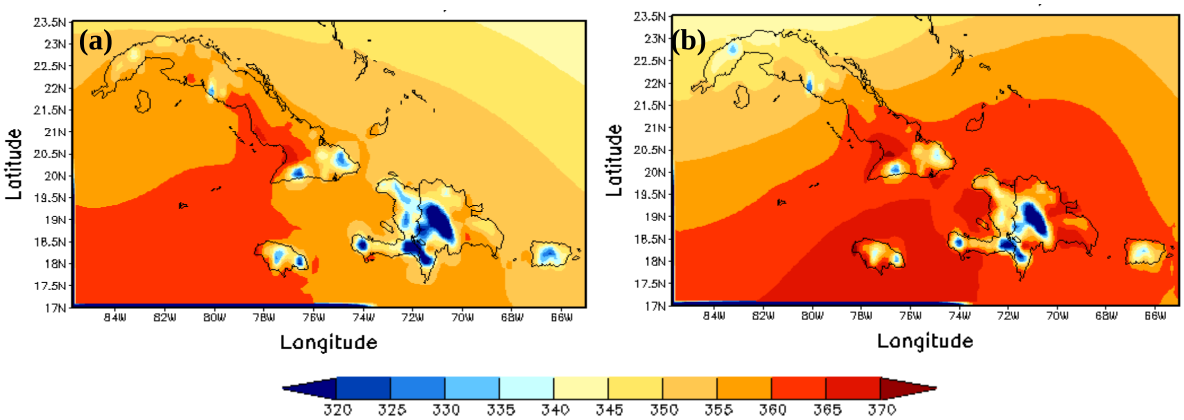

Figure 6.12 Incident Surface Flux of Longwave Radiation of RAMS. (a) Neutral data (March 1990), and (b) El Niño (March 1998) event data.

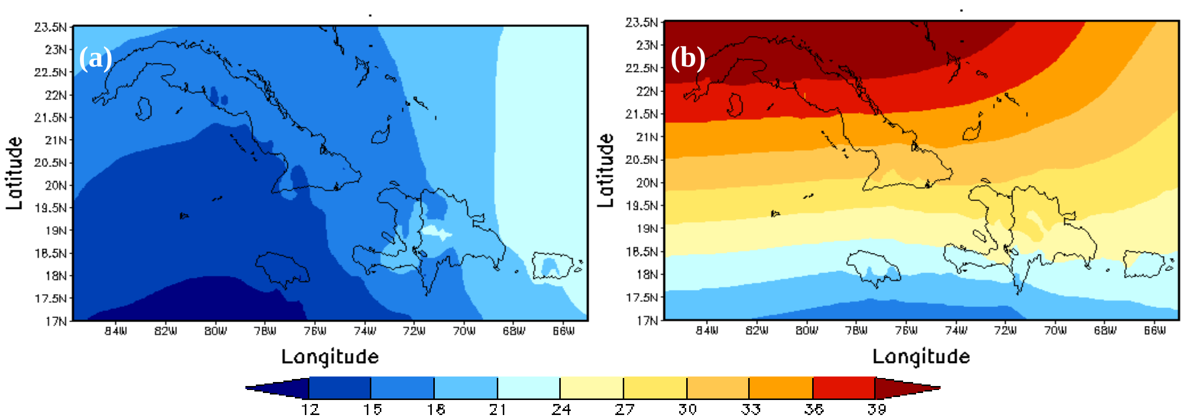

Figure 6.13 Vertical Wind Shear of RAMS. (a) Neutral data (March 1990), and (b) El Niño (March 1998) event data.

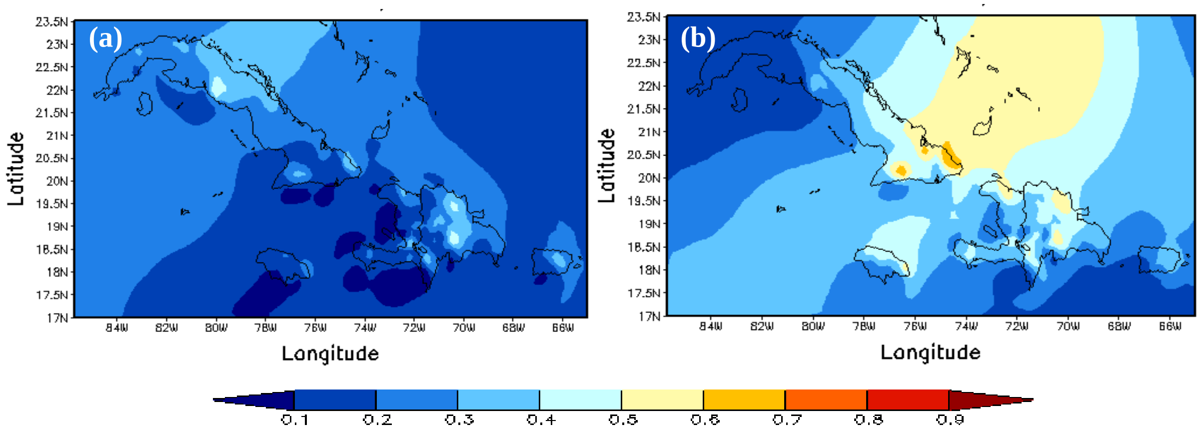

Figure 6.14 Cloud Cover Fraction of RAMS. (a) Neutral data (March 1990), and (b) El Niño (March 1998) event data.

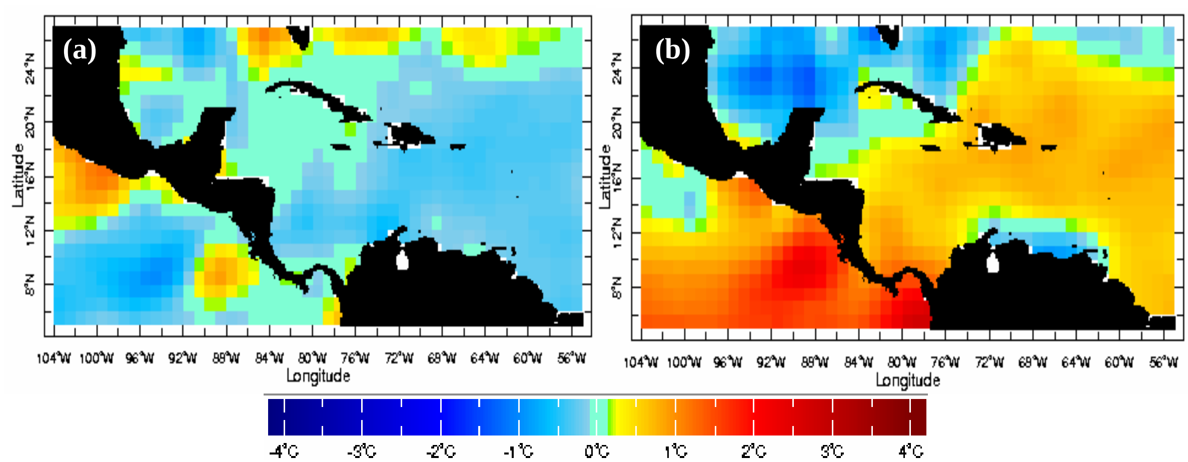

Figure 6.15 Sea Surface Temperature Anomaly observed. (a) Neutral data (March 1990), and (b) El Niño (March 1998) event data.

7 CONCLUSIONS AND FUTURE WORK

7.1 Conclusions

The statistical test was able to detect pulse change along the time series, being more efficient when it was used for annual time series. But in the monthly analysis the same change was also detected.

A significant increment during 1940 to 1960 and especially in December 1957 was reported to sunspot time series. No relations were found with any event registered.

Respect to the annual carbon dioxide, the stochastic behavior did not exhibit any change. But between 1985 until 1989 are observed several positive values which do not have the normal behavior of the rest and to this range of time (1985-1989) there were no significant eruptions.

Sunspot number and volcanic eruptions can not explain the global warming in the last century. Then, the concurrent global warming may be attributed to the anthropogenic causes such as high emission of CO_2 deposited over the Earth.

The sunspots and CO_2 exhibited a significant trend during the evaluated period, but the effect of carbon dioxide in the increase the air temperature is bigger than sunspot.

Global air temperature shows that the cold period started in 1964 and finished in 1979. The hottest period started on 2002 up to present time (2006). The Earth is heating specially with more intensity in the NH and this is the possible reason that Arctic sea is melting faster in this area.

The cooling effect registered in the Earth to the middle of the last century did not have relation with the volcanic eruption, other external forces created the cooling period.

The correlation between the global air temperature and the CO_2 time series the entire correlation between both series is of 29 % (1958-2005). But there is a correlation of 72% in the period 1958-1983 and other of 12% between 1984-2005. In addition, a poor correlation (19%) was found between the annual anomaly of the global air temperature and sunspot.

All Caribbean islands are increasing their AST, except Cuba, while Jamaica is warming faster than the rest of the islands. In addition, each island has a different AST behavior. However, the regional scales can have different results.

The minimum AST of Puerto Rico is increasing faster than maximum AST. The maximum AST was sensitive to El Niño event that occurred in 1982/1983. The maximum air temperature shows a climate change in March 1983. The minimum AST was also sensitive to

El Niño but of the 1997/1998 because finds a change in March 1998. The “difference analysis” shows the maximum AST begin to decrease from 1985 until now.

The lower cloud cover amount contributes to a lower incident radiation reflection resulting in an increment of the incoming energy. The decreasing cloud cover contributes to the imbalance of the energy on the earth. It has been pointed out that high cloud tended to warm the planet and low cloud cools the Earth. The decreasing trend of low cloud is contributing to the global warming.

The statistical test detected a change in the global middle cloud amount from October 1997 until February 1998 and in the Caribbean middle cloud amount was found in March 1998. There is evidence of a relation between El Niño 1997/1998 and the middle cloud amount.

The percent of decreasing Caribbean LCA is major than global LCA. With these characteristics more energy will fall over the Caribbean and it can explain why the rate of increase in the Caribbean is faster that Global AST.

The change detected in global and Caribbean Sea levels could be attributed to the thermal expansion as consequence of the excessive SST increase during El Niño event 1997/1998.

Simulation results show that the incident surface flux of longwave radiation, vertical wind shear and cloud cover fraction indicate an increment in March 1998 with respect to March 1990.

According to the simulation model the increase of middle cloud in March 1998 was caused by the increase of the SST and VWS. The increase of LW could be the cause of the increase of the minimum temperature in PR.

7.2 Future Work

To obtain data of minimum and maximum air surface temperature to Cuba, Republic Dominican, Haiti and Jamaica. Next, to each series applies the statistical analysis and to appreciate the climate behavior of the Caribbean region.

To apply the procedure statistical to detect a climate changes over more variables as sea surface temperature, ocean deep temperatures, aerosols and ozone time series, because these variables are important in the relation between atmosphere-ocean interactions.

To apply a new statistical technique which can detect change in tendency and to complement to the statistical analysis proposed in the present work. In this way, the specific date where a time series changes could be simulated.

To find the specifics months with the changed variables, to use RAMS to simulate these months and to understand the physical phenomena leading to the changes.

To find any relation between the changes of carbon dioxide behavior of year 1983 to 1985, the change in the temperature difference in PR and cloud cover in the same period. There is a probability that these changes are related.

REFERENCES

1. Angeles-Malaspina, Moisés E. 2005. An Assessment of Future Caribbean Climate Change Using "Business as Usual" Scenario by Coupling GCM Data and RAMs. Thesis of Master of Science in Mechanical Engineering, University of Puerto Rico-Mayagüez Campus.

2. Australian Government: Bureau of Meteorology, (2007), S.O.I. (Southern Oscillation Index) Archives, http://www.bom.gov.au/climate/current/soihtm1.shtml

3. Australia Government of Metrologic, (2007), Long Paddock, http://www.longpaddock.qld.gov.au/Products/AustraliasVariableClimate/ENSO-Year_Classification/index.html.

4. Barnett, T.P. Hasselman, K., M. Chelliah, T. Delworth, G. Hergel, P. Jones, E. Ramsmusson, E. Roeckner, C Ropelewski, B. Santer and S. Tett (1999), Detection and Attribution of Recent Climate Change: A Status Report, Bull. Am. Meteorol. Soc. Vol. 80 No. 12, December 1999.

5. Battisti D., Bitz M., Moritz R. (1997) Do General Circulation Models Underestimate the Natural Variability in the Arctic Climate? Journal Climate, Vol. 10: 1909 – 1920.

6. Box G. and Jenkins G., (1976), Time Series Analysis – Forecasting and Control, Holden-Day Inc.

7. Boston University, (2002), Overview of the Climate System, Climate and Vegetation Research Group, http://cybele.bu.edu/courses/gg312fall02/chap01/chap01.html

8. Brockwell, P. & Davis R. (2002), Introduction to Time Series and Forecasting, 2nd ed., Springer-Verlag New York, Inc.

9. Changnon S. A., Pielke R. A. Jr., Changnon D., Sylves R. T., and Pulwarty R., (2000) Human Factors Explain the Increased Losses from Weather and Climate Extremes; Bull. Am. Meteorol. Soc.; 81, 437 – 442.

10. Chatfield, C., (2004), The Analysis of Time Series: An Introduction, 6th ed., CRC Press LLC.

11. Chen J., Carlson B. and Del Genio A., (2002), Evidence for Strengthening of the Tropical General Circulation in the 1990s, Science, VOL 295: 838 – 841.

12. Church J., White N., Coleman R., Lambeck K. and Mitrovica J., (2004), Estimates of the Regional Distribution of Sea Level Rise over the 1950–2000 Period, Journal of Climate, Volume 17: 2609 – 2625.

13. Comarazamy, Daniel E., (2001), Atmospheric Modeling of the Caribbean Region: Precipitacion and Wind Analysis in Puerto Rico for April 1998, Thesis of Master of Science in Mechanical Engineering, University of Puerto Rico-Mayagüez Campus.

14. Demaria Mark, (1996), The Effect of Vertical Shear on Tropical Cyclone Intensity Change, Journal of the Atmospheric sciences, Vol. 53 Nº 14, 2076-2087.

15. Demenocal P., (2005), Science and Society, Department of Earth and Environmental Sciences - Columbia University, http://www.ldeo.columbia.edu/edu/dees/V1003/

16. Droxler A., (2005), Ocean and Global Change, Earth Science – Rice University, http://www.owlnet.rice.edu/~esci107/.

17. Easterling D. R., Horton B., Jones P. D., Peterson T. C., Karl T. R., Parker D. E., Salinger M. J., Razuvayev V., Plummer N., Jamason P. and Folland C. K., (1997), Maximum and Minimum Temperature Trends for the Globe; Science, 277, 364 – 367.

18. Easterling D. R., Meehl G. A., Parmesan C., Changnon S. A., Karl T. R. and Mearns L. O. (2000) Climate Extremes: Observations, Modeling, and Impacts; Science, 289, 2068 – 2074.

19. Feldstein, S. B. (2002). The Recent Trend and Variance Increase of the Annular Mode, Am. Meteorol. Soc. Vol., Vol. 15 No. 12, 1 January 2001.

20. Francis J. and Hunter E., (2006), New Insight Into the Disappearing Arctic Sea Ice, Eos, Vol. 87, No. 46.

21. Frich, P., L. V. Alexander, P. Della-Marta, B. Gleason, M. Haylock, A. Klein Tank, and T. Peterson, (2002) Observed coherent changes in climatic extremes during the second half of the twentieth century, Clim. Res., 19, 193–212.

22. Goldenberg S., Landsea C., Mestas-Nuñez A. and Gray W., (2001), The Recent Increase in Atlantic: Causes and Implications, Science, Vol. 293: 474 – 478.

23. Hanley D., Bourassa M., O'Brien J., Smith S., and Spade E., (2003), A Quantitative Evaluation of ENSO Indices, Journal of Climate, 16: 1249-1258.

24. Hansen, J (2005). A slippery slope: How much global warming constitutes "dangerous anthropogenic interference"? Climatic Change, 68: 269–279.

25. Hansen, J. and Ruedy, R., (1999) GISS Analysis of Surface Temperature Change, Journal of Geophysical Research, Vol. 104, NO. D24, pp 30,997–31,022.

26. Hartkamp D., De Beurs K., Stein A. and White W., (1999), Interpolation Techniques for Climate Variables, Sustainable Maize and Wheat Systems for the Poor, http://www.cimmyt.org/Research/nrg/pdf/NRGGIS%2099_01.pdf.

27. Huntingford C., Stott P., Allen M., and Lambert H., (2006) Incorporating model uncertainty into attribution of observed temperature change, Geophys. Res. Lett., Vol. 33, L05710.

28. Intergovernmental Panel on Climate Change, (2001): Climate Change: The Scientific Basic – Summary for Policymakers, Working Group I, Cambridge University Press.

29. Intergovernmental Panel on Climate Change, (2001), Climate Change: The Scientific Basis, Cambridge University Press.

30. Intergovernmental Panel on Climate Change, (2005), Special Report on Carbon Dioxide Capture and Storage, Summary for Policymakers and Technical Summary - Working Group III.

31. Intergovernmental Panel on Climate Change, (2007), Climate Change: Impacts, Adaptation and Vulnerability. Working Group II Contribution to the Fourth Assessment Report of IPCC.

32. Intergovernmental Panel on Climate Change, (2007), Climate Change: The Physical Science Basis - Summary for Policymakers. Working Group I to the Fourth Assessment Report of the IPCC.

33. Kalnay E. and Cai M., (2003), Impact of urbanization and land-use change on climate, Nature, 423: 528 – 531.

34. Kalnay E., Kanamitsu E., Kistler R., Collins W., Deaven D., Gandin L., Iredell M., Saha S., White G., Woollen J., Zhu Y., Chelliah M., Ebisuzaki W., Higgins W., Janowiak J., Mo K. C., Ropelewski C., Wang J., Leetmaa A., Reynolds R., Jenne Roy and Joseph D. (1996). The NCEP/NCAR 40-Year Reanalysis Project. Bull. Amer. Meteor. Soc., 77, 437-471.

35. Keeling, D. and Whorf T. (2005). Atmospheric CO2 records from sites in the SIO air sampling network. In Trends: A Compendium of Data on Global Change. Carbon Dioxide Information Analysis Center, Oak Ridge National Laboratory, U.S. Department of Energy, Oak Ridge, Tenn., U.S.A. Available in wet site: http://cdiac.ornl.gov/trends/co2/sio-mlo.htm.

36. Lean Judith, (2005), Living with a Variable Sun, Physics Today, June 2005, pp 32 – 38.

37. Leuliette, E., Nerem R., and G. Mitchum, (2004). Calibration of TOPEX/Poseidon and Jason altimeter data to construct a continuous record of mean sea level change. Marine Geodesy, 27(1-2), 79-94.

38. Levitus S., Antonov J., Boyer T. and Stephens C., (2000), Warming of the world oceans, Science, 287, 2225-2229.

39. Levitus S. Antonov J., and Boyer T., (2005), Warming of the world ocean, 1955-2003, Geophysical Research Letters, 32, L02604.

40. Lombard A., Cazenave1 A., Yves Le Traon P., Guinehut S. and Cabanes C., (2006), Perspectives on present-day sea level change: a tribute to Christian le Provost, Ocean Dynamics, Vol. 56: 445-451.

41. Maes, C., J. Picaut and S. Belamari, (2005), Importance of salinity barrier layer for the buildup of El Niño. Journal of Climate, Volume 18: 104-118.

42. Meehl G., Washington W., Wigley T., Arblaster J., and Dai A., (2003), Solar and Greenhouse Gas Forcing and Climate Response in the Twentieth Century, Journal of Climate, Volume 16: 426 – 444.

43. Meehl G., Washington W., Ammann C., Arblaster J., Wigley T., and Tebaldi C., (2004), Combinations of Natural and Anthropogenic Forcings in Twentieth-Century Climate, Journal of Climate, Volume 17: 3721 – 3727.

44. Menne, Matthew J., (2005), Abrupt Global Temperature Change and the Instrumental Record, 85th AMS Conference, P4.3.

45. Milly P., Cazenave A. and Gennero M., (2003), Contribution of climate-driven change in continental water storage to recent sea-level rise, PNAS, Vol.:100: 13158–13161.

46. Miranda P. and Tomé A. (2005), Piecewise linear fitting and trend changing points of climate parameters, 85th AMS Conference, P1.9.

47. Montgomery, D. (2001), Introduction to Statistical Quality Control, 4th Edition, John Wiley & Sons, Inc.

48. Moran J., (2002), Online Weather Studies, 2th Edition, American Meteorological Society.

49. National Oceanic and Atmospheric Administration's, Earth system Research laboratory – Physical Sciences Division, (2007) Multivariate ENSO Index (MEI), http://www.cdc.noaa.gov/people/klaus.wolter/MEI/mei.html

50. National Oceanic and Atmospheric Administration's, National Weather Service – Climate Prediction Center, (2007) Cold & Warm Episodes by Season, http://www.cpc.noaa.gov/products/analysis_monitoring/ensostuff/ensoyears.shtml

51. National Technical Information Service, (1984), Atmospheric Science and Power Production, U.S. Department of Energy.

52. Oku, Y., Ishikawa, H., Haginoya, S., Ma, Y., (2006): Recent Trends in Land Surface Temperature on the Tibetan Plateau. Journal of Climate, Vol. 19 Issue 12, p 2995-3003.

53. Peterson T., Taylor M., Demeritte R., Duncombe D., Burton S., Thompson F., Porter A., Mejia M., Villegas E., Semexant Fils R., Klein Tank A., Martis A., Warner R., Joyette A., Mills W., Alexander L., and Gleason B., (2002), Recent changes in climate extremes in the Caribbean region, Journal of Geophysical Research, VOL. 107, NO. D21, 4601.

54. Quispe, W. (2006). Sieve Bootstrap en Series de Tiempo de Nubosidad en el Caribe. Tesis de Maestria en Ciencias en Matematica, Universidad de Puerto Rico-Recinto de Mayagüez.

55. Quality America Inc. (2007), When to Use an EWMA Chart, Quality Publishing, http://www.qualityamerica.com/.

56. Ramirez N. and Julca O. (2006), Detection of a Local Climate Change, 86th AMS Conference, P2.14.

57. Ramirez, N., and Sastri, T., (1997), Transient Detection with an Application to a Chemical Processes, Computer and Industrial Engineering, 32, No. 4, pp 891-908.

58. Reck Ruth, (1993), Overview of Global Greenhouse Effects, U.S. Department of Energy, Office of Energy Research, Office of Health and Environmental Research. http://www.osti.gov/bridge/servlets/purl/10192250-PTINyH/10192250.PDF.

59. Retana, J. & Villalobos, R (2003). "Impacto social del fenómeno El Niño: Un recuento de 1977 - 1978", Top. Meteoro. Oceanog. 10 (1) 36-40.

60. Roberts, S. W. (1959), Control Chart Tests Based on Geometric Moving Averages, Technometrics, Vol. 1.

61. Robock A. (2000). Volcanic Eruptions and Climate, Reviews of Geophysics, 38, 2: 191–219.

62. Rossow, W.B. and Schiffer, R.A. (1999). Advances in understanding clouds from ISCCP. Bulletin of American Meteorological Society, 80, 2261-2287.

63. Salinger, M. J. (2005), "Climate Variability and Change: Past, Present and Future – an overview", Climate Change, 70: 9-29.

64. Santer B. D., Wigley T. M. L., Mears C., Wentz F. J, Klein S. A., Seidel D. J., Taylor K. E., Thorne P. W., Wehner M. F., Gleckler P. J., Boyle J. S., Collins W. D., Dixon K. W., Doutriaux C., Free M., Fu Q., Hansen J. E., Jones G. S., Ruedy R., Karl T. R., Lanzante J. R., Meehl G. A., Ramaswamy V., Russell G. and Schmidt G. A., (2005) Amplification of Surface Temperature Trends and Variability in the Tropical Atmosphere, Science, 309: 1551 – 1556.

65. Schar C, Vidale Pl, Luthi D, Frei C, Haberli C, Liniger MA, and C. Appenzeller, (2004); The role of increasing temperature variability in European summer heatwaves; Nature, 427: 332-335.

66. She C., Krueger D., (2004), Impact of natural variability in the 11-year mesopause region temperature observation over Fort Collins, CO (41_N, 105_W), Advances in Space Research, Vol. 34, 330–336.

67. Smith R., Wigley T. and Santer B. (2002), A Bivariate Time Series Approach to Anthropogenic Trend Detection in Hemispheric Mean Temperatures. Journal of Climate, 16: 1228 – 1240.

68. Stott P. and Kettleborough J., (2002). Origins and estimates of uncertainty in predictions of twenty-first century temperature rise, Nature, Vol. 416: 723 – 726.

69. Stott P., Mitchell J., Allen M., Delworth T., Gregory J., Meehl G., and Santer B., (2006), Incorporating model uncertainty into attribution of observed temperature change, Journal of Climate, Volume 19: 3055 – 3069.

70. US Global Change Research Program, (2000), Climate Change Impacts on the United States: The Potential Consequences of Climate Variability and Change, http://www.usgcrp.gov/usgcrp/Library/nationalassessment/overviewclimate.htm.

71. Velazquez L, Alexander, (2002), Urban Heat Island Effect Analysis for San Juan, Puerto Rico, Thesis of Master of Science in Mechanical Engineering, University of Puerto Rico-Mayagüez Campus.

72. Vecchi G. and Harrison D., (2006), The Termination of the 1997–98 El Niño. Part I: Mechanisms of Oceanic Change, Journal of Climate, Volume 19: 2633 – 2646.

73. Vinnikov K., Robock A., Stouffer R., Walsh J., Parkinson C., Cavalieri D., Mitchell J., Garrett D., Zakharov V. (1999). Global Warming and Northern Hemisphere Sea Ice Extent, SCIENCE, Vol. 286: 1934 – 1937.

74. Walko R., and Tremback C. (2006), Regional Atmospheric Modeling System, Model Input Namelist Parameters, http://www.atmet.com/html/docs/rams/ug60-model-namelist-1.4.pdf.

75. Walko R., Tremback C. and Hertenstein R. (1995), Regional Atmospheric Modeling System, User's Guide 3b, http://www.atmet.com/html/docs/rams/user_3b.ps.

76. Weier J., (2003), A Delicate Balance, Signs of Change in the Tropics, NASA – Earth Observatory. http://eobglossary.gsfc.nasa.gov/Study/DelicateBalance/balance.html.

APPENDIX A

Find the change in an uncorrelated or correlated time series

```
% The simulation of ARIMA (p, q) model, where p and/or q can be any value
% equal o major than 0.
clear, clc
close all
global TIME
global fuertes
global qqq
load dat.txt
data=dat(:,11); % Here the anomaly variable is selected, where the seasonal
                % and tendency component are eliminated and its ARMA model
                % is already identifying.
x=data;
back_value=5; % Value to put the change detected
%%%%%%%%%%%%%%%%%%%%%%%%%%%%%%%%%%%%%%%%%
%%%%%%%%%%%THIS IS APPLIED TO MONTHLY ANALYSIS%%%%%%%%%
% For this month time series an ARMA (2, 1) model is fitting.
p=2; %AR
q=1; %MA
filename='JA_total'; % The name with the result will be save
variable_title='Jamaica Mean Temp.'; % The title of the variable
year_init=1948; % Year when the series begging
months_init=1; % Month when the series begging
year_finl=2005; % Year when the series ending
months_finl=12; % Month when the series ending
time=year_series(months_init,year_init,months_finl,year_finl); % Function to obtain a year
                                                                %time series
find_change=changes_monthly(x,p,q,time,TIME, back_value,filename, variable_title);
% This is the function employed to detected a change in monthly time series.
%============================================================
%============================================================

%%%%%%%%%%%%%%%%%%%%%%%%%%%%%%%%%%%%%%%%%
%%%%%%%%%%%THIS IS APPLIED TO ANNUAL ANALYSIS%%%%%%%%%
% For this annual time series an ARMA (0, 1) model is fitting.
p=0; %AR
q=1; %MA
filename='JA_annually'; % The name with the result will be save
```

```
% variable_title='Annual Jamaica Mean Temp.'; % The title of the variable selected
serie=x;x=[]; % The same monthly series is selected to convert to annual series
for i=1:12 % Number of months
   eval(['Y' num2str(i) '=serie(i:12:end);']);
end
% %annual (Jan-Dec),winter (Dec-Feb),spring (Mar-May), summer (Jun-Aug),
% %autumn (Sep-Nov),warm (May-Oct), cold (Nov-Apr) and hurricane (Jun-Nov).
n=length(Y12);
for i=2:n
   s1(i-
1)=(Y1(i)+Y2(i)+Y3(i)+Y4(i)+Y5(i)+Y6(i)+Y7(i)+Y8(i)+Y9(i)+Y10(i)+Y11(i)+Y12(i))/12;
%anual
    s2(i-1)=(Y12(i-1)+Y1(i)+Y2(i))/3;% invierno
    s3(i-1)=(Y3(i)+Y4(i)+Y5(i))/3;%primavera
    s4(i-1)=(Y6(i)+Y7(i)+Y8(i))/3;%verano
    s5(i-1)=(Y10(i)+Y11(i)+Y9(i))/3;%otoño
    s6(i-1)=(Y5(i)+Y6(i)+Y7(i)+Y8(i)+Y9(i)+Y10(i));%caliente
    s7(i-1)=(Y11(i-1)+Y12(i-1)+Y1(i)+Y2(i)+Y3(i)+Y4(i));%frio
    s8(i-1)=(Y6(i)+Y7(i)+Y8(i)+Y9(i)+Y10(i)+Y11(i));%huracanes
 end
 for i=1:12
    eval(['clear Y' num2str(i) '']);
 end
 ann_series=[s1' s2' s3' s4' s5' s6' s7' s8']; % Until here the annual series are obtained in the %
following order: annual, winter, spring, summer, autumn, warm, cold and hurricane.
 x=ann_series(:,1); % The annual time series is selected
 TIME=1949:2005;time=TIME;
 find_change=changes_annually(x,p,q,time,TIME, back_value,filename, variable_title);
% This is the function employed to detected a change in annual time series.
%=====================================================================
%=====================================================================

eval(['save ' filename ' fuertes cambios']) % here the values where a change is detected are
saved.
```

APPENDIX A1

Description of "changes_monthly" function

```
function find_change=changes_monthly(x,p,q,time,TIME, back_value,filename,
variable_title)
global fuertes
global qqq
```

```
%%%%%%%%%%%%%%%%%%%%%%%%%%%%%%%%%%%%%%%%%%%%%%%
%%%%%%%%% %%%% Identification ARMA model (p, q)%%%%%%%%%%%%
%  A(q) y(t) = [B(q)/F(q)] u(t-nk) + [C(q)/D(q)] e(t)
w=x;  % The variable is selected
[n,c]=size(x);
nb=1;      % it must be included always
nc=q;      % nc= orden MA
nd=p;      % nd= orden AR
cambios=[];fuertes={};
M=36:12:120; % Number of baseline to each model

for qqq=1:length(M)
   if nc>0 | nd>0 % Here they are selected the correlated series
      % m=input('Enter window size for model fitting (before detection ) m > 50 and < n  ' )
      m=M(qqq);
      nf=0;
      nk=0;
      nn=[nb nc nd nf nk];
      y1=w(1:m);         % data to model fitting
      cero1=zeros(m,1);   % zeros for model fitting, so the another input (to Box
                  % -Jenkins) is considered zeros and it is easy model a
                  % ARMA model
      z1=[y1 cero1];      % input for model fitting
      mo1=bj(z1,nn);      % model fitting
      y2=w(m+1:n);      % data for forecasting
      m2=n-m;          % m2 values to predict n=total number of values m=values to fit
      cero2=zeros(m2,1);  % ceros to forecast
      z2=[y2 cero2];        % data for forecast
      z3=[z1; z2];       % data using in fitting and forecast
      w_est=predict(mo1,z3,1);    % estimation of the simulated process
      e=w - w_est;    % noise to introduce ewma

%%%%%%%%%%%%%%%%%%%%%%%%%%%%%%%%%%%%%%%%%%%%%%%

%%%%% %%%%%%%% Parameters for EWMA %%%%%%%%%%%%%%%%%%%%

      e_m=e(1:m);     % noise to design control limits
      mu=mean(e_m);
      sig=std(e_m);
      LL=3;
      lambda=0.2;
      U(1)=0;
      L(1)=0;
```

```
    ew(1)=mu;
    UI=[];
    LI=[];
    fuer=[];
    for i=2:n
      sq=sqrt(lambda/(2-lambda)*(1-(1-lambda)^(2*i)));
      U(i)=mu+LL*sig*sq;
      L(i)=mu-LL*sig*sq;
      ew(i)=lambda*e(i)+(1-lambda)*ew(i-1);
      if ew(i)>U(i)
        UI=[UI;ew(i) TIME(i,:)];
        fuer=[fuer; time(i) ew(i) i];
      end
      if ew(i)<L(i)
        LI=[LI;ew(i) TIME(i,:)];
        fuer=[fuer; time(i) ew(i) i];
      end
    end
    if length(UI)>0
      [B,IX] = sort(UI(:,1),'descend');
      UI_2=(UI(IX,:));IX=[];
    else
      UI_2=zeros(1,3);
    end
    if length(LI)>0
      [B,IX] = sort(LI(:,1),'ascend');
      LI_2=(LI(IX,:));IX=[];
    else
      LI_2=zeros(1,3);
    end
    mu=mu*ones(1,n);
  else % Here they are selected the uncorrelated series
    % m=input('Enter the baseline to the model (before detection ) m > 50 and < n  ' )
    m=M(qqq);
    e=x;
%%%%%%%%%%%%%%%%%%%%%%%%%%%%%%%%%%%%%%%%

%%%%% %%%%%%%% Parameters for EWMA %%%%%%%%%%%%%%%%%%%%

    e_m=e(1:m);     % noise to desing control limits
    mu=mean(e_m);
    sig=std(e_m);
    LL=3;
```

```
    lambda=0.2;
    U(1)=0;
    L(1)=0;
    ew(1)=mu;
    UI=[];
    LI=[];
    fuer=[];
    valores=[];
    for i=2:n
        sq=sqrt(lambda/(2-lambda)*(1-(1-lambda)^(2*i)));
        U(i)=mu+LL*sig*sq;
        L(i)=mu-LL*sig*sq;
        ew(i)=lambda*e(i)+(1-lambda)*ew(i-1);
        if ew(i)>U(i)
            UI=[UI;ew(i) TIME(i,:)];
            fuer=[fuer; time(i) ew(i) i];
        end
        if ew(i)<L(i)
            LI=[LI;ew(i) TIME(i,:)];
            fuer=[fuer; time(i) ew(i) i];
        end
    end
    if length(UI)>0
        [B,IX] = sort(UI(:,1),'descend');
        UI_2=(UI(IX,:));IX=[];
    else
        UI_2=zeros(1,3);
    end
    if length(LI)>0
        [B,IX] = sort(LI(:,1),'ascend');
        LI_2=(LI(IX,:));IX=[];
    else
        LI_2=zeros(1,3);
    end
    mu=mu*ones(1,n);
end

figure(1)
plot(time,w,'LineWidth',2)
title({['Anomaly: ', variable_title,];['Model ARMA (',num2str(p),','...
    ,num2str(q),')']},'FontSize',25)
xlabel('Time','FontSize',20)
```

```
ylabel('Variation','FontSize',20)
set(gca,'fontsize',18)
figure(2)
if length(fuer)>0
   plot(time,ew,'b',time,mu,'g',time,U,'r',time,L,'r')
   hline1 = line(time,ew,'LineWidth',2);
   text(fuer(1,1),fuer(1,2),[,num2str(TIME(fuer(1,3),1)),'/'...
      ,num2str(TIME(fuer(1,3),2)), ],...
   'Position',[time(fuer(1,3)- back_value), fuer(1,2)],'FontSize',18)
   title({[' EWMA Chart for the ', variable_title,];['Baseline: '...
      ,num2str(m),' months']},'FontSize',25)
   xlabel('Time','FontSize',20)
   ylabel('EWMA','FontSize',20)
   set(gca,'fontsize',18)
   hold on
   [oo pp]=size(fuer);
   for i=1:oo;
      plot(fuer(i,1),fuer(i,2),'*r')
      hold on
   end
   newname1=[num2str(m) '_' filename '_' num2str(TIME(fuer(1,3),1)) '_'...
       num2str(TIME(fuer(1,3),2)) '_orig_data'];
   newname_1=[num2str(m) '_' filename '_' num2str(TIME(fuer(1,3),1)) '_'...
       num2str(TIME(fuer(1,3),2)) '_orig_data.eps'];
   saveas(1,[newname1],'jpg')
   saveas(1,[newname_1],'psc2')
   newname2=[num2str(m) '_' filename '_' num2str(TIME(fuer(1,3),1)) '_'...
       num2str(TIME(fuer(1,3),2)) '_EWMA'];
    newname_2=[num2str(m) '_' filename '_' num2str(TIME(fuer(1,3),1)) '_'...
       num2str(TIME(fuer(1,3),2)) '_EWMA.eps'];
   saveas(2,[newname2],'jpg')
   saveas(2,[newname_2],'psc2')
   cambios=[cambios;TIME(fuer(1,3),1) TIME(fuer(1,3),2)];
else
   plot(time,ew,'b',time,mu,'g',time,U,'r',time,L,'r')
   hline1 = line(time,ew,'LineWidth',2);
   title({[' EWMA Chart for the ', variable_title,];['Baseline: '...
      ,num2str(m),' months']},'FontSize',25)
   xlabel('Time','FontSize',20)
   ylabel('EWMA','FontSize',20)
   newname1=[num2str(m) '_' filename '_nochange_orig_data'];
   newname_1=[num2str(m) '_' filename '_nochange_orig_data.eps'];
```

```
        saveas(1,[newname1],'jpg')
        saveas(1,[newname_1],'psc2')
        newname2=[num2str(m) '_' filename '_nochange_EWMA'];
        newname_2=[num2str(m) '_' filename '_nochange_EWMA.eps'];
        saveas(2,[newname2],'jpg')
        saveas(2,[newname_2],'psc2')
        fuer=zeros(1,2);
        cambios=[cambios; fuer(1,:)];
    end
    fuertes{qqq,1}={UI_2;LI_2};
    fuertes{qqq,2}=mu(1);
    fuer=[];mu=[];U=[];L=[];ew=[];e=[];UI_2=[];LI_2=[];
    close all
end

% All figures are saved in the concurrent directory.
```

The same procedure is made to annual analysis.

APPENDIX A2

Description of "year_series(months_init, year_init, months_finl, year_finl)" function

```
function time=year_series(months_init,year_init,months_finl,year_finl)
global TIME
years=(year_init:year_finl)';
MESES=(1:12)';
meses=MESES/12;
time=[];TIME=[];
for i=1:length(years)
    t=years(i)*ones(12,1);
    TIME=[TIME;t MESES];
    time=[time;t+meses];
end
dif=12-months_finl;
time=time(months_init:end-dif);
TIME=TIME(months_init:end-dif,:);
```

APPENDIX B
Localization Caribbean Stations

TABLE B.1 The number of station data from the Caribbean area.

COUNTRY	No.	CODE	DUP.	YEAR		NAME STATION	LOCALIZATION	
				BEG.	END		Latitude	Longitude
CUBA	1	(4067) 831-0000	0	1952	1970	CABO SAN ANTO	21.87	-84.95
			1	1971	1980	CABO SAN ANTO	21.87	-84.95
	2	(4067) 831-3000	0	1952	1981	ISABEL RUBIO,	22.17	-84.1
	3	(4067) 831-7000	0	1952	1981	PASO REAL DE	22.55	-83.3
			1	1971	1980	PASO REAL DE	22.55	-83.3
	4	(4067) 832-5000	0	1899	1991	CASA BLANCA,	23.17	-82.35
			1	1951	1990	CASA BLANCA,	23.17	-82.35
			2	1971	1980	CASA BLANCA,	23.17	-82.35
			3	1987	1995	CASA BLANCA,	23.17	-82.35
	5	(4067) 834-3001	0	1961	1980	SANTA CLARA /UNIV.	22.43	-79.9
	6	(4067) 834-8000	0	1952	1981	CAIBARIEN, VI	22.52	-79.45
	7	(4067) 834-9000	0	1961	1981	SANCTI SPIRIT	21.93	-79.45
			1	1971	1980	SANCTI SPIRIT	21.93	-79.45
	8	(4067) 835-3000	0	1952	1981	NUEVITAS,CAMA	21.53	-77.25
	9	(4067) 835-5000	0	1961	1981	CAMAGUEY, CAM	21.4	-77.85
			1	1971	1980	CAMAGUEY, CAM	21.4	-77.85
			2	1961	1970	CAMAGUEY, CAM	21.4	-77.85
	10	(4067) 836-0000	0	1952	1981	CABO CRUZ, GR	19.85	-77.23
			1	1971	1980	CABO CRUZ, GR	19.85	-77.23

	11	(4067) 836-4001	0	1961	1980	SANTIAGO DE CUBA/UNIV	20.05	-75.82
	12	(4067) 836-7000	0	1945	2003	GUANTANAMO,OR	19.9	-75.13
			1	1946	1981	GUANTANAMO,OR	19.9	-75.13
			2	1961	1970	GUANTANAMO,OR	19.9	-75.13
	13	(4067) 836-8001	0	1971	1980	GUANTANAMO/INST.TEC.	20.13	-75.2
	14	(4067) 836-9000	0	1952	1981	PUNTA DE MAIS	20.25	-74.15
			1	1971	1980	PUNTA DE MAIS	20.25	-74.15
DOMINICAN REPUBLIC	1	(4077) 845-1001	0	1961	1980	MONTE CRISTI	19.85	-71.63
			1	1951	1960	MONTE CRISTI	19.85	-71.63
	2	(4077) 845-8001	0	1951	1990	PUERTO PLATA	19.8	-70.7
	3	(4077) 846-0000	0	1961	1981	SANTIAGO	19.47	-70.7
	4	(4077) 846-0001	0	1961	1970	JARABACOA	19.12	-70.63
	5	(4077) 846-0002	0	1951	1970	LA VEGA DOMINICAN REPUBLIC	19.2	-70.5
			1	1971	1980	LA VEGA DOMINICAN REPUBLIC	19.2	-70.5
	6	(4077) 846-0003	0	1951	1970	SAN FRANCISCO DE MACORIS D	19.3	-70.3
	7	(4077) 846-0004	0	1961	1970	SAN JOSE DE LAS MATAS	19.33	-70.93
	8	(4077) 846-0005	0	1961	1970	MONCION	19.4	-71.15
	9	(4077) 846-0006	0	1951	1970	VALVERDE MAO DOMINICAN ZEP	19.6	-71.1
			1	1971	1980	VALVERDE MAO DOMINICAN ZEP	19.6	-71.1
	10	(4077) 846-4001	0	1971	1980	SANTIAGO DE LOS CABAL	19.43	-69.77
	11	(4077) 846-4002	0	1961	1980	CABRERA	19.63	-69.9
	12	(4077) 846-6001	0	1951	1970	SANCHEZ DOMINICAN REPUBLIC	19.2	-69.6
			1	1971	1980	SANCHEZ DOMINICAN REPUBLIC	19.2	-69.6
	13	(4077) 846-6002	0	1951	1970	SAMANA DOMINICAN REPUBLIC	19.2	-69.3
			1	1971	1980	SAMANA DOMINICAN REPUBLIC	19.2	-69.3
	14	(4077) 846-7000	0	1951	1981	SABANA DE LA	19.05	-69.38
			1	1971	1980	SABANA DE LA	19.05	-69.38
	15	(4077) 846-7001	0	1952	1970	EL SEYBO DOMINICAN REPUBLI	18.8	-69
			1	1971	1980	EL SEYBO DOMINICAN REPUBLI	18.8	-69

	16	(4077) 847-0001	0	1952	1970	NEYBA DOMINICAN REPUBLIC	18.5	-71.4
	17	(4077) 847-0002	0	1951	1970	SAN JUAN DE LA MAGUANA DOM	18.8	-71.2
			1	1971	1980	SAN JUAN DE LA MAGUANA DOM	18.8	-71.2
	18	(4077) 847-0003	0	1961	1980	CONSTANZA	18.9	-70.73
			1	1961	1970	CONSTANZA	18.9	-70.73
	19	(4077) 847-3001	0	1951	1970	MONTE PLATA DOMINICAN REPU	18.8	-69.8
			1	1971	1980	MONTE PLATA DOMINICAN REPU	18.8	-69.8
	20	(4077) 847-3002	0	1961	1980	COTUI	19.05	-70.13
			1	1961	1970	COTUI	19.05	-70.13
	21	(4077) 847-9001	0	1951	1970	LA ROMANA DOMINICAN REPUBL	18.4	-69
			1	1971	1980	LA ROMANA DOMINICAN REPUBL	18.4	-69
	22	(4077) 847-9002	0	1951	1981	CABO ENGANO DOMINIC	18.62	-68.33
			1	1971	1980	CABO ENGANO DOMINIC	18.62	-68.33
	23	(4077) 848-2000	0	1954	1981	BARAHONA	18.22	-71.1
			1	1971	1980	BARAHONA	18.22	-71.1
	24	(4077) 848-2001	0	1951	1970	AZUA DOMINICAN REPUBLIC	18.5	-70.7
	25	(4077) 848-4001	0	1951	1970	SAN CRISTOBAL DOMINICAN RE	18.4	-70.1
			1	1971	1980	SAN CRISTOBAL DOMINICAN RE	18.4	-70.1
	26	(4077) 848-5000	0	1971	1980	LAS AMERICAS	18.43	-69.67
	27	(4077) 848-5001	0	1952	1970	SAN PEDRO DE MACORIS DOMIN	18.5	-69.3
			1	1971	1980	SAN PEDRO DE MACORIS DOMIN	18.5	-69.3
	28	(4077) 848-6000	0	1951	1991	SANTO DOMINGO	18.43	-69.88
			1	1961	1970	SANTO DOMINGO	18.43	-69.88
			2	1987	2004	SANTO DOMINGO	18.43	-69.88
HAITI	1	(4117) 843-9000	0	1899	1967	PORT-AU-PRINC	18.57	-72.3
			1	1991	1993	PORT-AU-PRINC	18.57	-72.3
JAMAICA	1	(4137) 838-7001	0	1931	1960	NEGRIL POINT LIGHTHOUSE JA	18.3	-78.4
			1	1961	1970	NEGRIL POINT LIGHTHOUSE JA	18.3	-78.4
	2	(4137) 838-8000	0	1938	1991	MONTEGO BAY/S	18.5	-77.92

			1	1962	1990	MONTEGO BAY/S	18.5	-77.92
			2	1987	2005	MONTEGO BAY/S	18.5	-77.92
	3	(4137) 839-7000	0	1943	1991	KINGSTON/NORM	17.93	-76.78
			1	1955	1990	KINGSTON/NORM	17.93	-76.78
			2	1987	2005	KINGSTON/NORM	17.93	-76.78
	4	(4137) 839-7001	0	1961	1970	CINCHONA GARDENS JAMAICA	18.1	-76.7
	5	(4137) 839-9000	0	1951	1970	MORANT POINT	17.92	-76.18
PUERTO RICO	1	(4357) 852-6000	0	1899	1991	SAN JUAN/INT.	18.43	-66
			1	1955	2005	SAN JUAN/INT.	18.43	-66
			2	1951	1990	SAN JUAN/INT.	18.43	-66
			3	1961	1980	SAN JUAN/INT.	18.43	-66
			4	1945	1962	SAN JUAN/INT.	18.43	-66
			5	1984	1993	SAN JUAN/INT.	18.43	-66
	2	(4357) 852-6003	0	1899	1960	AGUIRRE PUERTO RIC	18	-66.2
	3	(4357) 852-6004	0	1951	1980	PONCE	18.02	-66.57
	4	(4357) 852-6005	0	1951	1970	LAJAS SUBSTATION PUERTO RI	18.1	-67.1
			1	1971	1980	LAJAS SUBSTATION PUERTO RI	18.1	-67.1
	5	(4357) 852-6006	0	1951	1979	BARRANQUITAS	18.17	-66.32
	6	(4357) 852-6007	0	1899	1970	MAYAGUEZ PUERTO RIC	18.2	-67.1
			1	1971	1980	MAYAGUEZ PUERTO RIC	18.2	-67.1
	7	(4357) 852-6008		1951	1980	JUNCOS	18.25	-65.92
	8	(4357) 852-6010	0	1951	1970	COLOSO	18.38	-67.15
			1	1951	1970	COLOSO	18.38	-67.15
		(4357) 852-6011	0	1971	1980	COLOSO	18.38	-67.15
	9	(4357) 852-6012	0	1951	1980	ISABELA SUBSTATION	18.47	-67.07
	10	(4357) 852-6013	0	1951	1980	ARECIBO	18.47	-66.7
	11	(4357) 852-6014	0	1949	1970	BORINQUEN/AIRPORT	18.5	-67.13
	12	(4357) 853-5002	0	1971	1980	HUMACAO	18.13	-65.83
	13	(4357) 853-5003	0	1947	2003	ROOSEVELT ROADS	18.25	-65.63
	14	(4357) 853-5004	0	1899	1970	FAJARDO PUERTO RIC	18.3	-65.7

			1	1971	1980	FAJARDO PUERTO RIC	18.3	-65.7
	15	24256	1	1970	2005	ADJUNTAS SUBSTATION	18.17	-66.8
	16	24224	1	1969	1980	AGUIRRE	17.97	-66.22
	17	24260	1	1906	1966	AIBONITO 1 S	18.13	-66.26
	18	24262	1	1931	1999	ARECIBO 3 ESE	18.45	-66.67
	19	24264	1	1980	2005	ARECIBO OBSERVATORY	18.35	-66.75
	20	24283	1	1955	2005	CANOVANAS	18.38	-65.89
	21	24290	1	1955	2002	CAYEY 1 E	18.11	-66.15
	22	24293	1	1969	2005	CERRO MARAVILLA	18.16	-66.56
	23	24297	1	1899	2005	COLOSO	18.38	-67.16
	24	24300	1	1931	2005	COROZAL SUBSTATION	18.33	-66.36
	25	24304	1	1931	2005	DORADO 2 WNW	18.47	-66.31
	26	24305	1	1937	2005	DOS BOCAS	18.34	-66.67
	27	24308	1	1931	1996	FAJARDO	18.31	-65.65
	28	24316	1	1911	2005	GUAYAMA 2 E	17.98	-66.09
	29	24321	1	1957	2005	GURABO SUBSTATION	18.26	-65.99
	30	24324	1	1931	1996	HUMACAO 2 SSE	18.13	-65.82
	31	24327	1	1901	2005	ISABELA SUBSTATION	18.46	-67.16
	32	24334	1	1931	2005	JUANA DIAZ CAMP	18.05	-66.5
	33	24335	1	1931	2005	JUNCOS 1 SE	18.23	-65.91
	34	24337	1	1900	2005	LAJAS SUBSTATION	18.03	-67.07
	35	24340	1	1903	1991	LARES	18.28	-66.88
	36	24343	1	1959	2005	MAGUEYES ISLAND	17.97	-67.05
	37	24344	1	1900	2005	MANATI 2 E	18.43	-66.47
	38	24346	1	1969	2005	MARICAO 2 SSW	18.15	-66.99
	39	24349	1	1899	2003	MAUNABO	18.01	-65.9
	40	24351	1	1957	2005	MAYAGUEZ AIRPORT	18.25	-67.15
	41	24350	1	1900	2005	MAYAGUEZ CITY	18.19	-67.14
	42	24355	1	1980	2005	MONA ISLAND 2	18.03	-66.53
	43	24370	1	1969	2005	PICO DEL ESTE	18.27	-65.76
	44	24374	1	1954	2005	PONCE 4 E	18.03	-66.53

	45	24379	1	1955	2000	QUEBRADILLAS	18.47	-66.94
	46	24382	1	1968	2005	RINCON	18.34	-67.25
	47	24389	1	1959	2005	RIO PIEDRAS EXP STN	18.39	-66.05
	48	24400	1	1957	2005	SAN JUAN WSFO AP	18.44	-66
	49	24405	1	1955	1997	SAN SEBASTIAN 2 WNW	18.35	-67.01
	50	24410	1	1982	2005	TORO NEGRO FOREST	18.17	-66.49
	51	24412	1	1957	2005	TRUJILLO ALTO 2 SSW	18.33	-66.02
	52	24413	1	1931	2002	UTUADO	18.26	-66.69
	53	24417	1	1955	1995	YABUCOA 1 NNE	18.06	-65.87

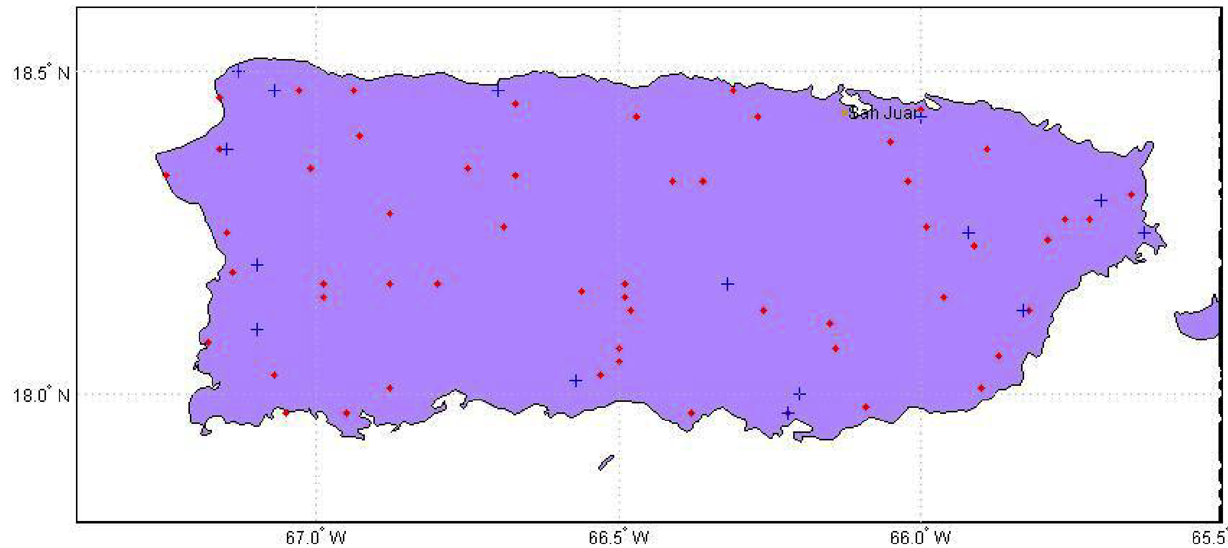

Figure B.1 Localization of 53 Puerto Rico Stations.

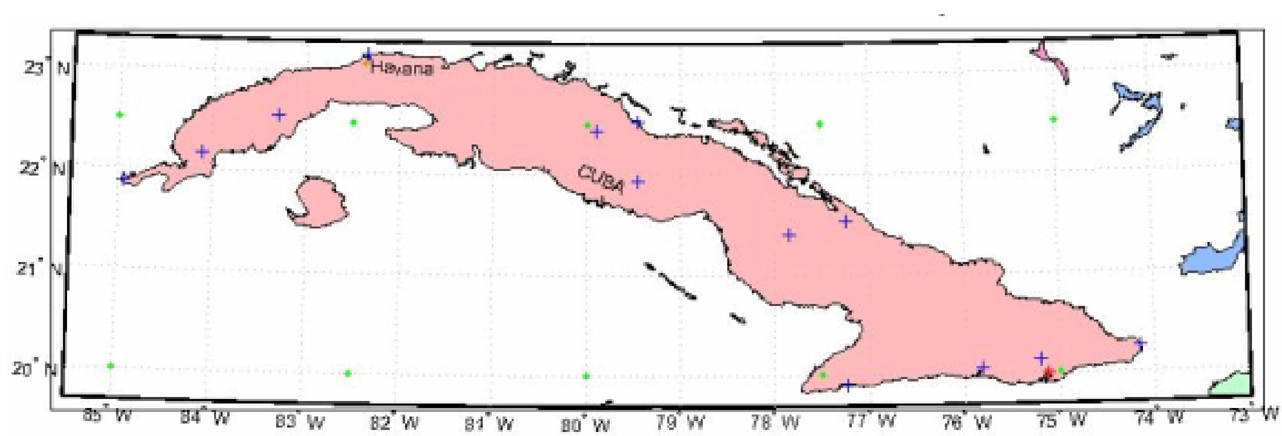

Figure B.2 Localization of 14 Cuba Stations.

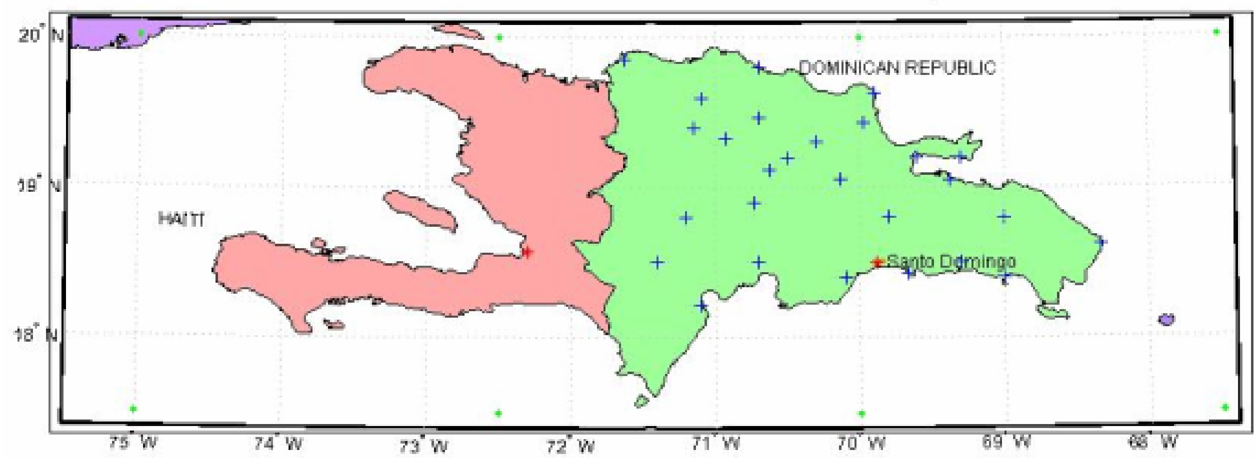

Figure B.3 Localization of 1 Haiti and 28 Republic Dominic stations.

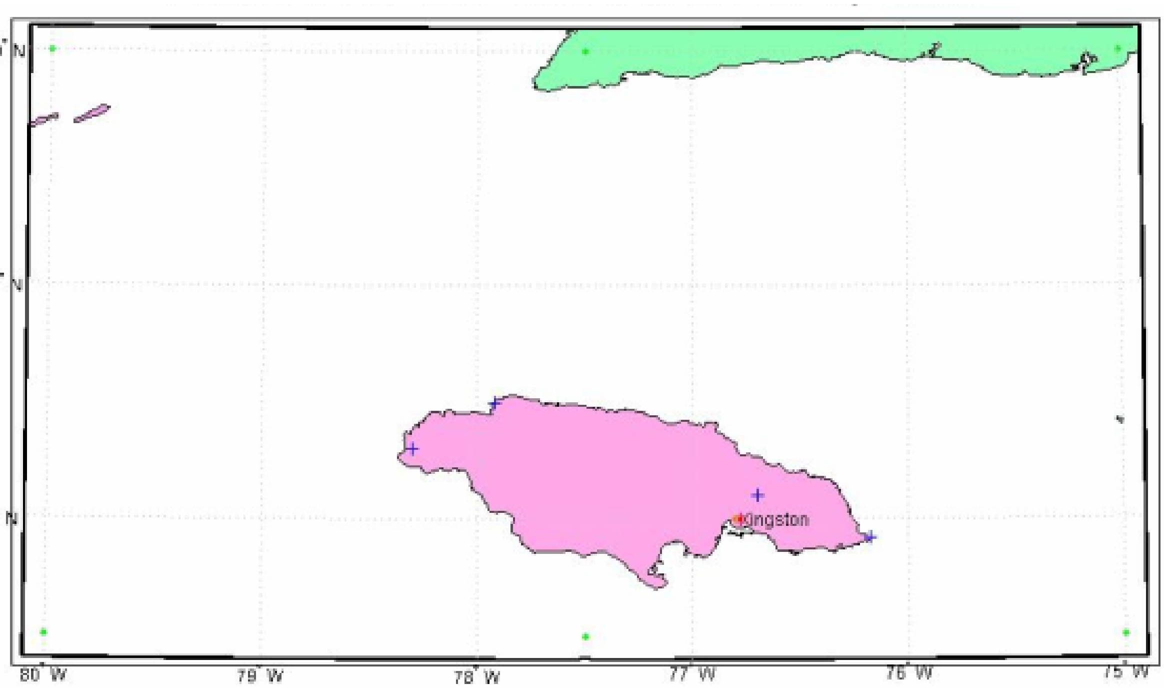

Figure B.4 Localization of 5 Jamaica stations.

APPENDIX C

The goal is to obtain the station air temperature of a missing value by using NCEP air temperature,

$$T_{station} = a + bT_{NCEP}$$

where, T_{NCEP} are the values employed to predict and $T_{station}$ are the values that will be predicted; square minimum method was used to fit the equation.
First, it was necessary to obtain the values of "a" and "b", next, with these values will be predicted the missing values to exact time.

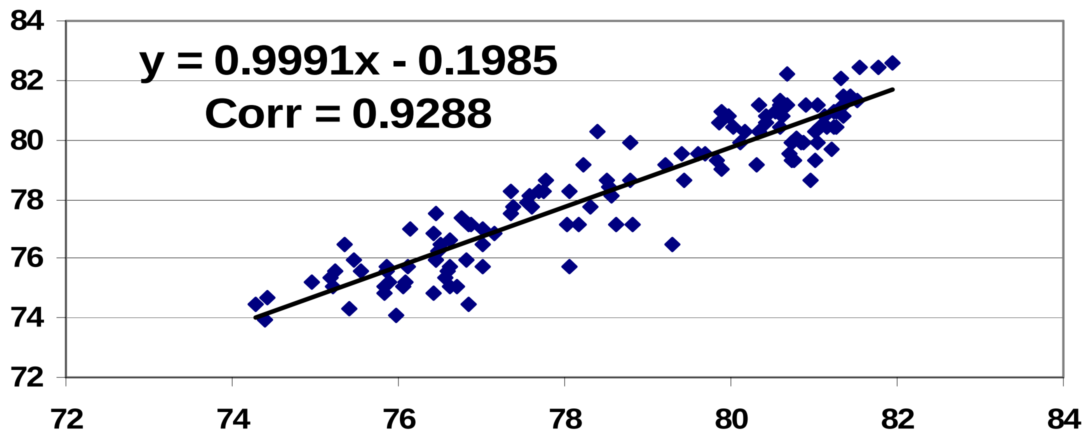

Figure C.1 Correlation between the observed and NCEP mean air surface temperature to PR. The Correlation between the station and NCEP air temperature is big and with this result can estimate the missing values.

TABLE C.1 Correlation value to the Caribbean area.

Country	Variable	Correlation Value
Puerto Rico	Mean AST	0.9288
	Minimum AST	0.9684
	Maximum AST	0.9018
Cuba	Mean AST	0.8992
	Minimum AST	0.9534
	Maximum AST	0.9476
Republic Dominican	Mean AST	0.8788
Haiti	Mean AST	0.8948
Jamaica	Mean AST	0.9076
	Average value	0.9200

Appendix D
Average Temperature in the Caribbean

In relation of the different behavior of the temperature shown in the section 6.1.2.A, about the Caribbean, was necessary to appreciate what is its behavior around the Caribbean. So, we employ NCEP monthly temperature from January 1948 until December 2005 and they were made an average to each point, to latitude and longitude specific, by obtaining the Figure D.1.

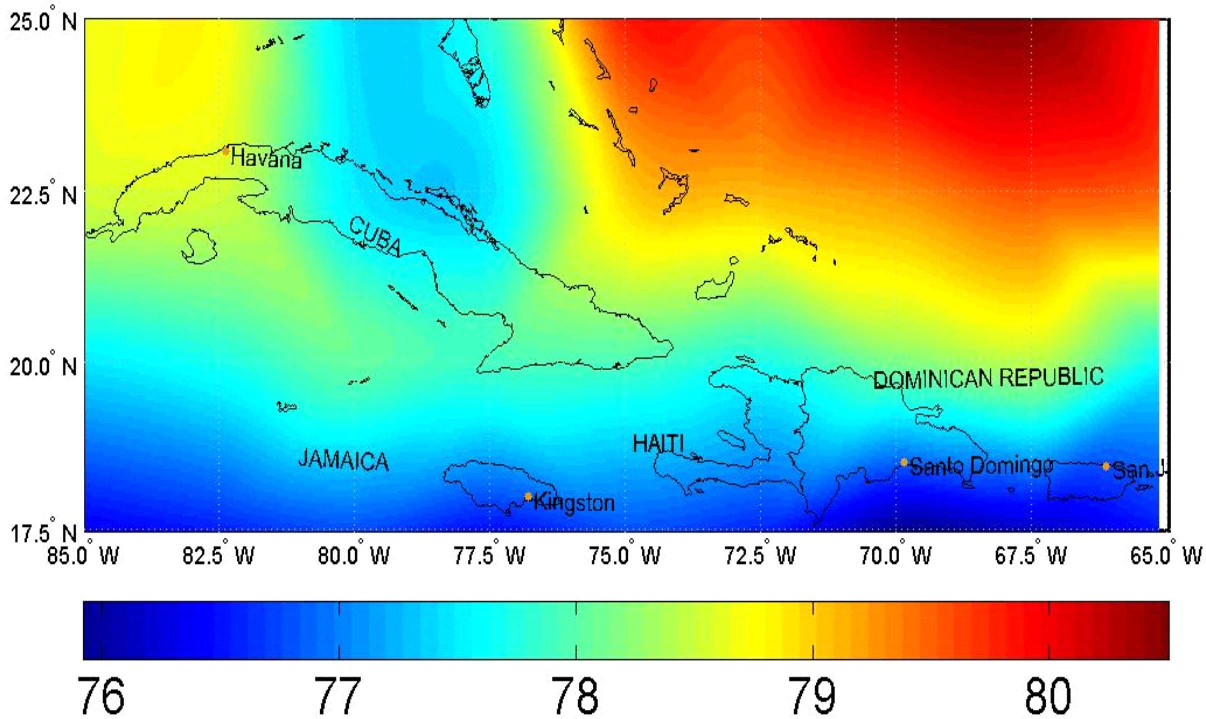

Figure D.1 Time Series Averages of Mean Air Surface Temperature from January 1948 until December 2005.

Figure D.1 shows that Caribbean has not the same behavior; each region has a special climatology. Northeast area is hotter than south area with respect to the middle of the Caribbean area. But the another restlessness was that Figure D.1 only shows the specific temperature but it is not clear with respect to each area is faster increasing or decreasing its temperature. Then, a linear equation was made

$$T_{NCEP} = a + bt$$

Where, ***t*** goes to 1 until the length of the NCEP time series, ***a*** is the intercept and ***b*** is the slope of the linear regression, and T_{NCEP} are the values of the temperature. Where the slope is going to indicate increase or decrease velocity of the Caribbean area. Figure D.2 shows this analysis and the slope was multiplied by 1000. This shows that the west area is increasing faster.

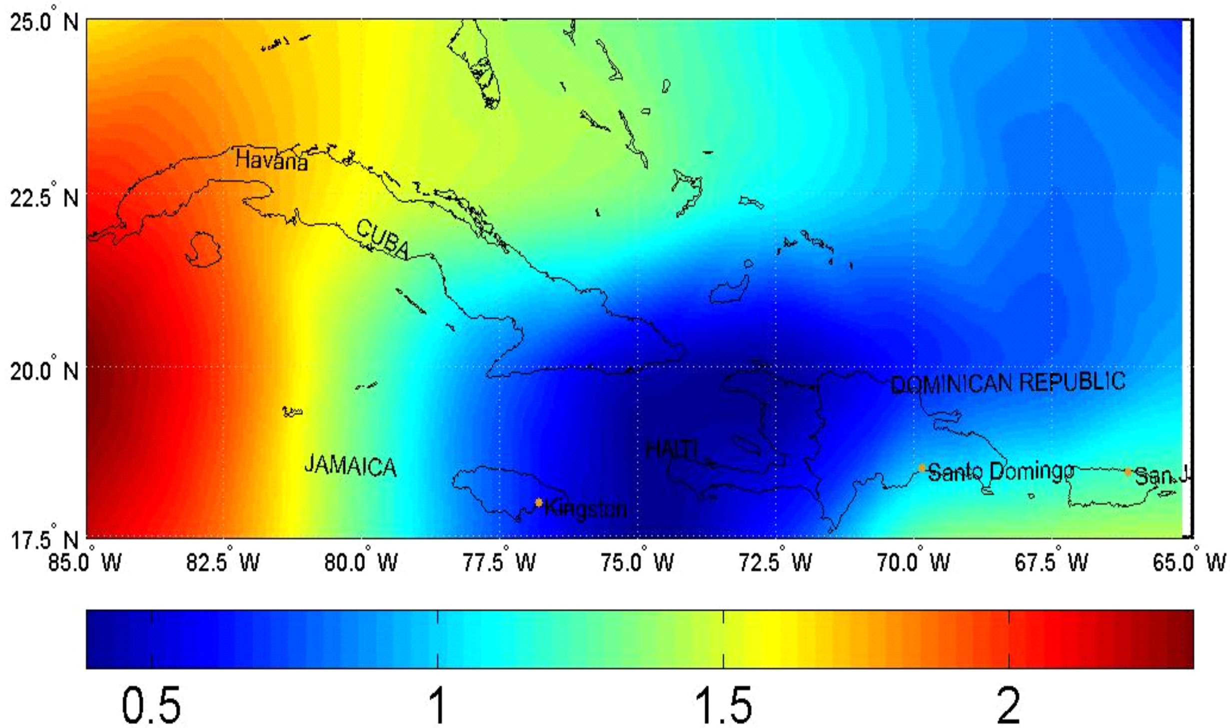

Figure D.2 Slope (x1000) of Mean Air Surface Temperature from January 1948 until December 2005.

APPENDIX E
Classification based in Southern Oscillation Index (SOI) of Jun - Nov

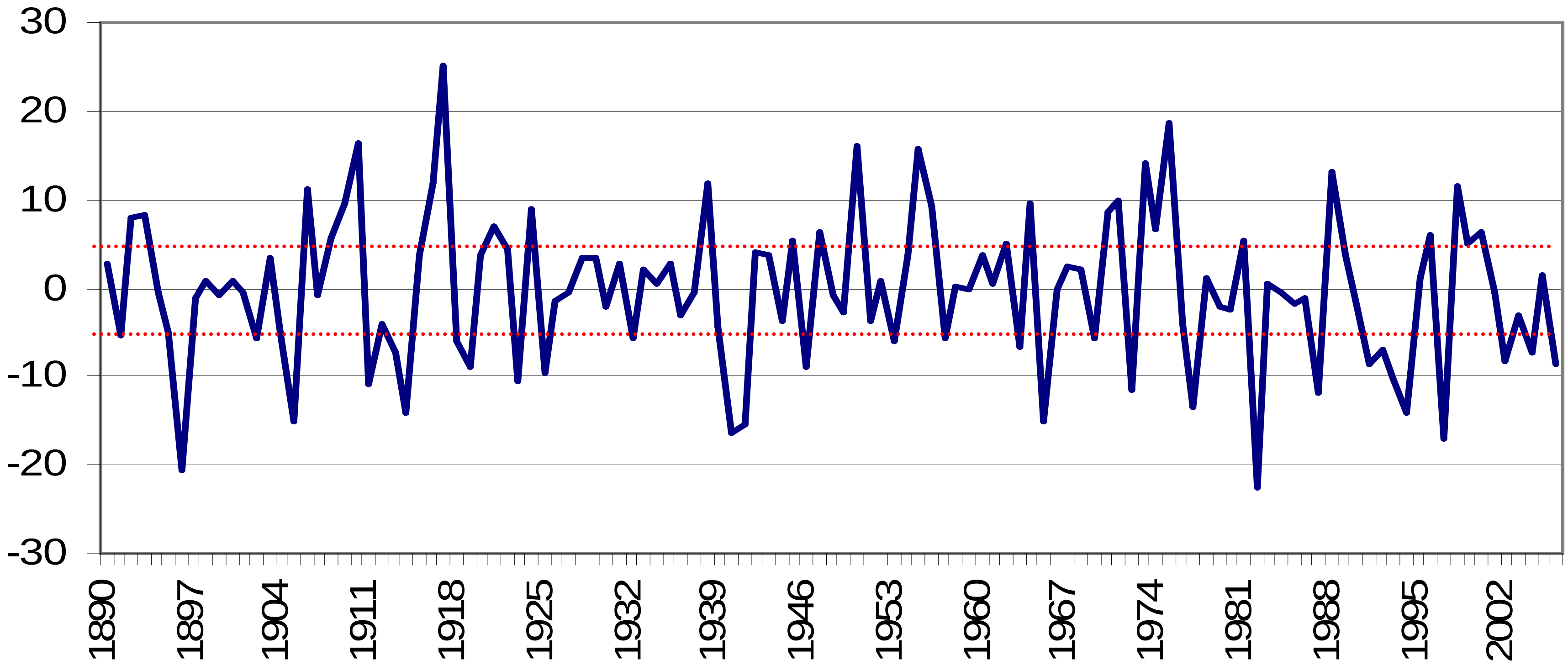

Figure E.1 Southern Oscillation Index (SOI) of Jun - Nov.

(a)

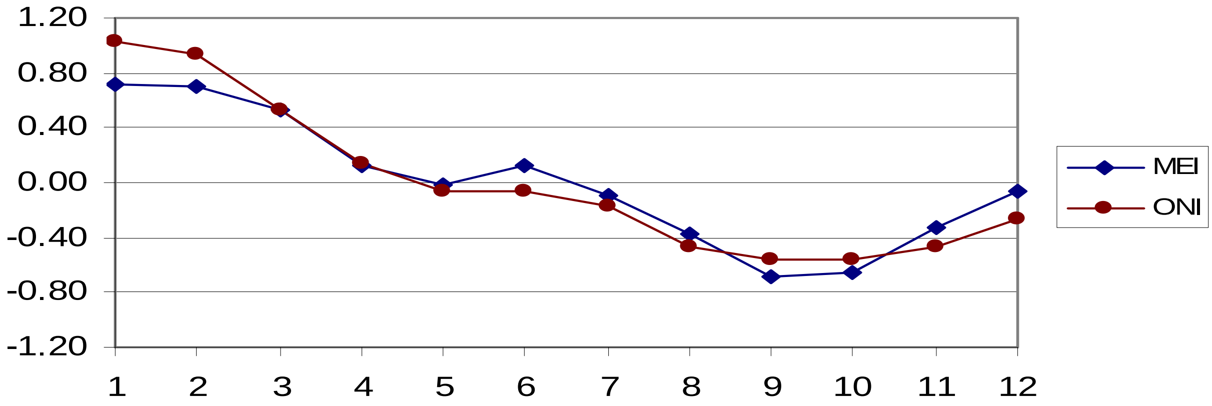

(b)

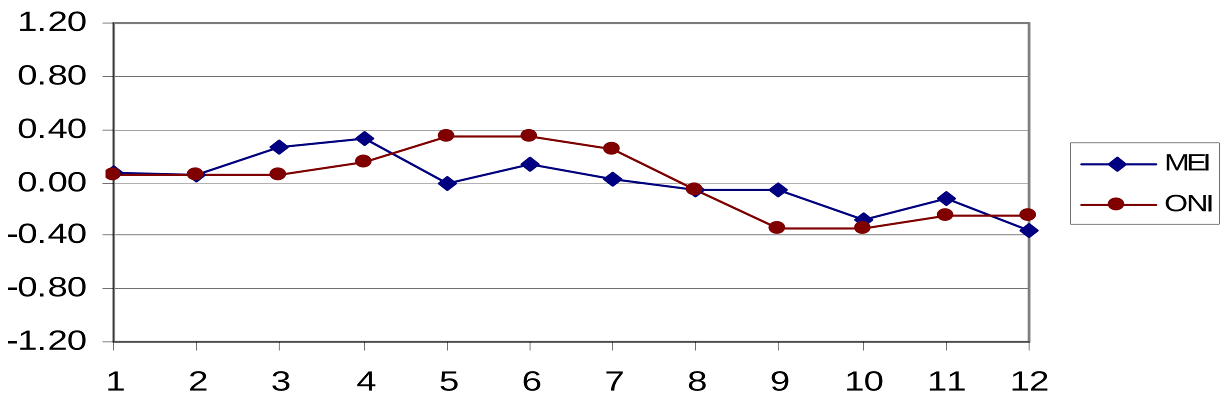

(c)

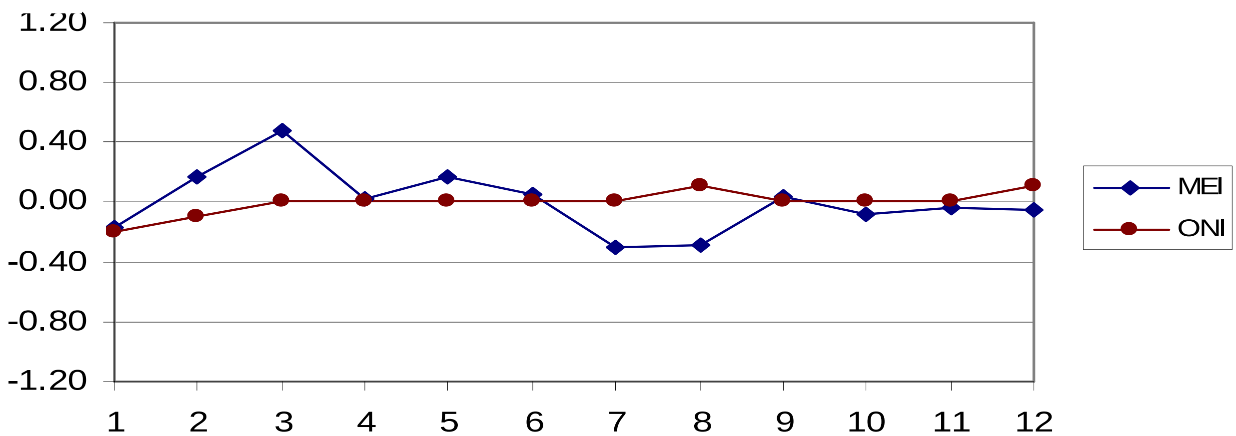

Figure E.2 MEI (blue) and ONI (brown) index to the year (a), 1959, (b) 1961 and (c) 1990.

APPENDIX F
Comparison between Simulated and Observed data to March 1998

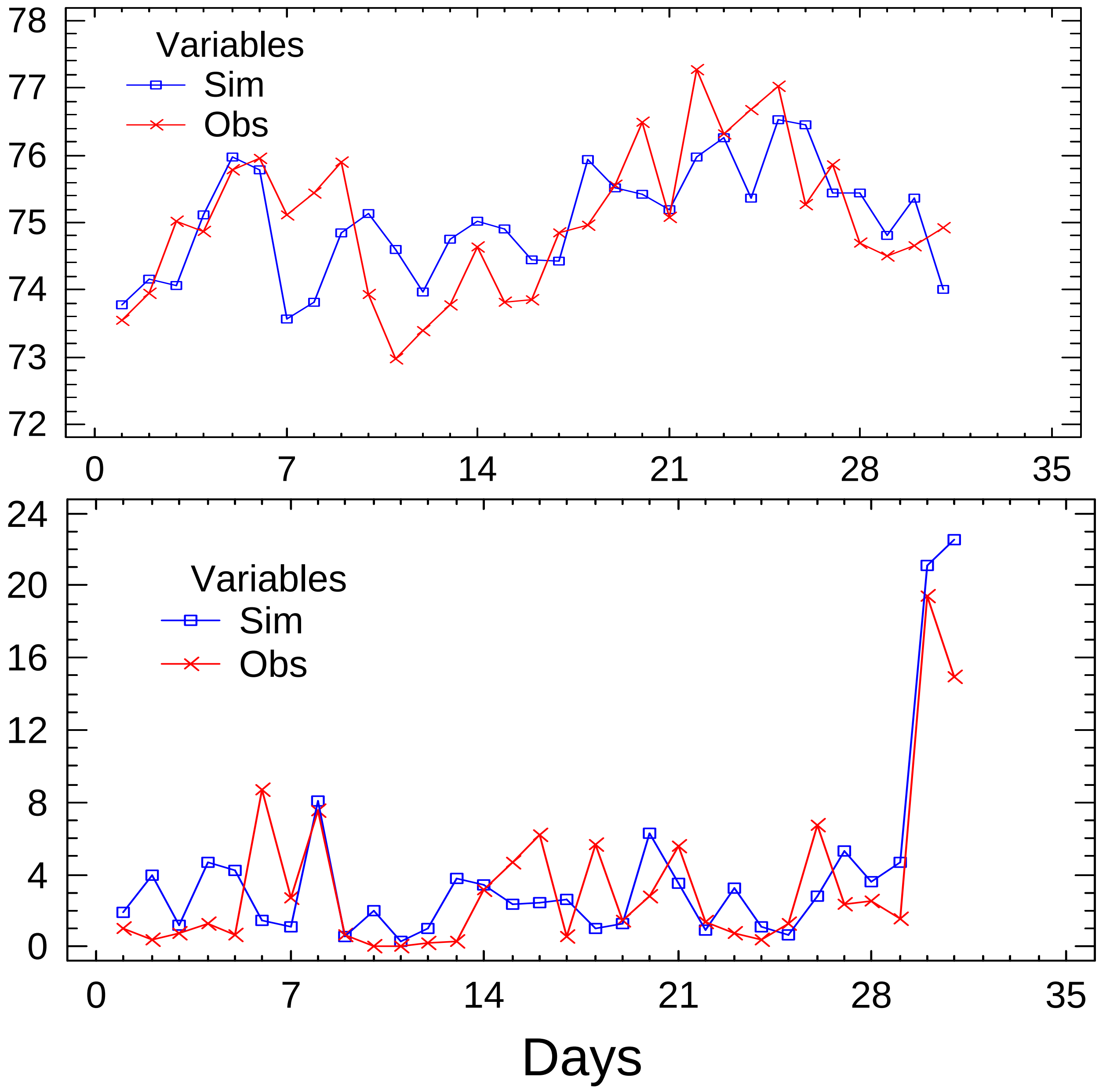

Figure F.1 Simulated (blue) and Observed (red) data from 27 COOP stations in PR to (a), The temperature (ºF), and (c) The Rainfall (mm).